PROTEINS THAT CONTROL THE GEOMETRY OF CILIARY ENDS

by

PANAGIOTA LOUKA

(Under the Direction of Jacek Gaertig)

ABSTRACT

Microtubules are cytoskeletal polymers that are inherently dynamic, switching between phases of elongation and shrinkage. Their dynamic behavior is tightly regulated in order to create organized groups and networks of microtubules that perform diverse cellular functions. One of the most complex microtubule organizations is found in cilia, organelles containing an axoneme core made of nine radially arranged compound (fused wall) microtubules. For most of their length these compound microtubules have a doublet conformation and are composed of a complete A-tubule and an incomplete B-tubule. However, in all cilia studied to date, the B-tubules are shorter than A-tubules giving rise to two main longitudinal compartments of the axoneme; the middle segment (in which the outer microtubules have both the A and B-tubule) and the distal segment (in which the outer microtubules have only the A-tubule extensions). The middle and distal axoneme segment have different functions. The middle segment drives ciliary motility while the distal segment is the side of cilium assembly and signaling in sensory cilia. The existence of longitudinal compartments in the cilium relies on the precise regulation of the termination points of A and B-tubules. Therefore, cilia provide a good opportunity to study how microtubules differentiate within the same functional network. The aim of this study was to explore the mechanisms that regulate the geometry of the distal segment in cilia and determine if

this structural organization serves a particular function. We discovered that the plus-ends of complete (A-tubules) and incomplete (B-tubules) microtubules in cilia are biochemically distinct. We show that FAP256/CEP104 protein localizes to the ends of complete microtubules and promotes their polymerization whereas CHE-12/Crescerin and ARMC9 proteins localize to the ends of B-tubules where they promote their polymerization and depolymerization, respectively. Changes in the length of microtubule subtypes affect the geometry of the distal segment, which correlates with defects in the motile and sensory functions of cilia. Importantly, mutation in FAP256/CEP104 and ARMC9 cause Joubert syndrome, a severe neurological developmental disorder, and our results suggest that defects in distal segment geometry may underlie the disease pathology.

INDEX WORDS: FAP256/CEP104, CHE-12/Crescerin, ARMC9, cilia, Joubert Syndrome, microtubules, TOG, B-tubules

PROTEINS THAT CONTORL THE GEOMETRY OF CILIARY ENDS

by

PANAGIOTA LOUKA

B.S., National and Kapodistrian University of Athens, Greece, 2009

M.S., Boise State University, 2012

A Dissertation Submitted to the Graduate Faculty of The University of Georgia in Partial Fulfillment of the Requirements for the Degree

DOCTOR OF PHILOSOFY

ATHENS, GEORGIA

2018

PROTEINS THAT CONTROL THE GEOMETRY OF CILIARY ENDS

by

PANAGIOTA LOUKA

Major Professor: Jacek Gaertig
Committee: Karl F. Lechtreck
Marcus Fechheimer
Scott T. Dougan

Electronic Version Approved:

Suzanne Barbour
Dean of the Graduate School
The University of Georgia
May 2018

DEDICATION

Dedicated to all the scientists who laid the foundation that made my work possible.

ACKNOWLEDGEMENTS

I would like to express my deepest gratitude to my mentor Jacek Gaertig for his guidance, constant encouragement and constructive criticism that helped me become an independent researcher. His love for science created an ideal work environment where I was constantly encouraged to share my ideas and discuss new findings in my field and other areas of research. I will be forever grateful to Jacek for everything he has done for me and for encouraging me to pursue a career in science. I am also grateful to my committee members, Dr Lechtreck, Dr Fechheimer and Dr Dougan, for their valuable input on my project that helped shape the final product.

I am grateful to all my friends in Athens, GA who became my family away from home. I would like to thank Zacharias Arnos who has been my motivation and strength all these years. Last but not least I would like to thank my parents for always letting me chose my own path in life and my sisters and brother for their constant support.

TABLE OF CONTENTS

CHAPTER 1

INTRODUCTION AND LITERATURE REVIEW

Microtubules

Microtubules, actin and intermediate filaments are the main components of the cytoskeleton. Microtubules are used as rails for the transport of cargoes in the cytosol, direct cell migration, establish cell polarity, provide a binding platform for signaling molecules, and drive chromosome segregation during mitosis. These diverse cellular functions rely on the dynamic behavior of microtubules (exchange of subunits) and their ability to organize into bundles and networks.

Microtubules are hollow cylindrical polymers made of heterodimers of α- and β-tubulin. The tubulin heterodimers are arranged head-to-tail to form protofilaments. Lateral contacts between 10 or more protofilaments form microtubules that have intrinsic polarity, with α-tubulin exposed on one end (minus-end) and β-tubulin on the other (plus-end) (Desai and Mitchison, 1997). While most microtubules are single tubules typically made of 13 protofilaments (Tilney et al., 1973), some presumably specialized microtubules have an atypical protofilament number including 11 and 15 protofilament microtubules in *C. elegans* (Chalfie and Thomson, 1982; Chretien et al., 1992; Wade et al., 1990) and cilia and centrioles have compound fused-wall microtubules made of multiple subfibers (see below). Thus, the same monomer can be used to assemble an amazing diversity of polymeric structures. Some of the big largely unanswered questions about the microtubule organization deal with the mechanisms and significance of generation of microtubules with diverse lattice organization.

Microtubule Properties

The first step towards microtubule polymerization is the nucleation, which refers to an initially slow formation of polymeric "seeds" that once present support a much faster polymer elongation. Spontaneous microtubule nucleation is energetically unfavored because it requires formation of unstable intermediates of tubulin oligomers (reviewed in (Roostalu and Surrey, 2017)). *In vivo* these assembly intermediates are stabilized by proteins that promote nucleation (Roostalu and Surrey, 2017). However, *in vitro* microtubules can form from purified tubulin at higher tubulin concentrations and studies on these artificial polymers revealed some fundamental properties of microtubules. *In vitro* experiments with reconstituted microtubules showed that the exchange of tubulin subunits takes place primarily at the ends of microtubules (Rothwell et al., 1985). Nucleation and polymerization take place in the presence of a minimal concentration of tubulin, called the critical concentration (Cc). Importantly, the Cc of tubulin is much lower at the plus-end as compared to the minus-end, hence microtubules grow primarily by polymerization at the plus-end (Desai and Mitchison, 1997). The rates of depolymerization are similar between the plus and minus end and free microtubule minus-ends undergo depolymerization at tubulin concentrations above the Cc for the plus end. The process in which the plus end grows and minus end shrinks is called treadmilling, a behavior of microtubules, which allows them to seemingly move in the cytoplasm (Rodionov and Borisy, 1997). However, this is a rare phenomenon *in vivo* because most microtubule minus-ends are anchored at microtubule organizing centers like the centrosome or are capped by minus end binding proteins. Mitchison and Kirschner were the first to observe that growing and shrinking microtubules co-exist in the same sample of *in vitro* reconstituted microtubules and that the plus ends frequently transition from growth to shrinkage (catastrophe) and vice versa (rescue) (Mitchison and Kirschner, 1984). They named this

phenomenon “dynamic instability”. Individual microtubules undergo catastrophes under assembly-favoring conditions showing that dynamic instability is stochastic (Mitchison and Kirschner, 1984). Importantly, *in vivo,* the dynamic instability of microtubules is highly regulated by microtubule-binding proteins (discussed later) (Cassimeris et al., 1988).

Because it is an intrinsic property of microtubules, the explanation for dynamic instability must be derived from the microtubule structure. Studies of tubulin and microtubules at the near atomic resolution revealed conformational changes in the tubulin dimers that take place during polymerization and depolymerization. Both α- and β-tubulin bind a single molecule GTP. The addition of tubulin dimers to the plus end is associated with GTP hydrolysis only on β-tubulin (Weisenberg et al., 1976), that occurs promptly but with a sufficient delay allowing for formation of a “GTP cap” containing freshly added subunits (that have not yet hydrolyzed their GTP) at the end of growing microtubules (Carlier and Pantaloni, 1981). The hydrolysis of GTP correlates with changes in the microtubule lattice conformation that destabilize tubulin lateral interactions and promote depolymerization (Alushin et al., 2014). However, depolymerization does not occur as long as a minimal GTP cap is present, which somehow stabilizes the microtubule end (Hyman et al., 1992; Tran et al., 1997; Walker et al., 1989). The GTP cap is lost when the rate of polymerization is slower than the rate of GTP hydrolysis, and this induces a catastrophe (Voter et al., 1991; Walker et al., 1991). Interestingly, older microtubules undergo catastrophes more frequently than younger microtubules at the same total tubulin concentration (Gardner et al., 2011) suggesting that the polymers accumulate changes over time that somehow reduce the size of the GTP cap.

The transitions from microtubule depolymerization to polymerization (rescues) are less understood. Although the rate of tubulin polymerization *in vitro* increases with increasing

concentrations of tubulin, the frequency of rescues is very low and is independent of tubulin concentration (Walker et al., 1988). There is some evidence that rescue events occur in places where microtubules retain remnants of GTP-tubulin (GTP-islands) that were detected both *in vitro* and *in vivo* using antibodies specific to GTP-β-tubulin (Dimitrov et al., 2008; Nakata et al., 2011; Seetapun et al., 2012; Thoma et al., 2010; Tropini et al., 2012). How the GTP- islands form is unclear. One possibility is some tubulin that is added at the growing end (as part of the GTP cap) somehow escapes GTP hydrolysis as the microtubule elongates. Furthermore, recent studies indicate that GTP- islands form by internal incorporation of GTP-tubulin in places where microtubules bend and experience lattice breaks (de Forges et al., 2016).

In vivo, the frequencies of catastrophes and rescues are regulated to tune the microtubule dynamics and adapt the microtubule networks for specific functions. For example during the mitotic anaphase, microtubules that connect to kinetochores shrink whereas interpolar microtubules elongate (Saxton and McIntosh, 1987). This suggests the presence of mechanisms that regulate the intrinsic properties of individual microtubules within a functional network such as the spindle. Microtubule associated proteins (MAPs) and molecular motors are known to regulate the microtubule dynamics by accelerating the rates of polymerization and depolymerization, or changing the frequencies of transitions (rescue, catastrophes or pauses) (reviewed in (Desai and Mitchison, 1997)). MAPs can be grouped into proteins that bind to the microtubule wall or to polymer ends. Lattice-binding proteins typically bind to multiple tubulin subunits and either stabilize or sever the microtubules, whereas proteins that bind to the microtubule ends act as polymerization or depolymerization regulators.

Microtubule Associated Proteins

MAPs that track the microtubule plus-end (+TIPs) are a structurally and functionally diverse group of proteins that recognize the plus ends and regulate their dynamics (reviewed in (Akhmanova and Steinmetz, 2008)). The specificity of +TIPs for the microtubule plus-end is mediated by their microtubule-binding domains that recognize distinct conformations present at the plus-end. However, some +TIPs (including the well studied EB proteins) can recognize both the plus and minus ends when these ends grow (Goodwin and Vale, 2010). They are still called +TIPs because the minus end is less dynamic and the majority of growing ends are plus-ends. Those +TIPs that recognize the growing plus and minus ends likely sense the GTP cap that is present at both plus and minus ends as long as they grow and acquire new tubulin. Going back to the plus end that is studied in most cases, the growing microtubule end has three structurally distinct regions: curved tubulin dimers at outer edge of the plus-end (GTP-tubulin); followed by slightly straightened tubulin dimers (GDP + Pi-tubulin); and straight tubulin dimers (GDP-tubulin). The depolymerizing microtubule plus-end has a different conformation in which protofilaments curve outward and peel off and tubulin dimers are highly curved (Nicholson et al., 1999). One class of +TIPs uses TOG domains (Tumor Overexpressed Gene) to track the microtubule plus-end (Al-Bassam and Chang, 2011). TOG domains are microtubule-binding domains that recognize curved tubulin characteristic of unpolymerized tubulin and tubulin at the newly formed microtubule plus-end (Ayaz et al., 2014; Ayaz et al., 2012). TOG domains are made of 6 antiparallel alpha helixes with divergent primary structure that folds into conserved tubulin binding motifs (Al-Bassam et al., 2007). Three TOG domain protein families are known: CLASP, Stu2/XMAP215 and CHE-12/Crescerin. Proteins of the CLASP family have three TOG domains that likely interact with highly curved tubulin that may be present at the plus end of

depolymerizing microtubules (Leano et al., 2013). This interaction is believed to inhibit both depolymerization and polymerization and promote microtubule pause. Proteins of the Stu2/XMAP215 family use an array of TOG domains to promote microtubule plus end polymerization (Ayaz et al., 2014; Ayaz et al., 2012; Brouhard et al., 2008; Fox et al., 2014; Widlund et al., 2011). The Stu2-TOG1 domain binds to curved tubulin, which explains the presence of Stu2 family proteins at the extreme plus-end of microtubules (Ayaz et al., 2012). Typically, these proteins have two or more TOG domains which allow them to simultaneously bind to tubulin already added to the growing end and bring an unpolymerized tubulin subunit to this end (Ayaz et al., 2012). CHE-12/Crescerin is the most recent TOG family described (Das et al., 2015). Crescerin family proteins have multiple TOG-domains. The Crescerin-TOG2 domain is structurally similar to Stu2-TOG1 domain and is also likely to interact with curved tubulin. CHE-12/Crescerin proteins are predicted to be microtubule polymerases; however, they form a distinct protein family whose members are specifically associated with cilia (Das et al., 2015), in contrast to CLASP and Stu2/XMAP215 proteins that regulate the cytoplasmic and mitotic microtubules. Our work shows that CHE-12/crescerin promotes polymerization of ciliary microtubules and specifically acts on the B-tubule (see chapter 2). It is interesting to note that seemingly small conformational changes in the TOG domains confer the specificity of these proteins for a particular microtubule lattice organization.

The most well studied class of +TIPs is the family of End Binding proteins (EBs). The founding member of this class is EB1, which uses an N-terminal Calponin Homology (CH) domain to recognize an assembly intermediate conformation (GDP + Pi microtubule lattice) at the growing microtubule end (Zanic et al., 2009). The CH domain bridges two protofilaments by binding at the crossroads of four neighboring tubulin dimers (Maurer et al., 2012; Zhang et al.,

2015). EB1 forms the core of the "+TIP network" by transporting other +TIPs to the microtubule plus-end (Akhmanova and Steinmetz, 2010). Optometric inactivation of EB1 in the living cell leads to a rapid loss of a number of other +TIPs, attenuates the microtubule growth and promotes catastrophes (van Haren et al., 2018). Thus, multiple +TIPs cooperate to modulate microtubule dynamics.

Certain MAPs promote microtubule depolymerization. This group includes depolymerizing kinesin-related proteins (some of which lack the ability to walk on the microtubule surface) that destabilize the microtubule ends: kinesin-13, kinesin-8 and kinesin-4. The end depolymerizing function of the non-motile kinesin-13 involves binding to protofilaments that peel off at the ends of depolymerizing microtubules (Ogawa et al., 2004; Shipley et al., 2004). Kinesin-4 and kinesin-8 proteins track the end of a growing microtubule and promote catastrophe through a yet unknown mechanism (He et al., 2014) (Niwa et al., 2012; Wang et al., 2016).

Defects in the regulation of microtubule dynamics *in vivo* can affect multiple cellular functions. For example, a loss of microtubule plus end polymerases, like XMAP215, leads to reduced rate of microtubule assembly and reduces the size of the mitotic spindle (mini spindle phenotype) (Cullen et al., 1999). On the other hand a loss of kinesin-13 leads to elongated spindles in *Drosophila* cells (Goshima et al., 2005). Therefore, through modulation of microtubule dynamics, MAPs regulate the length of microtubules and affect the organization of microtubule networks.

Cilia

Cilia are conserved microtubule-based organelles that project from the cell surface. The presence of one or more cilia per cell correlates with the cilium function. A single cilium per cell is used mainly as a sensory organelle (primary cilium) whereas multiple cilia per cell are mainly used as motile organelles (motile cilia). The sensory primary cilia are found in animals and are involved in many functions including animal body patterning, organogenesis, and sensory perception. The discovery of signaling pathways mediated through primary cilia (Huangfu et al., 2003) and ciliary diseases caused by mutations in cilia-associated proteins (Afzelius, 1976; Pazour et al., 2000) brought this organelle to the spotlight. Motile cilia are present in most eukaryotes (with exception of most land plants and fungi). Cilia are used for locomotion, generation of fluid flow along the cell or tissue surface, the movement of particles such as mucus across a tissue surface as well as signaling between cells. Importantly, defects in both primary and motile cilia are known to cause a plethora of human genetic diseases collectively called ciliopathies (see next section) (Reiter and Leroux, 2017).

Ciliopathies

Ciliopathies are classified as first-order when the causative mutation is in a ciliary gene, or second-order when the causative mutation is not in a ciliary gene but affects cilia function (reviewed in (Reiter and Leroux, 2017)). The first documented ciliopathy was a case of a male patient with both infertility and sinusitis/bronchitis whose cilia (sperm and respiratory) lacked dynein arms (Afzelius, 1976). In humans, motile cilia are present in the node of the developing embryo (where they are required for establishing the left-right body axis), in the airways where they power the mucociliary transport, in the oviducts for transporting oocytes and in sperm to

power its movement. Mutations that affect ciliary motility typically result in the development of primary ciliary dyskinesia syndrome (PCD) characterized by situs inversus (body asymmetry reversal), respiratory problems and infertility. Sensory primary cilia are found in almost all cells of the human body and are involved in sensing environmental or intercellular cues. For example, cilia in the eye are important for light perception, in the nose for odor perception, in the kidney for sensing flow and in the brain for signaling pathways like Hedgehog (Hh). Defects in primary cilia result in the development of a number of diverse syndromes including retinal dystrophy, polycystic kidney disease, mental disabilities and neurodevelopmental disorders like Joubert syndrome (JS) (Reiter and Leroux, 2017). Two of the proteins we studied here (chapter 2) are confirmed JS proteins (Srour et al., 2015; Van De Weghe et al., 2017). To date, mutations in more than 35 ciliary genes are known to cause JS (Mitchison and Valente, 2017). Joubert syndrome proteins cluster near the basal body, transition zone and the tip of cilia. Although our knowledge of the molecular defects underpinning this syndrome is increasing, it is still unclear how defects in primary cilia function cause JS.

Ultrastructure of cilia

The first report linking cilia function to the organelle's structure was published in 1964, with the identification of *Chlamydomonas* motility mutants that carried structurally defective cilia lacking specific parts such as radial spokes or central microtubules (Randall et al., 1964). Our knowledge of the cilium structure exploded with advancements in electron microscopy, which allowed for characterization of cilia up to the subnanometer resolution (with the more recent use of cryo-electron tomography). Cilia have one of the most complex microtubule organizations in the eukaryotic cell. Cilia originate from basal bodies that are cylindrical

arrangements of nine triplet microtubules, two of which elongate to form the core structure of the cilium, the axoneme. In principle the basal body is a modified centriole that is used to nucleate an axoneme of the cilium. In some organisms, including mammalian cells, the centriole serves in the mitotic spindle as the centrosome and later in interphase becomes the basal body to support cilium formation (and the basal body converts into the centriole in the subsequent mitotis). In most motile cilia a central pair of microtubules (CP) is present in the center of the axoneme (9+2 axoneme). Near the tip of the cilium the doublets transition to singlets. Thus, the cilium has multiple structurally and likely functionally distinct longitudinal segments that have microtubules with a different wall organization; the basal body (nine triplet microtubules), the transition zone and middle axoneme (nine doublet microtubules) and the distal axoneme segment (nine singlet microtubules) (Figure 1).

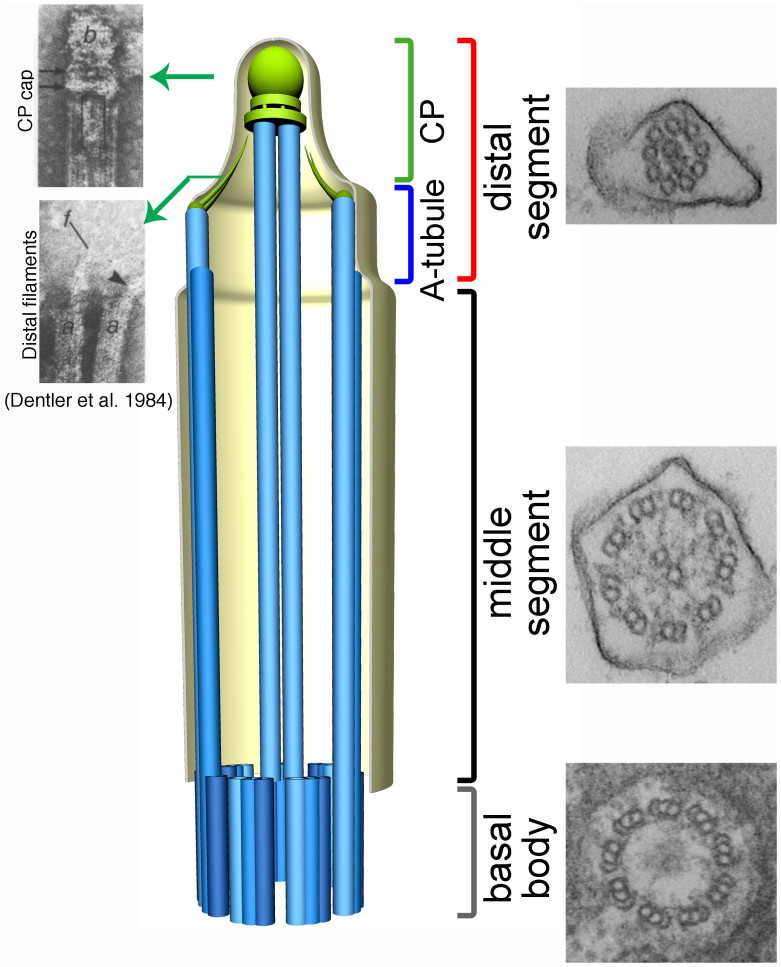

Figure 1. Ultrastructure of a motile cilium

The Basal Body

The base of each cilium has the basal body from which the main framework of the cilium, the axoneme, grows. Basal bodies are modified centrioles that are specialized in ciliation. They are cylindrical structures with a nine-fold symmetry made of nine triplet microtubules; one complete (13 protofilament) A-tubule and two incomplete (10 protofilament) subfibers: the B-tubule that is attached to the side of the A-tubule and the C-tubule that is attached to the side of the B-tubule. The framework for basal body and centriole assembly is established by its cartwheel present in the basal region. The main component of the cartwheel is SAS-6, a protein that oligomerizes to form radially arranged spokes with a nine-fold symmetry. Several layers of

SAS-6 rings are vertically stacked to form the cartwheel (reviewed in (Guichard et al., 2018). At the periphery of every spoke the γ-tubulin ring complex (γTuRC) and γ-tubulin small complex (γTuSC) nucleate the assembly of A-tubules (reviewed in (Guichard et al., 2018)). These complexes were originally isolated as 25 nm ring structures made of repeating units of γ-tubulin and associated proteins (reviewed in (Kollman et al., 2011)). Gamma-tubulin complexes have a broader role as they also support the assembly of cytoplasmic singlet microtubules. Lateral interactions of γ-tubulin monomers resemble the lateral contacts between protofilaments and the γ-tubulin ring is believed to form a structural template for nucleation of 13 protofilament microtubules (Aldaz et al., 2005; Rice et al., 2008). It is not clear whether γ-tubulin also contributes as structural template for the assembly of the (incomplete) B and C-tubules. However, certain other tubulin types have been implicated in the formation of B- and C-tubules (but it is still not clear whether they act as templates in the manner similar to γ-tubulin). The tubulin superfamily includes isotypes from α to η though only α, β and γ-tubulins are conserved in all eukaryotes (Turk et al., 2015). Loss of δ-tubulin results in a loss of C-tubules (Chang and Stearns, 2000; Dutcher and Trabuco, 1998; Garreau de Loubresse et al., 2001; O'Toole et al., 2003) and loss of ε-tubulin results in loss of both C and B-tubules from basal bodies (Chang et al., 2003; Dupuis-Williams et al., 2002; Dutcher et al., 2002). Loss of δ or ε-tubulin in mammalian cells results in centrioles with singlet microtubules (Wang et al., 2017). These results suggest that δ and ε-tubulins maybe involved in the assembly or maintenance of incomplete tubules in the basal bodies and centrioles.

Microtubule doublets (or triplets) are not known to form outside of organelles like the centrosome and basal body. In the presence of high amounts of tubulin unusual structures called hooks form on the microtubule surface *in vitro* that resemble the incomplete tubules of doublets

and triplets (Euteneuer and McIntosh, 1980). These artificial hooks are rarely closed (like the B- or C-tubules) suggesting that formation of the incomplete tubules in cilia requires additional proteins, not just tubulin at high concentration. A recent cryo-electron tomography study revealed that the inner wall of both A and B-tubules is covered with a dense network of globular and filamentous "microtubule inner proteins" or MIPs. The tubulin-MIP interfaces are highly conserved in ciliated organisms suggesting they are important for the doublet (and perhaps triplet) architecture (Ichikawa et al., 2017). The triplet and doublet microtubules are also extremely stable as compared to rather fragile cytoplasmic or mitotic singlet microtubules. This means that triplet and doublet microtubules resist conditions that readily depolymerize singlet microtubules such as cold or certain microtubule drugs (e.g. colchicine). Furthermore, the doublets and triplets are less dynamic, they do not show behaviors known for cytoplasmic microtubules such as dynamic instability (Kochanski and Borisy, 1990). However, the doublets and triplets are not static after their assembly is completed. For example, tubulin is incorporated at a slow rate at the distal (plus) ends of axonemes (Marshall and Rosenbaum, 2001).

The role of triplet microtubule organization in the basal body (or centriole more broadly) function is not clear. Some basal bodies including those in cilia of *C. elegans* and *Drosophila* neurons, are made of doublet microtubules (Jana et al., 2016; Nechipurenko et al., 2017). Interestingly, the basal bodies of *Drosophila* sperm have triplet basal body microtubules (Jana et al., 2016). An increasing body of evidence suggests that the triplet organization is important for the structural stability of centrioles and basal bodies (Chang et al., 2003; Chang and Stearns, 2000; Dupuis-Williams et al., 2002; Dutcher and Trabuco, 1998; Garreau de Loubresse et al., 2001; Wang et al., 2017). For example a loss of the C-tubule in the ciliate *Paramecium*, may lead to progressive loss of B-tubules and the entire triplets (Garreau de Loubresse et al., 2001).

Interestingly, the C-tubules in centrioles are slightly shorter than the B- and A-tubules, but the functional significance of this organization is unknown (Paintrand et al., 1992). The mechanism that regulates the length of C-tubules is unclear. More broadly, it is not known how the termination points of any subfibers are regulated. My experiments (see chapter 2) address this exact and large gap in knowledge – how the longitudinal segments of cilia form through regulation of microtubule ends. My work is relevant to the formation of three main segments of cilia: the basal body, middle and distal segment.

Transition zone

The basal bodies dock to the plasma membrane with the plus ends of microtubules oriented toward the membrane. The termination of C-tubules and the elongation of the doublets forms the axoneme that is associated with expansion of the plasma membrane culminating in the generation of the cell projection on the cell surface. The axonemal doublets are linked to the ciliary membrane near the base of the cilium. The area between the termination of C-tubules and the membrane links is the transition zone. While the basic components of the transition zone are conserved, the exact structural organization varies among different species (reviewed in (Fisch and Dupuis-Williams, 2011)). Defects in proteins that localize to the transition zone often lead to changes in the protein composition of cilia and their membrane suggesting that the transition zone may function as a "ciliary gate" that regulates protein entry into the cilium (reviewed in (Garcia-Gonzalo and Reiter, 2017)).

Middle segment

The part of the cilium that starts above the transition zone and contains the doublet microtubules is called the middle segment. Typically, the middle segment is the main or longest part of the cilium. With some rare exceptions, for example, in the olfactory cilia the distal segment is the main part of the cilium as noted below. In motile cilia a central pair of microtubules forms in the center of the axoneme above the transition zone through a poorly understood mechanism that may involve an initial microtubule polymerization in the distal portion of the axoneme and its subsequent docking above the basal body (Lechtreck et al., 2013). Central microtubules are encaged in a dense sheath of proteins that form projections. Each of the two central microtubules is structurally unique, carrying a different subset of projections (Loreng and Smith, 2017). The central pair is essential for motility in cilia that beat asymmetrically, that is have a distinct power and recovery stroke (Huang et al., 1979; Lewin, 1954), whereas it is absent from cilia that produce a vortex like symmetrical movement (i.g 9+0 nodal cilia) (Nonaka et al., 1998). The CP projections physically interact with the force-generating proteins that decorate the A-tubules with a 96 nm periodicity. The three major motility-associated protein complexes are the outer and inner dynein arms and radial spokes. Dynein arms project from the A-tubule towards the B-tubule of the neighboring doublet and radial spokes project from the A-tubule towards the central pair (Nicastro et al., 2006) (Figure 2). Loss of radial spokes leads to formation of more than two central microtubules suggesting that the number of central microtubules is regulated through lateral spatial constraints generated by the radial spokes (Lechtreck et al., 2013; Nakazawa et al., 2014). Inner dynein arms promote sliding of the outer doublets. The sliding of doublets is transformed into axoneme bending, because the minus ends of doublets are stably anchored in the cytoplasm and doublets are interconnected through the

nexin dynein regulatory complex (Bower et al., 2013; Satir, 1968; Summers and Gibbons, 1971). The activity of inner dynein arms is regulated by physical contacts between radial spokes and the central pair projections (Oda et al., 2014). One important function of the CP-radial spoke complexes is to confer switching of dynein arm activation cycles on the two sides of the axoneme as the cilium cycles between the power and the recover stroke. Outer dynein arms regulate the beat frequency and their activity is affected by certain tubulin Post-Translational Modifications (PTMs) of the B-tubule (Kamiya, 2002; Kubo et al., 2010; Suryavanshi et al., 2010). In *Chlamydomonas* a loss of the CP or radial spokes can eliminate the asymmetric waveform, but the affected cilia can still beat symmetrically (Brokaw and Kamiya, 1987).

The middle segment of primary cilia (non-motile) is relatively understudied and its only function may be to provide certain length and rigidity to the cilium. To date no middle segment proteins specific to primary cilia have been identified. Interestingly, primary cilia have a relatively short middle segment when compared to the motile cilia (Reese, 1965; Williams et al., 2014).

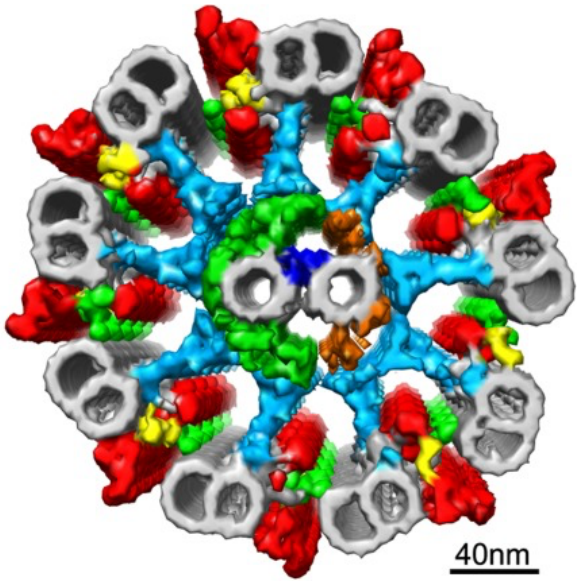

Figure 2. Cryotomography of *Chlamydomonas* flagellum seen from the tip.

Grey: microtubule doublets and CP. Red and yellow: inner and outer dynein arms. Light blue: radial spokes. Light green: nexin. Green, blue and orange around the CP: CP projections. Reproduced with permission from (Ishikawa, 2013).

Distal segment

In all cilia studied to date, B-tubules terminate below A-tubules defining the proximal boundary of the distal segment that contains singlet microtubules (A-tubules in primary cilia and A-tubules and CP in motile cilia) (Figure 1). Even though all cilia have a distal segment its dimensions vary in different cell types, presumably reflecting functional adaptions of cilia. For example, in the immotile 9+2 olfactory cilia the distal segment accounts for 80% of the cilium length (reviewed in (McEwen et al., 2008). The distal segment length varies in different sensory cilia of *C. elegans* specialized for different functions (Inglis et al., 2007; Mukhopadhyay et al., 2007). Mammalian primary cilia have particularly long distal segments and signaling molecules are enriched in this region (Haycraft et al., 2005). The distal segment in motile cilia of the unicellular algae *Chlamydomonas* is relatively short measuring 4% of the total cilium length, which becomes 30% longer during sexual mating (Mesland et al., 1980). Taken together these observations show that the length of the distal segment is regulated and its length may be functionally important.

The distal segment is poorly studied and has not been assigned a ciliary role yet. However, a number of activities, some of which are of critical importance, are known to take place within this region including: 1) axoneme assembly and disassembly; 2) turnaround of intraflagellar transport (IFT) trains; 3) production of extracellular vesicles; and 4) events associated with activation of certain signaling pathways including the essential (in mammalian

embryonic development) Hh signaling. To be more precise, we know that certain important activities take place within the distal segment, but it is not clear why the distal segment has a prominent region of singlet microtubules that varies in length depending on the type of cilia and physiological conditions. Furthermore, we do not know how the unique organization of the distal segment is established. To illustrate the question further, one could imagine that all cilia are made of a ring of triplet microtubules (or doublet microtubules) from the base to the tip. And yet this has never been observed in nature, which brings the question of the function of segmental divisions in the cilium and the mechanism of segment differentiation.

Axoneme assembly and disassembly: The distal segment contains the plus-ends of axonemal microtubules, which is the site of cilium assembly and disassembly (Marshall and Rosenbaum, 2001; Viswanadha et al., 2014). Ciliary proteins are synthesized in the cytoplasm and transported to the tip of cilia through diffusion or IFT (reviewed in (Lechtreck et al., 2017)). IFT was discovered in 1993 as a bidirectional movement of particles inside *Chlamydomonas* flagella (Kozminski et al., 1993). Two types of IFT cargo platform complexes or "trains" exist; the anterograde trains powered by kinesin-2 motors that (in the middle segment) move primarily on B-tubules, and the retrograde trains powered by a subtype of cytoplasmic dynein, IFT dynein that move primarily on A-tubules (Cole et al., 1998; Kozminski et al., 1995; Pazour et al., 1999; Pazour et al., 1998; Signor et al., 1999; Stepanek and Pigino, 2016). Biochemically the IFT trains are made of two multiprotein complexes IFT-A and IFT-B. Proteins that are part of the IFT-B complex are more important for the anterograde transport, while proteins forming the IFT-A complex are more important for the retrograde transport. Cargo loading on IFT could be direct or indirect through the use of cargo adaptors (reviewed in (Lechtreck, 2015)). Cargo loading takes place at the base of cilia and unloading generally occurs at the tip of cilia though occasionally

some cargos may be unloaded along the axoneme length. At the tip of cilia cargos are released and IFT is reorganized, to associate with the minus-end directed motor for retrograde transport (Pedersen et al., 2005). What triggers IFT turnover at the tip of cilia is an active area of research. IFT affects the rate of axonemal microtubule polymerization by delivering tubulin to the ciliary tip where the axoneme assembles. Tubulin transport by IFT is upregulated during cilia assembly and returns to base levels when cilia are full length (Craft et al., 2015). Defects in IFT affect the length of cilia showing that IFT is involved in the cilium length regulation, but its role in the cilium structural organization is not known (reviewed in (Ludington et al., 2015)). However, in the *Drosophila* sperm and some organisms such as *Plasmodium*, cilia form in the cytoplasm without IFT (Briggs et al., 2004; Han et al., 2003; Sarpal et al., 2003). These motile cilia are structurally normal suggesting that IFT is not needed for the structural organization of ciliary compartments. Moreover, IFT is not needed for the formation of centrioles and basal bodies, which also have structurally distinct longitudinal compartments. Our work shows that cilia length mutants defective in IFT have well-organized distal segments (see chapter 2). Therefore, although IFT is essential for cilia length regulation and the assembly of cilia that form at the plasma membrane, it is not important for the regulation of the distal segment geometry.

The cilium length is also influenced by microtubule depolymerization that contributes to what is known as the cilium disassembly pathway. Depolymerization of the axoneme is mediated through the activity of kinesin-13 (Dawson et al., 2007; Piao et al., 2009; Vasudevan et al., 2015), kinesin-8 (Niwa et al., 2012; Wang et al., 2016), Kif-7 (He et al., 2014), and NRK2/CNK2 kinases (Hilton et al., 2013; Wloga et al., 2006). It appears that some of these factors act by depolymerizing the plus or distal ends of axonemal microtubules. When some of these proteins are lost, the axonemes become much longer.

In contrast to the well-documented role of +TIPs in the regulation of cytoplasmic microtubule plus-end dynamics, very little is known about the regulation of microtubule end dynamics in axonemal microtubules. Only three +TIP proteins are known to be present in cilia, namely Kif7 (Endoh-Yamagami et al., 2009; He et al., 2014), EB1 (Pedersen et al., 2003) and FAP256/CEP104 (Satish Tammana et al., 2013). Loss of Kif7 in mice leads to elongated cilia with a possibly disorganized distal segment (He et al., 2014). EB1 tracks the plus-ends of axonemal microtubules (Harris et al., 2016; Pedersen et al., 2003). However, it remains to be tested if it creates a +TIP network at the ends of axonemal microtubules similar to its function in cytoplasmic microtubules. FAP256/CEP104 a TOG domain protein, is known to interact with EB1 in cell extracts (Jiang et al., 2012; Rezabkova et al., 2016) and thus it is likely to localize to the tip of cilia through EB1. Loss of FAP256/CEP104 disrupts cilium structure at the tip; however, its exact effect on the axoneme is not known (Satish Tammana et al., 2013). My work shows that FAP256 promotes assembly of a subset of axonemal microtubules (A-tubules) (chapter 2).

Activation of signaling pathways: Certain activated signaling molecules are enriched in the distal segment of primary and sensory cilia. For example, in the presence of an agonist, the GPCR SSTR3 accumulates at the ciliary distal segment likely through interaction with Kif7 (Ye et al., 2018). Activation of Hh signaling pathway leads to accumulation of Gli and Sufu in the distal segment (Haycraft et al., 2005). Cilia defects that lead to mislocalization or reduction in the level of Gli transcription factors affect Hh signaling and vertebrate development (reviewed in (Reiter and Leroux, 2017)). It remains to be explored how the unique architecture of the distal segment supports sensory functions.

In motile cilia the distal segment can be further divided into the A-tubule region containing outer singlets and the CP and the CP region containing only CP extensions (Figure 1). Even though the motility-associated proteins are restricted in the middle segment, central microtubules terminate distal to the A-tubule and are linked to the ciliary membrane (Dentler, 1980; Miller et al., 1990; Sale and Satir, 1977). The minus ends of the CP microtubules are not anchored and thus the link of plus ends to the membrane may restrict the central pair movement. The length of the CP region varies in different species but its function is not known. For example, the single motile cilium of *Micromonas* has a CP region that accounts for 80% of the total length (Omoto and Witman, 1981), whereas the CP region in *Tetrahymena* that uses ~500 cilia for locomotion is 8% of the total cilium length. Perhaps the length of the CP correlates with the amount of force produced to power locomotion.

Ciliary capping structures

Intriguingly, the plus-ends of complete microtubules, namely the A-tubules and CP, are capped by distinct structures while no caps where detected at the ends of B-tubules. The ends of A-tubules carry the elongated distal filaments (DFs) and the central microtubules have the larger spherical central microtubule cap (CMC) (Dentler, 1980; Dentler and Rosenbaum, 1977; Sale and Satir, 1977). The ciliary caps are present in diverse cilia in both protists and animals, though their structure varies in different species and cell types (reviewed in (Fisch and Dupuis-Williams, 2011)). The ciliary caps were first described over 30 years ago, but their composition and function remain enigmatic. Sentan, a small calcium-binding protein, is the only protein known to localize near the structures linking the A-tubules to the ciliary membrane in mouse tracheal cells

(Kubo et al., 2008). However, the function of Sentan has not yet been studied and this protein type is limited to vertebrate species.

The caps in the ciliate *Tetrahymena,* the model organism used in this study, are among the best described. The DFs are thin long filaments with their proximal side inserted in the A-tubule lumen and the distal side linked to the plasma membrane (Dentler, 1980). The CMC is a larger and more elaborate structure that links the CP ends to the membrane. Two plates link a bead structure to the plus-ends of both CP microtubules and thin projections link the bead to the membrane. The CMC and distal end of CP are covered by a helical filament that is thought to stabilize the cap on the microtubule (Dentler, 1980, 1984). The spherical bead may allow the CP to rotate and twist around itself, a property that is believed to be important for cilia bend propagation (Fisch and Dupuis-Williams, 2011). The caps are present during cilia assembly as well as during cilia resorption (Dentler and Rosenbaum, 1977; Portman et al., 1987). Surprisingly, the CMC is believed to block tubulin addition to the plus-end of central microtubules raising the question of how tubulin exchange is taking place *in vivo* in the presence of caps (Dentler and Rosenbaum, 1977; Johnson and Rosenbaum, 1992).

Axonemal Microtubules

Axonemal microtubules are perhaps the most complex group of microtubules that work coordinately to assemble and support the function of cilia. In addition to differences in the number of protofilaments that make up the CP, the A-,B- and C-tubule and presence of distinct caps at their plus ends, axonemal tubulin carries unique post-translational modifications (PTMs) that may have co-evolved with cilia.

PTMs generate the tubulin code that is read by MAPs and locally regulates the microtubule-based functions (Verhey and Gaertig, 2007). Detyrosination, polyglutamylation and polyglycylation are modifications of the carboxy-terminal tubulin tails (CTTs) on the surface of the microtubule lattice (reviewed in (Wloga et al., 2017)). Intriguingly, all these PTMs are enriched on B-tubules (Johnson, 1998; Kubo et al., 2010; Lechtreck and Geimer, 2000; Multigner et al., 1996; Suryavanshi et al., 2010) and my work showed that polyglycylation is exclusively present in the middle segment (chapter 2). What confers the specificity of the modifying enzymes (all of which have been identified in recent years (reviewed in (Gadadhar et al., 2017))) for the B-tubule lattice is not known. One possible explanation is that the surface of the A-tubule and CP microtubules is obscured by motility associated proteins preventing the modifying enzymes from acting on these microtubules (Wloga et al., 2017). However, there are rare cases where the CP microtubules are polyglutamylated, including *Drosophila melanogaster* and *Lytechinus pictus* sperm (Hoyle et al., 2008). Polyglutamylation is also asymmetrically distributed among the individual axoneme doublets (Prigent et al., 1996). Thus, the heterogeneity in PTMs exists not only among different tubules in cilia, but also within the same type of a tubule. Tubulin modifications in cilia are surprisingly complex showing the presence of a sophisticated yet unknown mechanism that establishes the tubulin code depending on the tubulin subunit position on a microtubule.

Abnormalities in the levels of PTMs that are enriched on B-tubules affect cilia function. Mutations of glutamic acid residues on the CTT of tubulin, the substrate for polyglycylation and polyglutamylation, are lethal in *Tetrahymena.* Mutant cells divide 2-3 times before they die during which time ultrastructural analysis of cilia showed the presence of severe defects including partial loss of B-tubules (Thazhath et al., 2002; Xia et al., 2000). Loss of enzymes that

glutamylate tubulin in zebrafish results in open B-tubules (Pathak et al., 2011). On the other hand a loss of the deglutamylating enzymes in *C. elegans* causes progressive loss of cilia function likely due to B-tubule instability and loss (O'Hagan et al., 2011). Therefore, alterations in the level of PTMs affect the stability of B-tubules and consequently the cilium structure and function. PTMs also affect the activity of MAPs. For example, glutamylation is essential for inner dynein arm activity (Kubo et al., 2010; Suryavanshi et al., 2010) and it increases the speed and processivity of molecular motors *in vitro* (Sirajuddin et al., 2014).

B-tubules are not associated with any known MAPs (perhaps with exception of the tubulin modifying enzymes), whereas different subsets of MAPs localize to A-tubules and the CP. As mentioned earlier, A-tubules are covered by 96 nm repeat protein complexes and different projection proteins associate with each of the CP microtubules (reviewed in (Loreng and Smith, 2017; Mitchell and Smith, 2009). How MAPs distinguish between different subtypes of complete microtubules (that are made of the same tubulin and have the same 13 protofilament organization) is not known. The luminal space of A and B-tubules is covered with MIPs that are thought to stabilize the doublet structure (Ichikawa et al., 2017). Luminal proteins on A-tubules project across the tubulin lattice (Ichikawa et al., 2017) and this may contribute to the association with 96 nm repeats. Cryo-EM of the luminal surface of CP may provide more information regarding the differences between A-tubules and CP and shed more light into the compartmentalization of MAPs in cilia.

Another fascinating aspect of axonemal microtubules is the difference in their length with CP being longer than A-tubules and A-tubules longer than B-tubules. As discussed earlier, this organization is evolutionarily conserved and therefore likely serves important functions. However, the mechanism that regulates the position of microtubule ends to establish the cilium's

structural compartments is not known. The length of cytoplasmic microtubules *in vivo* depends on tubulin concentration and presence of +TIPs that regulate the plus-end dynamics. In cilia, tubulin concentration is regulated by IFT (Craft et al., 2015), which likely affects all microtubules equally. Only a handful of proteins are known to localize to the tip of cilia. However their effect on the dynamics of microtubule subtypes is not known (He et al., 2014; Kubo et al., 2008; Niwa et al., 2012; Pedersen et al., 2003; Satish Tammana et al., 2013; Vasudevan et al., 2015).

In this study, we used *Tetrahymena thermophila* to explore the function of the distal segment by identifying and studying proteins that localize to the ends of axonemal microtubules. We identified three proteins that regulate the dynamics of a subset of axonemal microtubules and consequently determine the position of axonemal microtubule ends. We show that changes in the dimension of the distal segment correlate with defects in ciliary motility and cilia based sensory functions in both motile cilia of a protist and sensory cilia of an animal (*C. elegans*). Our work provides the first evidence connecting defects in the distal segment organization to Joubert syndrome.

Tetrahymena thermophila as a model system

Tetrahymena thermophila is a unicellular, multiciliated, fresh water organism that has been used as a model system by cell biologists since 1923, when laboratory cultures of *Tetrahymena* were first established (Lwoff, 1923). This unicellular organism has structural and functional complexity comparable to human cells. *Tetrahymena* cells are polarized; they have a "mouth", the oral apparatus, in the anterior end of the cell and two contractile vacuole pores at the posterior that are used for osmoregulation. Before each division, cells create a new posterior

end in the anterior half and a new anterior end in the posterior half. This patterning is used to explore conserved pathways related to cell polarity and pattern formation (Jiang et al., 2017). *Tetrahymena* is used as a model system in many areas of research including gene rearrangement, membrane fusion and vesicle secretion (reviewed in (Ruehle et al., 2016)). *Tetrahymena* as a model system led to the Nobel Prize winning discoveries of ribozymes (Kruger et al., 1982) and telomerase and telomere function (Greider and Blackburn, 1985). Other notable discoveries made using *Tetrahymena* include the discovery of the first motor, dynein (Gibbons and Rowe, 1965), and the discovery of the first histone modifying enzyme and genesis of the "histone code" (Brownell et al., 1996). With its genome annotated and new advances in whole genome sequencing forward genetic screens are now more feasible (Jiang et al., 2017). The inherent homologous recombination of *Tetrahymena* enables genetic manipulations for multiple gene deletions and gene tagging under inducible or native regulatory elements (Dave et al., 2009; Gaertig et al., 2013). *Tetrahymena* is an especially attractive system for studying cilia biology. Each cell is covered by ~500 cilia that are structurally and biochemically similar to animal cilia. The large number of cilia per cell is ideal for biochemical and structural studies of these organelles. *Tetrahymena* cells can be induced to release their cilia and regrow new ones allowing us to study the process of cilia assembly (Gaertig et al., 2013). All cilia of *Tetrahymena* are motile cilia used for locomotion, feeding and cell to cell communication. Thus, using *Tetrahymena* we can study cilia structure, motility and cilia based sensory functions.

References

Afzelius, B.A. (1976). A human syndrome caused by immotile cilia. Science (New York, NY) *193*, 317-319.

Akhmanova, A., and Steinmetz, M.O. (2008). Tracking the ends: a dynamic protein network controls the fate of microtubule tips. Nature reviews Molecular cell biology *9*, 309-322.

Akhmanova, A., and Steinmetz, M.O. (2010). Microtubule +TIPs at a glance. Journal of cell science *123*, 3415-3419.

Al-Bassam, J., and Chang, F. (2011). Regulation of microtubule dynamics by TOG-domain proteins XMAP215/Dis1 and CLASP. Trends in cell biology *21*, 604-614.

Al-Bassam, J., Larsen, N.A., Hyman, A.A., and Harrison, S.C. (2007). Crystal structure of a TOG domain: conserved features of XMAP215/Dis1-family TOG domains and implications for tubulin binding. Structure (London, England : 1993) *15*, 355-362.

Aldaz, H., Rice, L.M., Stearns, T., and Agard, D.A. (2005). Insights into microtubule nucleation from the crystal structure of human gamma-tubulin. Nature *435*, 523-527.

Alushin, G.M., Lander, G.C., Kellogg, E.H., Zhang, R., Baker, D., and Nogales, E. (2014). High-resolution microtubule structures reveal the structural transitions in alphabeta-tubulin upon GTP hydrolysis. Cell *157*, 1117-1129.

Ayaz, P., Munyoki, S., Geyer, E.A., Piedra, F.A., Vu, E.S., Bromberg, R., Otwinowski, Z., Grishin, N.V., Brautigam, C.A., and Rice, L.M. (2014). A tethered delivery mechanism explains the catalytic action of a microtubule polymerase. eLife *3*, e03069.

Ayaz, P., Ye, X., Huddleston, P., Brautigam, C.A., and Rice, L.M. (2012). A TOG:alphabeta-tubulin complex structure reveals conformation-based mechanisms for a microtubule polymerase. Science (New York, NY) *337*, 857-860.

Bower, R., Tritschler, D., Vanderwaal, K., Perrone, C.A., Mueller, J., Fox, L., Sale, W.S., and Porter, M.E. (2013). The N-DRC forms a conserved biochemical complex that maintains outer doublet alignment and limits microtubule sliding in motile axonemes. Molecular biology of the cell *24*, 1134-1152.

Briggs, L.J., Davidge, J.A., Wickstead, B., Ginger, M.L., and Gull, K. (2004). More than one way to build a flagellum: comparative genomics of parasitic protozoa. Current biology : CB *14*, R611-612.

Brokaw, C.J., and Kamiya, R. (1987). Bending patterns of Chlamydomonas flagella: IV. Mutants with defects in inner and outer dynein arms indicate differences in dynein arm function. Cell motility and the cytoskeleton *8*, 68-75.

Brouhard, G.J., Stear, J.H., Noetzel, T.L., Al-Bassam, J., Kinoshita, K., Harrison, S.C., Howard, J., and Hyman, A.A. (2008). XMAP215 is a processive microtubule polymerase. Cell *132*, 79-88.

Brownell, J.E., Zhou, J., Ranalli, T., Kobayashi, R., Edmondson, D.G., Roth, S.Y., and Allis, C.D. (1996). Tetrahymena histone acetyltransferase A: a homolog to yeast Gcn5p linking histone acetylation to gene activation. Cell *84*, 843-851.

Carlier, M.F., and Pantaloni, D. (1981). Kinetic analysis of guanosine 5'-triphosphate hydrolysis associated with tubulin polymerization. Biochemistry *20*, 1918-1924.

Cassimeris, L., Pryer, N.K., and Salmon, E.D. (1988). Real-time observations of microtubule dynamic instability in living cells. The Journal of cell biology *107*, 2223-2231.

Chalfie, M., and Thomson, J.N. (1982). Structural and functional diversity in the neuronal microtubules of Caenorhabditis elegans. The Journal of cell biology *93*, 15-23.

Chang, P., Giddings, T.H., Jr., Winey, M., and Stearns, T. (2003). Epsilon-tubulin is required for centriole duplication and microtubule organization. Nature cell biology *5*, 71-76.

Chang, P., and Stearns, T. (2000). Delta-tubulin and epsilon-tubulin: two new human centrosomal tubulins reveal new aspects of centrosome structure and function. Nature cell biology *2*, 30-35.

Chretien, D., Metoz, F., Verde, F., Karsenti, E., and Wade, R.H. (1992). Lattice defects in microtubules: protofilament numbers vary within individual microtubules. The Journal of cell biology *117*, 1031-1040.

Cole, D.G., Diener Dr Fau - Himelblau, A.L., Himelblau Al Fau - Beech, P.L., Beech Pl Fau - Fuster, J.C., Fuster Jc Fau - Rosenbaum, J.L., and Rosenbaum, J.L. (1998). Chlamydomonas kinesin-II-dependent intraflagellar transport (IFT): IFT particles contain proteins required for ciliary assembly in Caenorhabditis elegans sensory neurons.

Comartin, D., Gupta, G.D., Fussner, E., Coyaud, E., Hasegan, M., Archinti, M., Cheung, S.W., Pinchev, D., Lawo, S., Raught, B*., et al.* (2013). CEP120 and SPICE1 cooperate with CPAP in centriole elongation. Current biology : CB *23*, 1360-1366.

Craft, J.M., Harris, J.A., Hyman, S., Kner, P., and Lechtreck, K.F. (2015). Tubulin transport by IFT is upregulated during ciliary growth by a cilium-autonomous mechanism. The Journal of cell biology *208*, 223-237.

Cullen, C.F., Deak, P., Glover, D.M., and Ohkura, H. (1999). mini spindles: A gene encoding a conserved microtubule-associated protein required for the integrity of the mitotic spindle in Drosophila. The Journal of cell biology *146*, 1005-1018.

Das, A., Dickinson, D.J., Wood, C.C., Goldstein, B., and Slep, K.C. (2015). Crescerin uses a TOG domain array to regulate microtubules in the primary cilium. Molecular biology of the cell *26*, 4248-4264.

Dave, D., Wloga, D., and Gaertig, J. (2009). Manipulating ciliary protein-encoding genes in Tetrahymena thermophila. Methods in cell biology *93*, 1-20.

Dawson, S.C., Sagolla, M.S., Mancuso, J.J., Woessner, D.J., House, S.A., Fritz-Laylin, L., and Cande, W.Z. (2007). Kinesin-13 regulates flagellar, interphase, and mitotic microtubule dynamics in Giardia intestinalis. Eukaryotic cell *6*, 2354-2364.

de Forges, H., Pilon, A., Cantaloube, I., Pallandre, A., Haghiri-Gosnet, A.M., Perez, F., and Pous, C. (2016). Localized Mechanical Stress Promotes Microtubule Rescue. Current biology : CB *26*, 3399-3406.

Dentler, W.L. (1980). Structures linking the tips of ciliary and flagellar microtubules to the membrane. Journal of cell science *42*, 207-220.

Dentler, W.L. (1984). Attachment of the cap to the central microtubules of Tetrahymena cilia. Journal of cell science *66*, 167-173.

Dentler, W.L., and Rosenbaum, J.L. (1977). Flagellar elongation and shortening in Chlamydomonas. III. structures attached to the tips of flagellar microtubules and their relationship to the directionality of flagellar microtubule assembly. The Journal of cell biology *74*, 747-759.

Desai, A., and Mitchison, T.J. (1997). Microtubule polymerization dynamics. Annual review of cell and developmental biology *13*, 83-117.

Dimitrov, A., Quesnoit, M., Moutel, S., Cantaloube, I., Pous, C., and Perez, F. (2008). Detection of GTP-tubulin conformation in vivo reveals a role for GTP remnants in microtubule rescues. Science (New York, NY) *322*, 1353-1356.

Dupuis-Williams, P., Fleury-Aubusson, A., de Loubresse, N.G., Geoffroy, H., Vayssie, L., Galvani, A., Espigat, A., and Rossier, J. (2002). Functional role of epsilon-tubulin in the assembly of the centriolar microtubule scaffold. The Journal of cell biology *158*, 1183-1193.

Dutcher, S.K., Morrissette, N.S., Preble, A.M., Rackley, C., and Stanga, J. (2002). Epsilon-tubulin is an essential component of the centriole. Molecular biology of the cell *13*, 3859-3869.

Dutcher, S.K., and Trabuco, E.C. (1998). The UNI3 gene is required for assembly of basal bodies of Chlamydomonas and encodes delta-tubulin, a new member of the tubulin superfamily. Molecular biology of the cell *9*, 1293-1308.

Endoh-Yamagami, S., Evangelista, M., Wilson, D., Wen, X., Theunissen, J.W., Phamluong, K., Davis, M., Scales, S.J., Solloway, M.J., de Sauvage, F.J.*, et al.* (2009). The mammalian Cos2 homolog Kif7 plays an essential role in modulating Hh signal transduction during development. Current biology : CB *19*, 1320-1326.

Euteneuer, U., and McIntosh, J.R. (1980). Polarity of midbody and phragmoplast microtubules. The Journal of cell biology *87*, 509-515.

Fisch, C., and Dupuis-Williams, P. (2011). Ultrastructure of cilia and flagella - back to the future! Biology of the cell / under the auspices of the European Cell Biology Organization *103*, 249-270.

Fox, J.C., Howard, A.E., Currie, J.D., Rogers, S.L., and Slep, K.C. (2014). The XMAP215 family drives microtubule polymerization using a structurally diverse TOG array. Molecular biology of the cell *25*, 2375-2392.

Gadadhar, S., Bodakuntla, S., Natarajan, K., and Janke, C. (2017). The tubulin code at a glance. Journal of cell science *130*, 1347-1353.

Gaertig, J., Wloga, D., Vasudevan, K.K., Guha, M., and Dentler, W. (2013). Discovery and functional evaluation of ciliary proteins in Tetrahymena thermophila. Methods in enzymology *525*, 265-284.

Garcia-Gonzalo, F.R., and Reiter, J.F. (2017). Open Sesame: How Transition Fibers and the Transition Zone Control Ciliary Composition. Cold Spring Harbor perspectives in biology *9*.

Gardner, M.K., Zanic, M., Gell, C., Bormuth, V., and Howard, J. (2011). Depolymerizing kinesins Kip3 and MCAK shape cellular microtubule architecture by differential control of catastrophe. Cell *147*, 1092-1103.

Garreau de Loubresse, N., Ruiz, F., Beisson, J., and Klotz, C. (2001). Role of delta-tubulin and the C-tubule in assembly of Paramecium basal bodies. BMC cell biology *2*, 4.

Gibbons, I.R., and Rowe, A.J. (1965). Dynein: A Protein with Adenosine Triphosphatase Activity from Cilia. Science (New York, NY) *149*, 424-426.

Goodwin, S.S., and Vale, R.D. (2010). Patronin regulates the microtubule network by protecting microtubule minus ends. Cell *143*, 263-274.

Goshima, G., Wollman, R., Stuurman, N., Scholey, J.M., and Vale, R.D. (2005). Length control of the metaphase spindle. Current biology : CB *15*, 1979-1988.

Greider, C.W., and Blackburn, E.H. (1985). Identification of a specific telomere terminal transferase activity in Tetrahymena extracts. Cell *43*, 405-413.

Guichard, P., Hamel, V., and Gonczy, P. (2018). The Rise of the Cartwheel: Seeding the Centriole Organelle. BioEssays : news and reviews in molecular, cellular and developmental biology.

Han, Y.G., Kwok, B.H., and Kernan, M.J. (2003). Intraflagellar transport is required in Drosophila to differentiate sensory cilia but not sperm. Current biology : CB *13*, 1679-1686.

Harris, J.A., Liu, Y., Yang, P., Kner, P., and Lechtreck, K.F. (2016). Single-particle imaging reveals intraflagellar transport-independent transport and accumulation of EB1 in Chlamydomonas flagella. Molecular biology of the cell *27*, 295-307.

Haycraft, C.J., Banizs, B., Aydin-Son, Y., Zhang, Q., Michaud, E.J., and Yoder, B.K. (2005). Gli2 and Gli3 localize to cilia and require the intraflagellar transport protein polaris for processing and function. PLoS genetics *1*, e53.

He, M., Subramanian, R., Bangs, F., Omelchenko, T., Liem, K.F., Jr., Kapoor, T.M., and Anderson, K.V. (2014). The kinesin-4 protein Kif7 regulates mammalian Hedgehog signalling by organizing the cilium tip compartment. Nature cell biology *16*, 663-672.

Hilton, L.K., Gunawardane, K., Kim, J.W., Schwarz, M.C., and Quarmby, L.M. (2013). The kinases LF4 and CNK2 control ciliary length by feedback regulation of assembly and disassembly rates. Current biology : CB *23*, 2208-2214.

Hoyle, H.D., Turner, F.R., and Raff, E.C. (2008). Axoneme-dependent tubulin modifications in singlet microtubules of the Drosophila sperm tail. Cell motility and the cytoskeleton *65*, 295-313.

Huang, B., Piperno, G., and Luck, D.J. (1979). Paralyzed flagella mutants of Chlamydomonas reinhardtii. Defective for axonemal doublet microtubule arms. The Journal of biological chemistry *254*, 3091-3099.

Huangfu, D., Liu, A., Rakeman, A.S., Murcia, N.S., Niswander, L., and Anderson, K.V. (2003). Hedgehog signalling in the mouse requires intraflagellar transport proteins. Nature *426*, 83-87.

Hyman, A.A., Salser, S., Drechsel, D.N., Unwin, N., and Mitchison, T.J. (1992). Role of GTP hydrolysis in microtubule dynamics: information from a slowly hydrolyzable analogue, GMPCPP. Molecular biology of the cell *3*, 1155-1167.

Ichikawa, M., Liu, D., Kastritis, P.L., Basu, K., Hsu, T.C., Yang, S., and Bui, K.H. (2017). Subnanometre-resolution structure of the doublet microtubule reveals new classes of microtubule-associated proteins. Nature communications *8*, 15035.

Inglis, P.N., Ou, G., Leroux, M.R., and Scholey, J.M. (2007). The sensory cilia of Caenorhabditis elegans. WormBook : the online review of C elegans biology, 1-22.

Ishikawa, T. (2013). 3D structure of eukaryotic flagella/cilia by cryo-electron tomography. Biophysics *9*, 141-148.

Jana, S.C., Bettencourt-Dias, M., Durand, B., and Megraw, T.L. (2016). Drosophila melanogaster as a model for basal body research. Cilia *5*, 22.

Jiang, K., Toedt, G., Montenegro Gouveia, S., Davey, N.E., Hua, S., van der Vaart, B., Grigoriev, I., Larsen, J., Pedersen, L.B., Bezstarosti, K.*, et al.* (2012). A Proteome-wide screen for mammalian SxIP motif-containing microtubule plus-end tracking proteins. Current biology : CB *22*, 1800-1807.

Jiang, Y.Y., Maier, W., Baumeister, R., Minevich, G., Joachimiak, E., Ruan, Z., Kannan, N., Clarke, D., Frankel, J., and Gaertig, J. (2017). The Hippo Pathway Maintains the Equatorial Division Plane in the Ciliate Tetrahymena. Genetics *206*, 873-888.

Johnson, K.A. (1998). The axonemal microtubules of the Chlamydomonas flagellum differ in tubulin isoform content. Journal of cell science *111 (Pt 3)*, 313-320.

Kamiya, R. (2002). Functional diversity of axonemal dyneins as studied in Chlamydomonas mutants. Int Rev Cytol *219*, 115-155.

Kochanski, R.S., and Borisy, G.G. (1990). Mode of centriole duplication and distribution. The Journal of cell biology *110*, 1599-1605.

Kollman, J.M., Merdes, A., Mourey, L., and Agard, D.A. (2011). Microtubule nucleation by gamma-tubulin complexes. Nature reviews Molecular cell biology *12*, 709-721.

Kozminski, K.G., Beech, P.L., and Rosenbaum, J.L. (1995). The Chlamydomonas kinesin-like protein FLA10 is involved in motility associated with the flagellar membrane. The Journal of cell biology *131*, 1517-1527.

Kozminski, K.G., Johnson, K.A., Forscher, P., and Rosenbaum, J.L. (1993). A motility in the eukaryotic flagellum unrelated to flagellar beating. Proceedings of the National Academy of Sciences of the United States of America *90*, 5519-5523.

Kruger, K., Grabowski, P.J., Zaug, A.J., Sands, J., Gottschling, D.E., and Cech, T.R. (1982). Self-splicing RNA: autoexcision and autocyclization of the ribosomal RNA intervening sequence of Tetrahymena. Cell *31*, 147-157.

Kubo, A., Yuba-Kubo, A., Tsukita, S., Tsukita, S., and Amagai, M. (2008). Sentan: a novel specific component of the apical structure of vertebrate motile cilia. Molecular biology of the cell *19*, 5338-5346.

Kubo, T., Yanagisawa, H.A., Yagi, T., Hirono, M., and Kamiya, R. (2010). Tubulin polyglutamylation regulates axonemal motility by modulating activities of inner-arm dyneins. Current biology : CB *20*, 441-445.

Leano, J.B., Rogers, S.L., and Slep, K.C. (2013). A cryptic TOG domain with a distinct architecture underlies CLASP-dependent bipolar spindle formation. Structure (London, England : 1993) *21*, 939-950.

Lechtreck, K.F. (2015). IFT-Cargo Interactions and Protein Transport in Cilia. Trends in biochemical sciences *40*, 765-778.

Lechtreck, K.F., and Geimer, S. (2000). Distribution of polyglutamylated tubulin in the flagellar apparatus of green flagellates. Cell motility and the cytoskeleton *47*, 219-235.

Lechtreck, K.F., Gould, T.J., and Witman, G.B. (2013). Flagellar central pair assembly in Chlamydomonas reinhardtii. Cilia *2*, 15.

Lechtreck, K.F., Van De Weghe, J.C., Harris, J.A., and Liu, P. (2017). Protein transport in growing and steady-state cilia. Traffic (Copenhagen, Denmark) *18*, 277-286.

Lewin, R.A. (1954). Mutants of Chlamydomonas moewusii with impaired motility. Journal of general microbiology *11*, 358-363.

Lin, Y.N., Wu, C.T., Lin, Y.C., Hsu, W.B., Tang, C.J., Chang, C.W., and Tang, T.K. (2013). CEP120 interacts with CPAP and positively regulates centriole elongation. The Journal of cell biology *202*, 211-219.

Loreng, T.D., and Smith, E.F. (2017). The Central Apparatus of Cilia and Eukaryotic Flagella. Cold Spring Harbor perspectives in biology *9*.

Ludington, W.B., Ishikawa, H., Serebrenik, Y.V., Ritter, A., Hernandez-Lopez, R.A., Gunzenhauser, J., Kannegaard, E., and Marshall, W.F. (2015). A systematic comparison of mathematical models for inherent measurement of ciliary length: how a cell can measure length and volume. Biophys J *108*, 1361-1379.

Lwoff, A. (1923). Sur la nutrition des infusoires. C R Acad Sci *176*, 928-930.

Mahjoub, M.R., Xie, Z., and Stearns, T. (2010). Cep120 is asymmetrically localized to the daughter centriole and is essential for centriole assembly. The Journal of cell biology *191*, 331-346.

Marshall, W.F., and Rosenbaum, J.L. (2001). Intraflagellar transport balances continuous turnover of outer doublet microtubules: implications for flagellar length control. The Journal of cell biology *155*, 405-414.

Maurer, S.P., Fourniol, F.J., Bohner, G., Moores, C.A., and Surrey, T. (2012). EBs recognize a nucleotide-dependent structural cap at growing microtubule ends. Cell *149*, 371-382.

McEwen, D.P., Jenkins, P.M., and Martens, J.R. (2008). Olfactory cilia: our direct neuronal connection to the external world. Current topics in developmental biology *85*, 333-370.

Mesland, D.A., Hoffman, J.L., Caligor, E., and Goodenough, U.W. (1980). Flagellar tip activation stimulated by membrane adhesions in Chlamydomonas gametes. The Journal of cell biology *84*, 599-617.

Miller, J.M., Wang, W., Balczon, R., and Dentler, W.L. (1990). Ciliary microtubule capping structures contain a mammalian kinetochore antigen. The Journal of cell biology *110*, 703-714.

Mitchell, D.R., and Smith, B. (2009). Analysis of the central pair microtubule complex in Chlamydomonas reinhardtii. Methods in cell biology *92*, 197-213.

Mitchison, H.M., and Valente, E.M. (2017). Motile and non-motile cilia in human pathology: from function to phenotypes. The Journal of pathology *241*, 294-309.

Mitchison, T., and Kirschner, M. (1984). Dynamic instability of microtubule growth. Nature *312*, 237-242.

Mukhopadhyay, S., Lu, Y., Qin, H., Lanjuin, A., Shaham, S., and Sengupta, P. (2007). Distinct IFT mechanisms contribute to the generation of ciliary structural diversity in C. elegans. The EMBO journal *26*, 2966-2980.

Multigner, L., Pignot-Paintrand, I., Saoudi, Y., Job, D., Plessmann, U., Rudiger, M., and Weber, K. (1996). The A and B tubules of the outer doublets of sea urchin sperm axonemes are composed of different tubulin variants. Biochemistry *35*, 10862-10871.

Nakata, T., Niwa, S., Okada, Y., Perez, F., and Hirokawa, N. (2011). Preferential binding of a kinesin-1 motor to GTP-tubulin-rich microtubules underlies polarized vesicle transport. The Journal of cell biology *194*, 245-255.

Nakazawa, Y., Ariyoshi, T., Noga, A., Kamiya, R., and Hirono, M. (2014). Space-dependent formation of central pair microtubules and their interactions with radial spokes. PLoS One *9*, e110513.

Nechipurenko, I.V., Berciu, C., Sengupta, P., and Nicastro, D. (2017). Centriolar remodeling underlies basal body maturation during ciliogenesis in Caenorhabditis elegans. eLife *6*.

Nicastro, D., Schwartz, C., Pierson, J., Gaudette, R., Porter, M.E., and McIntosh, J.R. (2006). The molecular architecture of axonemes revealed by cryoelectron tomography. Science (New York, NY) *313*, 944-948.

Nicholson, W.V., Lee, M., Downing, K.H., and Nogales, E. (1999). Cryo-electron microscopy of GDP-tubulin rings. Cell biochemistry and biophysics *31*, 175-183.

Niwa, S., Nakajima, K., Miki, H., Minato, Y., Wang, D., and Hirokawa, N. (2012). KIF19A is a microtubule-depolymerizing kinesin for ciliary length control. Developmental cell *23*, 1167-1175.

Nonaka, S., Tanaka, Y., Okada, Y., Takeda, S., Harada, A., Kanai, Y., Kido, M., and Hirokawa, N. (1998). Randomization of left-right asymmetry due to loss of nodal cilia generating leftward flow of extraembryonic fluid in mice lacking KIF3B motor protein. Cell *95*, 829-837.

O'Hagan, R., Piasecki, B.P., Silva, M., Phirke, P., Nguyen, K.C., Hall, D.H., Swoboda, P., and Barr, M.M. (2011). The tubulin deglutamylase CCPP-1 regulates the function and stability of sensory cilia in C. elegans. Current biology : CB *21*, 1685-1694.

O'Toole, E.T., Giddings, T.H., McIntosh, J.R., and Dutcher, S.K. (2003). Three-dimensional organization of basal bodies from wild-type and delta-tubulin deletion strains of Chlamydomonas reinhardtii. Molecular biology of the cell *14*, 2999-3012.

Oda, T., Yanagisawa, H., Yagi, T., and Kikkawa, M. (2014). Mechanosignaling between central apparatus and radial spokes controls axonemal dynein activity. The Journal of cell biology *204*, 807-819.

Ogawa, T., Nitta, R., Okada, Y., and Hirokawa, N. (2004). A common mechanism for microtubule destabilizers-M type kinesins stabilize curling of the protofilament using the class-specific neck and loops. Cell *116*, 591-602.

Omoto, C.K., and Witman, G.B. (1981). Functionally significant central-pair rotation in a primitive eukaryotic flagellum. Nature *290*, 708-710.

Paintrand, M., Moudjou, M., Delacroix, H., and Bornens, M. (1992). Centrosome organization and centriole architecture: their sensitivity to divalent cations. Journal of structural biology *108*, 107-128.

Pathak, N., Austin, C.A., and Drummond, I.A. (2011). Tubulin tyrosine ligase-like genes ttll3 and ttll6 maintain zebrafish cilia structure and motility. The Journal of biological chemistry *286*, 11685-11695.

Pazour, G.J., Dickert, B.L., Vucica, Y., Seeley, E.S., Rosenbaum, J.L., Witman, G.B., and Cole, D.G. (2000). Chlamydomonas IFT88 and its mouse homologue, polycystic kidney disease gene tg737, are required for assembly of cilia and flagella. The Journal of cell biology *151*, 709-718.

Pazour, G.J., Dickert, B.L., and Witman, G.B. (1999). The DHC1b (DHC2) isoform of cytoplasmic dynein is required for flagellar assembly. The Journal of cell biology *144*, 473-481.

Pazour, G.J., Wilkerson, C.G., and Witman, G.B. (1998). A dynein light chain is essential for the retrograde particle movement of intraflagellar transport (IFT). The Journal of cell biology *141*, 979-992.

Pedersen, L.B., Geimer, S., Sloboda, R.D., and Rosenbaum, J.L. (2003). The Microtubule plus end-tracking protein EB1 is localized to the flagellar tip and basal bodies in Chlamydomonas reinhardtii. Current biology : CB *13*, 1969-1974.

Pedersen, L.B., Miller, M.S., Geimer, S., Leitch, J.M., Rosenbaum, J.L., and Cole, D.G. (2005). Chlamydomonas IFT172 is encoded by FLA11, interacts with CrEB1, and regulates IFT at the flagellar tip. Current biology : CB *15*, 262-266.

Piao, T., Luo, M., Wang, L., Guo, Y., Li, D., Li, P., Snell, W.J., and Pan, J. (2009). A microtubule depolymerizing kinesin functions during both flagellar disassembly and flagellar assembly in Chlamydomonas. Proceedings of the National Academy of Sciences of the United States of America *106*, 4713-4718.

Piasecki, B.P., and Silflow, C.D. (2009). The UNI1 and UNI2 genes function in the transition of triplet to doublet microtubules between the centriole and cilium in Chlamydomonas. Molecular biology of the cell *20*, 368-378.

Portman, R.W., LeCluyse, E.L., and Dentler, W.L. (1987). Development of microtubule capping structures in ciliated epithelial cells. Journal of cell science *87 (Pt 1)*, 85-94.

Prigent, Y., Kann, M.L., Lach-Gar, H., Pechart, I., and Fouquet, J.P. (1996). Glutamylated tubulin as a marker of microtubule heterogeneity in the human sperm flagellum. Mol Hum Reprod *2*, 573-581.

Randall, J., Warr, J.R., Hopkins, J.M., and McVittie, A. (1964). A Single-Gene Mutation of Chlamydomonas Reinhardii Affecting Motility: A Genetic and Electron Microscope Study. Nature *203*, 912-914.

Reese, T.S. (1965). Olfactory Cilia in the Frog. The Journal of cell biology *25*, 209-230.

Reiter, J.F., and Leroux, M.R. (2017). Genes and molecular pathways underpinning ciliopathies. Nature reviews Molecular cell biology *18*, 533-547.

Rezabkova, L., Kraatz, S.H., Akhmanova, A., Steinmetz, M.O., and Kammerer, R.A. (2016). Biophysical and Structural Characterization of the Centriolar Protein Cep104 Interaction Network. The Journal of biological chemistry *291*, 18496-18504.

Rice, L.M., Montabana, E.A., and Agard, D.A. (2008). The lattice as allosteric effector: structural studies of alphabeta- and gamma-tubulin clarify the role of GTP in microtubule assembly. Proceedings of the National Academy of Sciences of the United States of America *105*, 5378-5383.

Rodionov, V.I., and Borisy, G.G. (1997). Microtubule treadmilling in vivo. Science (New York, NY) *275*, 215-218.

Roostalu, J., and Surrey, T. (2017). Microtubule nucleation: beyond the template. Nature reviews Molecular cell biology *18*, 702-710.

Rothwell, S.W., Grasser, W.A., and Murphy, D.B. (1985). Direct observation of microtubule treadmilling by electron microscopy. The Journal of cell biology *101*, 1637-1642.

Ruehle, M.D., Orias, E., and Pearson, C.G. (2016). Tetrahymena as a Unicellular Model Eukaryote: Genetic and Genomic Tools. Genetics *203*, 649-665.

Sale, W.S., and Satir, P. (1977). The termination of the central microtubules from the cilia of Tetrahymena pyriformis. Cell biology international reports *1*, 45-49.

Sarpal, R., Todi, S.V., Sivan-Loukianova, E., Shirolikar, S., Subramanian, N., Raff, E.C., Erickson, J.W., Ray, K., and Eberl, D.F. (2003). Drosophila KAP interacts with the kinesin II motor subunit KLP64D to assemble chordotonal sensory cilia, but not sperm tails. Current biology : CB *13*, 1687-1696.

Satir, P. (1968). Studies on cilia. 3. Further studies on the cilium tip and a "sliding filament" model of ciliary motility. The Journal of cell biology *39*, 77-94.

Satish Tammana, T.V., Tammana, D., Diener, D.R., and Rosenbaum, J. (2013). Centrosomal protein CEP104 (Chlamydomonas FAP256) moves to the ciliary tip during ciliary assembly. Journal of cell science *126*, 5018-5029.

Saxton, W.M., and McIntosh, J.R. (1987). Interzone microtubule behavior in late anaphase and telophase spindles. The Journal of cell biology *105*, 875-886.

Seetapun, D., Castle, B.T., McIntyre, A.J., Tran, P.T., and Odde, D.J. (2012). Estimating the microtubule GTP cap size in vivo. Current biology : CB *22*, 1681-1687.

Sharma, A., Gerard, S.F., Olieric, N., and Steinmetz, M.O. (2018). Cep120 promotes microtubule formation through a unique tubulin binding C2 domain. Journal of structural biology.

Shipley, K., Hekmat-Nejad, M., Turner, J., Moores, C., Anderson, R., Milligan, R., Sakowicz, R., and Fletterick, R. (2004). Structure of a kinesin microtubule depolymerization machine. The EMBO journal *23*, 1422-1432.

Signor, D., Wedaman, K.P., Orozco, J.T., Dwyer, N.D., Bargmann, C.I., Rose, L.S., and Scholey, J.M. (1999). Role of a class DHC1b dynein in retrograde transport of IFT motors and

IFT raft particles along cilia, but not dendrites, in chemosensory neurons of living Caenorhabditis elegans. The Journal of cell biology *147*, 519-530.

Sirajuddin, M., Rice, L.M., and Vale, R.D. (2014). Regulation of microtubule motors by tubulin isotypes and post-translational modifications. Nature cell biology *16*, 335-344.

Srour, M., Hamdan, F.F., McKnight, D., Davis, E., Mandel, H., Schwartzentruber, J., Martin, B., Patry, L., Nassif, C., Dionne-Laporte, A.*, et al.* (2015). Joubert Syndrome in French Canadians and Identification of Mutations in CEP104. Am J Hum Genet *97*, 744-753.

Stepanek, L., and Pigino, G. (2016). Microtubule doublets are double-track railways for intraflagellar transport trains. Science (New York, NY) *352*, 721-724.

Summers, K.E., and Gibbons, I.R. (1971). Adenosine triphosphate-induced sliding of tubules in trypsin-treated flagella of sea-urchin sperm. Proceedings of the National Academy of Sciences of the United States of America *68*, 3092-3096.

Suryavanshi, S., Edde, B., Fox, L.A., Guerrero, S., Hard, R., Hennessey, T., Kabi, A., Malison, D., Pennock, D., Sale, W.S.*, et al.* (2010). Tubulin glutamylation regulates ciliary motility by altering inner dynein arm activity. Current biology : CB *20*, 435-440.

Thazhath, R., Liu, C., and Gaertig, J. (2002). Polyglycylation domain of beta-tubulin maintains axonemal architecture and affects cytokinesis in Tetrahymena. Nature cell biology *4*, 256-259.

Thoma, C.R., Matov, A., Gutbrodt, K.L., Hoerner, C.R., Smole, Z., Krek, W., and Danuser, G. (2010). Quantitative image analysis identifies pVHL as a key regulator of microtubule dynamic instability. The Journal of cell biology *190*, 991-1003.

Tilney, L.G., Bryan, J., Bush, D.J., Fujiwara, K., Mooseker, M.S., Murphy, D.B., and Snyder, D.H. (1973). Microtubules: evidence for 13 protofilaments. The Journal of cell biology *59*, 267-275.

Tran, P.T., Walker, R.A., and Salmon, E.D. (1997). A metastable intermediate state of microtubule dynamic instability that differs significantly between plus and minus ends. The Journal of cell biology *138*, 105-117.

Tropini, C., Roth, E.A., Zanic, M., Gardner, M.K., and Howard, J. (2012). Islands containing slowly hydrolyzable GTP analogs promote microtubule rescues. PLoS One *7*, e30103.

Turk, E., Wills, A.A., Kwon, T., Sedzinski, J., Wallingford, J.B., and Stearns, T. (2015). Zeta-Tubulin Is a Member of a Conserved Tubulin Module and Is a Component of the Centriolar Basal Foot in Multiciliated Cells. Current biology : CB *25*, 2177-2183.

Van De Weghe, J.C., Rusterholz, T.D.S., Latour, B., Grout, M.E., Aldinger, K.A., Shaheen, R., Dempsey, J.C., Maddirevula, S., Cheng, Y.H., Phelps, I.G.*, et al.* (2017). Mutations in ARMC9, which Encodes a Basal Body Protein, Cause Joubert Syndrome in Humans and Ciliopathy Phenotypes in Zebrafish. Am J Hum Genet *101*, 23-36.

van Haren, J., Charafeddine, R.A., Ettinger, A., Wang, H., Hahn, K.M., and Wittmann, T. (2018). Local control of intracellular microtubule dynamics by EB1 photodissociation. Nature cell biology *20*, 252-261.

Vasudevan, K.K., Jiang, Y.Y., Lechtreck, K.F., Kushida, Y., Alford, L.M., Sale, W.S., Hennessey, T., and Gaertig, J. (2015). Kinesin-13 regulates the quantity and quality of tubulin inside cilia. Molecular biology of the cell *26*, 478-494.

Verhey, K.J., and Gaertig, J. (2007). The tubulin code. Cell cycle (Georgetown, Tex) *6*, 2152-2160.

Viswanadha, R., Hunter, E.L., Yamamoto, R., Wirschell, M., Alford, L.M., Dutcher, S.K., and Sale, W.S. (2014). The ciliary inner dynein arm, I1 dynein, is assembled in the cytoplasm and transported by IFT before axonemal docking. Cytoskeleton *71*, 573-586.

Voter, W.A., O'Brien, E.T., and Erickson, H.P. (1991). Dilution-induced disassembly of microtubules: relation to dynamic instability and the GTP cap. Cell motility and the cytoskeleton *18*, 55-62.

Wade, R.H., Chretien, D., and Job, D. (1990). Characterization of microtubule protofilament numbers. How does the surface lattice accommodate? Journal of molecular biology *212*, 775-786.

Walker, R.A., Inoue, S., and Salmon, E.D. (1989). Asymmetric behavior of severed microtubule ends after ultraviolet-microbeam irradiation of individual microtubules in vitro. The Journal of cell biology *108*, 931-937.

Walker, R.A., O'Brien, E.T., Pryer, N.K., Soboeiro, M.F., Voter, W.A., Erickson, H.P., and Salmon, E.D. (1988). Dynamic instability of individual microtubules analyzed by video light microscopy: rate constants and transition frequencies. The Journal of cell biology *107*, 1437-1448.

Walker, R.A., Pryer, N.K., and Salmon, E.D. (1991). Dilution of individual microtubules observed in real time in vitro: evidence that cap size is small and independent of elongation rate. The Journal of cell biology *114*, 73-81.

Wang, D., Nitta, R., Morikawa, M., Yajima, H., Inoue, S., Shigematsu, H., Kikkawa, M., and Hirokawa, N. (2016). Motility and microtubule depolymerization mechanisms of the Kinesin-8 motor, KIF19A. eLife *5*.

Wang, J.T., Kong, D., Hoerner, C.R., Loncarek, J., and Stearns, T. (2017). Centriole triplet microtubules are required for stable centriole formation and inheritance in human cells. eLife *6*.

Weisenberg, R.C., Deery, W.J., and Dickinson, P.J. (1976). Tubulin-nucleotide interactions during the polymerization and depolymerization of microtubules. Biochemistry *15*, 4248-4254.

Widlund, P.O., Stear, J.H., Pozniakovsky, A., Zanic, M., Reber, S., Brouhard, G.J., Hyman, A.A., and Howard, J. (2011). XMAP215 polymerase activity is built by combining multiple

tubulin-binding TOG domains and a basic lattice-binding region. Proceedings of the National Academy of Sciences of the United States of America *108*, 2741-2746.

Williams, C.L., McIntyre, J.C., Norris, S.R., Jenkins, P.M., Zhang, L., Pei, Q., Verhey, K., and Martens, J.R. (2014). Direct evidence for BBSome-associated intraflagellar transport reveals distinct properties of native mammalian cilia. Nature communications *5*, 5813.

Wloga, D., Camba, A., Rogowski, K., Manning, G., Jerka-Dziadosz, M., and Gaertig, J. (2006). Members of the NIMA-related kinase family promote disassembly of cilia by multiple mechanisms. Molecular biology of the cell *17*, 2799-2810.

Wloga, D., Joachimiak, E., Louka, P., and Gaertig, J. (2017). Posttranslational Modifications of Tubulin and Cilia. Cold Spring Harbor perspectives in biology *9*.

Xia, L., Hai, B., Gao, Y., Burnette, D., Thazhath, R., Duan, J., Bre, M.H., Levilliers, N., Gorovsky, M.A., and Gaertig, J. (2000). Polyglycylation of tubulin is essential and affects cell motility and division in Tetrahymena thermophila. The Journal of cell biology *149*, 1097-1106.

Ye, F., Nager, A.R., and Nachury, M.V. (2018). BBSome trains remove activated GPCRs from cilia by enabling passage through the transition zone. The Journal of cell biology.

Zanic, M., Stear, J.H., Hyman, A.A., and Howard, J. (2009). EB1 recognizes the nucleotide state of tubulin in the microtubule lattice. PLoS One *4*, e7585.

Zhang, R., Alushin, G.M., Brown, A., and Nogales, E. (2015). Mechanistic Origin of Microtubule Dynamic Instability and Its Modulation by EB Proteins. Cell *162*, 849-859.

CHAPTER 2

PROTEINS THAT CONTROL THE GEOMETRY OF CILAIRY ENDS[1]

[1]Louka, P. Vasudevan, K. Guha, M. Joachimiak, E. Wloga, D. Tomasi, R. Baroud, C. Dupuis-Williams, P. Galati, F. Pearson, C. Rice, L. Moresco, J. Yates III, J. Jiang, Y. Lechtreck, K. Dentler, W. and Gaertig, J. Submitted to *Journal of Cell Biology*, 20.4.18.

Abstract

Cilia, essential motile and sensory organelles, have several compartments: the basal body, transition zone, and the middle and distal axoneme segments. The distal segment accommodates key functions including cilium assembly and sensory activities. While the middle segment contains doublet microtubules (incomplete B-tubules fused to complete A-tubules), the distal segment contains only A-tubule extensions, and its existence requires coordination of microtubule length at the nanometer scale. We show that three conserved proteins, two of which are mutated in the ciliopathy, Joubert syndrome, determine the geometry of the distal segment by controlling the positions of specific microtubule ends. FAP256/CEP104 promotes A-tubule elongation. CHE-12/crescerin and ARMC9 act as positive and negative regulators of B-tubule length, respectively. Defects in the distal segment are associated with motile and sensory deficiencies of cilia. Our observations suggest that abnormalities in distal segment geometry cause a subset of Joubert syndrome cases.

Introduction

Microtubules function in groups, such as networks and bundles, within which the positions and dimensions of individual filaments have to be precisely coordinated in space and time. Cilia are conserved and important organelles that are built around a sophisticated bundle of microtubules, the axoneme. With few exceptions, motile cilia have a 9+2 axoneme containing nine outer and two central pair (CP) microtubules, while most sensory cilia have a 9+0 axoneme that lacks the CP. The ring of nine outer microtubules is the unifying feature of both motile and sensory cilia. For most of their length, the outer microtubules have a doublet conformation and are composed

of a “complete” A-tubule and an “incomplete” B-tubule that is fused to the A-tubule wall. Importantly, in all known cilia, the B-tubules are shorter than the A-tubules; this difference in length creates the distal ciliary segment made only of singlet microtubules (Fawcett and Porter, 1954) (Fig. 1A).

The distal segment is the site of axoneme assembly, and a preexisting A-tubule may function as a template for the B-tubule assembly (Ichikawa et al., 2017). In addition the distal segment may play a role in signaling because it tends to be relatively long in sensory cilia. In the olfactory cilia that are particularly long (~60 μm), the distal segment represents 80% of total cilium length and this compartment is enriched in signaling proteins that mediate olfaction (reviewed in (McEwen et al., 2008)). Important signaling proteins, including the Hedgehog (Hh) pathway components: Gli and Sufu, and the GPCR SSTR3, accumulate in the distal segment of the primary cilium in activated cells (Haycraft et al., 2005; Ye et al., 2018).

While the distal segment is a universal feature of all cilia, its molecular activities and the mechanism of biogenesis are not clear. In *C. elegans*, a subtype of the intraflagellar transport (IFT) motor, OSM-3 kinesin-II, is required for building the distal segment in cilia of amphid neurons (Mukhopadhyay et al., 2007; Perkins et al., 1986; Snow et al., 2004). However, OSM-3 is not needed for the distal segment assembly in other cilia of *C. elegans* (Mukhopadhyay et al., 2007) and in the olfactory cilia of mouse and zebrafish (Jiang et al., 2015a; Williams et al., 2014). Thus, unknown mechanisms individualize the lengths of microtubules across the axoneme, to establish its functional compartments, including the distal segment. Here we use the multiciliated protist *Tetrahymena,* to explore the biogenesis and function of the ciliary distal

segment. We found that three conserved ciliary proteins, FAP256/CEP104, CHE-12/crescerin and ARMC9, control the positions of the ends of specific axonemal microtubules, and consequently determine the geometry of the distal segment. Since mutations in two proteins studied here (ARMC9 and FAP256) cause Joubert syndrome, our observations suggest that abnormalities in the distal segment cause at least a subset of this ciliopathy, possibly by interfering with signaling molecules that operate near the ciliary tip.

Materials and Methods

Tetrahymena strains, culture and genome editing

Tetrahymena thermophila strains were grown at 30^{o}C in either SPP (Gorovsky, 1973) or MEPP (Orias and Rasmussen, 1976) media with antibiotics (Dave et al., 2009). CU428 strain was used as a wild type (*Tetrahymena* Stock Center, Cornell University, Ithaca, NY). Homologous DNA recombination was used to add sequences encoding epitope tags (GFP or 2xmNeonGreen-6xMyc-BirA*) (Shaner et al., 2013) to the ends of predicted open reading frames (ORFs) in the native loci or complete ORFs were inserted into *BTU1* locus for overexpression under the cadmium-inducible *MTT1* promoter (Dave et al., 2009; Gaertig et al., 2013). Micronuclear strains with disruptions of *FAP256A (TTHERM_00079820)*, *FAP256B (TTHERM_00584800)*, *CHE12A (TTHERM_00102840)*, *CHE12B (TTHERM_00193480)*, *ARMC9A (TTHERM_00723450)* and *ARMC9B (TTHERM_0042850)* genes were made by replacing a part of each ORF with *neo4* (Gaertig et al., 1994; Mochizuki, 2008) or *bsr2* (Couvillion and Collins,

2012) cassettes by biolistic transformation (Cassidy-Hanley et al., 1997; Dave et al., 2009). The knockout phenotype-expressing homokaryon strains were produced by mating of heterokaryons (Hai et al., 2000). The losses of the targeted fragments were confirmed by PCR using primers specific to the deleted sequences. The primers used to amplify the homology arms for gene targeting and to confirm the losses of targeted sequences are listed in the Supplemental Table S1.

Microscopic analyses of *Tetrahymena*

Cells were stained by immunofluorescence (Gaertig et al., 2013) using one or more of the following reagents: DAPI (Sigma-Aldrich, 0.5 μg/ml), antibodies directed to: α-tubulin (12G10, 1:30 dilution; Developmental Hybridoma Bank; (Jerka-Dziadosz et al., 2001)), polyglycylation (polyG, 2302 serum, 1:200, (Duan and Gorovsky, 2002)), polyglutamylation (polyE, 2304 serum, 1:100 (Shang et al., 2002)), centrin (20H5, 1:100, (Salisbury et al., 1988)), Myc (9E10, Developmental Hybridoma Bank, undiluted), or GFP (abcam6556, rabbit polyclonal, 1:100). The secondary antibodies conjugated to either FITC or Cy3 (Zymed Laboratories) were used at 1:250. Fluorescence imaging was performed either on a Zeiss LSM 710 confocal microscope, or Zeiss ELYRA S1 super-resolution structured illumination (SR-SIM) microscope, or total internal reflection microscope (TIRFM) as described (Jiang et al., 2015b). The density of cilia on the cell surface was calculated as the average number of cilia per μm on a confocal slice containing the widest cell circumference. To induce cilia regeneration, cells were deciliated as described (Calzone and Gorovsky, 1982).

The transmission electron microscopy TEM was done as described (Urbanska et al., 2015). To negatively stain isolated cilia, *Tetrahymena* cells were deciliated with dibucaine or low pH (Gaertig et al., 2013), and cilia were purified and negatively stained with 1% or 1.5% uranyl acetate (Suprenant and Dentler, 1988). To visualize the ciliary caps, purified cilia were extracted with 1% NP-40 in 50 mM Tris pH 7.4, 3 mM $MgSO_4$, 0.1 mM EGTA, 0.25 M sucrose, 1 mM DTT for 10 min, centrifuged, suspended in 50 mM PIPES pH 7.10, 3 mM $MgSO_4$, 0.1 mM EGTA, 0.25 M sucrose, 1 mM DTT, and 1 mM phenylmethylsulfonyl fluoride, and observed in a FEI Technai F20XT electron microscope. To measure the length of distal segment, whole cells were fixed with 2% paraformaldehyde in PHEM buffer (Gaertig et al., 2013), placed on formvar-coated grids and stained with 1.5% uranyl acetate. Images were obtained on a JEOL JEM1011 electron microscope and analyzed using NIH ImageJ (Schneider et al., 2012).

Phenotypic studies of *Tetrahymena*

The cell swimming velocity was determined using 30 sec video recordings of growing cells (1 ml at 1 x 10^4 cells/ml in a well of a 24-well plate,) using an AxioCam HS camera mounted on a Nikon Observer.A1 microscope with a 10x lens. The velocities were calculated using AxioVision software (Zeiss). The ciliary beat frequency was measured in *Tetrahymena* cells swimming in a microfluidic channel on an inverted microscope (Nikon TE2000) with a 60x objective lens. Videos were recorded using a Photron 1024PCI camera at 2000 fps. The observation area was a section of a long straight channel (33 μm in height and 50 μm in width). The cells were injected into the inlet of the channel using a controllable pressure source (Fluigent), after which the pressures between the inlet and outlet were equilibrated, to prevent

residual flow. The calculation of ciliary beat frequency was done as described (Funfak et al., 2014) (see Fig. S8). Briefly, a Matlab code (https://sites.google.com/site/crtoolbox/) was used to track the moving cell and align a series of consecutive images at the same position relative to the internal cell body markers (as if the cell was not moving). This "composite cell" was digitally unwrapped, to produce a rectangular segment around the cell's contour (Fig. S8A-B). A space-time mapping was used to produce a kymograph of ciliary beating activity across the cell surface (Fig. S8C-E). The ciliary beat frequency was obtained by auto-correlation on the signal in each column of the kymograph and searching for the time of the first peak.

Proximity biotinylation and mass spectrometry in *Tetrahymena cilia*

A codon optimized (for *T. thermophila*) BirA* coding region (Roux et al., 2012) was added to the 5' end of an ORF encoding NRK2-(K35R)-GFP expressed under *MTT1* promoter in the *BTU1* locus (Wloga et al., 2006). The expression of BirA*-NRK2-(K35R)-GFP and GFP-BirA* (also under *MTT1* promoter) was induced with 2.5 μg/μl $CdCl_2$ for 2 hr in the presence of 50 μM biotin. Cilia were isolated after low pH shock deciliation (Gaertig et al., 2013) and solubilized in lysis buffer (50 mM Tris pH 7.4, 500 mM NaCl, 0.4% SDS, 1 mM DTT) for 1 hr at room temperature. The lysate was frozen in liquid nitrogen and used for direct detection of biotinylated peptides by mass spectrometry (Schiapparelli et al., 2014). For every protein hit, a normalized spectral associate factor (NSAF) was calculated. mRNA expression patterns were analyzed using Co-regulation Data Harvester (Tsypin and Turkewitz, 2017).

Imaging of ciliary compartments in *C. elegans*

C. elegans strains were cultured as described (Brenner, 1974). Worms carrying the *che-12(mn389)* allele and integrated single-copy transgenes expressing KAP::GFP and OSM-3::mCherry were derived from a cross between strains *SP1620* (obtained from CGC) (Bacaj et al., 2008) and *EJP42* (Prevo et al., 2015). The PCR primers used for genotyping the *che-12(mn389) allele* are listed in Table S1. For measurements of the middle and distal segments of phasmid cilia, adult worms were paralyzed using 0.5 mM levamisole (Sigma-Aldrich) and imaged on a Zeiss Axioskop microscope with a Hamamatsu ORCA-ER camera operated using Openlab 4.0.2 software (Agilent Technologies). The images were analyzed using NIH ImageJ (Schneider et al., 2012).

Results

FAP256/CEP104, CHE-12/crescerin and ARMC9, are enriched near the boundaries of distal segment

FAP256/CEP104 is a TOG domain protein (Al-Jassar et al., 2017; Jiang et al., 2012; Rezabkova et al., 2016) that in *Chlamydomonas reinhardtii* is enriched near the ends of ciliary microtubules (Satish Tammana et al., 2013). Most TOG domains bind to tubulin in a "curved conformation" that is characteristic of the unpolymerized state and also transiently present at the growing microtubule plus end (Ayaz et al., 2014; Ayaz et al., 2012). *Tetrahymena thermophila* has two genes that encode FAP256/CEP104 homologs: *TTHERM_00079820* (*FAP256A*) and

TTHERM_00584800 (*FAP256B*). The most compatible known structure to the predicted single TOG-domains of FAP256A and FAP256B is TOG1 of yeast STU2 (based on the i-TASSER searches with no template specificity). A superimposition of the amino acid sequences of the TOG domains of either FAP256A or FAP256B on the 3D structure of TOG1 of STU2 revealed conservation of key amino acids at the interphases with curved tubulin (Fig. S1 and data not shown for FAP256B). Thus, FAP256A and B have TOG domains that may be compatible with the plus ends of microtubules including those present near the tips of cilia. Indeed, FAP256A-GFP was highly enriched near the tips of steady-state cilia (Fig. 1B, 1F, 1G, arrows, Movie S1), assembling cilia (Fig. 1C-E) and unciliated basal bodies (Fig 1G, green arrowheads). At the tips of most cilia of either live (using TIRFM) or fixed (using SR-SIM) cells, there were two dots of tagged FAP256A (Fig. 1B, F, G, Movie S1 note that the two dots move together indicating they are on the same cilium). We used immunogold TEM to localize FAP256A-GFP with higher resolution. At the ultrastructural level, the distal segment of a 9+2 cilium can be divided into two subcompartments: 1) the "A-tubule region" that contains the A-tubule (singlet) extensions and a portion of the CP, and 2) the more terminal "CP region" that contains only the central microtubules (Fig. 1A). On the electron micrographs of cilia or axonemes, we used the cross-section at which the cilium diameter first decreases due to the termination of B-tubules, as the proximal boundary of distal segment (blue arrow in Fig. 1A, 1H, see also Fig. 5E). The proximal boundary of the CP region was designated at the level where the axoneme becomes maximally thin (green arrow in Fig. 1A, 5E). The A-tubule region is located between these two landmarks (blue bracket in Fig. 1A, 5E). In cilia of cells expressing FAP256A-GFP, there was a strong enrichment of gold particles near the end of the CP and a weaker (but above background) signal scattered along the A-tubule region (Fig. 1H-I). We used an independent approach, based on

tubulin post-translational modifications (PTMs), to localize FAP256A-GFP. PolyG and polyE are antibodies that recognize PTMs that are specific to the B-tubules (Kubo et al., 2010; Lechtreck and Geimer, 2000; Suryavanshi et al., 2010). Immunogold TEM confirmed that the specific polyG signal ends within the B-tubule termination zone (Fig S2A-B). In SR-SIM, there is a gap of 840 +/- 200 nm between the proximal FAP256A-6xMyc dot and the distal end of either polyG (Fig. S3A, asterisks) or polyE (Fig. 1G, asterisk) signals, which places the proximal dot within the A-tubule region. Based on the frequency of TEM cross sections with different numbers of A-tubule profiles (Fig. S2C-K), we estimated that the termination points of the individual A-tubules spread over ~540 nm (Fig. S2L). Among the nine A-tubule ends, six of them terminate within ~100 nm from each other, which is below the resolution of SR-SIM. While the positions of the three remaining A-tubule ends are far enough from others to be resolved in principle, in practice the signal intensity of tagged FAP256A associated with a single microtubule end could be below the sensitivity of SR-SIM. Thus, the proximal FAP256A-GFP dot seen in SR-SIM likely corresponds to the cluster of several A-tubule ends. The two FAP256A-GFP dots (in SR-SIM) are separated by 590 +/- 90 nm, which corresponds to the length of the CP region (582+/- 234 nm, Fig. 5L). Thus, based on the combination of SR-SIM and TEM imaging, FAP256A-GFP colocalizes with the ends of complete microtubules: CP and A-tubules. We did not detect tagged FAP256B even after its overexpression.

CHE-12/crescerin is the only other known TOG domain protein in cilia (Das et al., 2015). *Tetrahymena* has two genes encoding CHE-12/crescerin: *TTHERM_00102840* (*CHE12A*) and *TTHERM_00193480* (*CHE12B*). In growing cells, CHE12A-GFP was enriched near the tips of shorter, assembling cilia and very close to the end of polyG, the marker of B-tubule ends (Fig.

2A arrow). In cells regenerating cilia after deciliation, most ciliary tips were positive for CHE12A-GFP (Fig. 2B and S4). CHE12B-6xMyc was detected near the tips of full-length cilia, also close to the end of either polyG or polyE signals (Fig. 2C, Fig. S3B). There was also a weak punctate presence of CHE12B along the length of mature cilia (Fig. 2C, S3B arrowheads) and TIRFM revealed that a subset of CHE12B-mNeonGreen particles diffused along the cilium length (Fig 2D-E, movie S2). The observed enrichment close the ends of polyG and polyE signals and the presence of TOG domains is consistent with targeting of CHE-12 to the ends of B-tubules.

We considered ARMC9A (TTHERM_00723450) as a potential distal segment protein, based on 1) its proximity to an overproduced NRK2 kinase, a known distal segment marker ((Wloga et al., 2006) and Fig. S5) revealed by BioID (Supplemental Table S2), and 2) the similarity of its mRNA expression pattern to that of FAP256A (Tsypin and Turkewitz, 2017; Xiong et al., 2013). ARMC9A and its paralog ARMC9B (TTHERM_00420850) are orthologs of the mammalian ARMC9, whose mutations cause Joubert syndrome and mental retardation (Kar et al., 2018; Van De Weghe et al., 2017). In most cilia, SR-SIM revealed an enrichment of ARMC9A-6xMyc very close to the end of polyG (Fig. 3A). In isolated cilia with partially splayed axonemes, there were multiple foci of ARMC9A-6xMyc corresponding to the ends of splayed microtubules (Fig. 3B). Immunogold TEM detection of ARMC9A-6xMyc revealed an enrichment of gold particles near the B-tubule termination zone (Fig. 3C-D). ARMC9B-6xMyc localized to the unciliated basal bodies (Fig. 3E arrowhead) and the tips of growing cilia (Fig. 3E, arrow shows assembling oral cilia). In SR-SIM, the GFP-FAP256A and ARMC9A-mNeon-6xMyc signals were separated by ~700 nm, consistent with their localizations to different compartments of distal segment (Fig.

3F). To conclude, we identified ARMC9 as a new distal segment protein that, like CHE-12, localizes near the ends of B-tubules.

FAP256, CHE12 and ARMC9 are important for cilia-based functions

To study the functions of FAP256, CHE12 and ARMC9, we created gene disruption strains (both paralogs were targeted for each of the three proteins). *Tetrahymena* cells use cilia for swimming, feeding by phagocytosis, and pair formation at the onset of conjugation. All three knockout strains swam slowly; the cells lacking ARMC9 (ARMC9-KO) were most affected and swam at the rate of 50% of the wild type (Fig. 4A, Movies S2-S6). The loss of ARMC9 also greatly reduced the rates of cell multiplication and phagocytosis (Fig. 4B, Fig. S6E). In the MEPP culture medium that bypasses the requirement for phagocytosis (Orias and Rasmussen, 1976), the ARMC9-KO cells grew as well as the wild type (Fig. S6F). Thus, the slow multiplication of ARMC9-KO is largely due to its reduced feeding rate. Introduction of GFP-ARMC9B transgene into ARMC9-KO cells partially rescued the phagocytosis defect (Fig. 4B).

The FAP256-KO and CHE12-KO cells had ~30% fewer, while the ARMC9-KO cells had 37% more cilia than the wild type, respectively (Fig. S6A-D, G). Because wild-type cells assemble more cilia in starvation ((Nelsen, 1978; Nelsen and Debault, 1978) and data not shown), the increased ciliation of ARMC9-KO cells could be a response to starvation caused by their slow phagocytosis. The length of cilia was normal in the FAP256-KO, reduced (by 16%) in CHE12-KO, and increased (by 14%) in ARMC9-KO cells (Fig. 5K). The ciliary beat frequency was reduced (by 15%) in FAP256-KO and unaffected in CHE12-KO cells (Fig. 4D). The ciliary

waveform appeared unaffected in the FAP256-KO and CHE-12-KO cells (Movie S4-S5). The ARMC9-KO cells showed the most severe defects in ciliary motility; many cilia (particularly those in the posterior cell region) were paralyzed or appeared to have incomplete power strokes (Fig. 4F, Movie S6). The non-paralyzed ARMC9-KO cilia beat at the frequency of 43% of the wild type (Fig. 4D).

Starved and sexually mature *Tetrahymena* cells form pairs to initiate conjugation. FAP256-KO cells almost completely failed to form pairs with wild-type cells of a complementary mating type and this defect was partially rescued by introduction of GFP-FAP256A transgene (Fig. 4C). Cilia-less mutants do not form pairs (data not shown). The FAP256-KO cells have fewer cilia that beat slowly. However, other mutants that have even fewer cilia (CHE12-KO) or swim more slowly (ARMC9-KO), formed pairs efficiently (Fig. 4C). Thus, the pair formation defect in the FAP256-KO cells does not appear to be a downstream effect of weak ciliary motility but rather reflects a deficiency in the cell-to-cell signaling that occurs during pair formation (Love and Rotheim, 1984; Wolfe et al., 1979). To explore this phenotype further, we examined the expression of mating type proteins; MTA and MTB (Cervantes et al., 2013). In the starved wild-type cells having the same mating type as FAP256-KO cells (mt IV), MTA4-GFP was detected in the anterior cell cortex, whereas MTB4-GFP was enriched near the anterior cell pole and at the tips of some anterior cilia (Fig. S7A, C). However, MTA4-GFP and MTB4-GFP were not detectable in the FAP256-KO cells (Fig. S7B, D). The levels MTA and MTB mRNAs were normal in FAP256-KO cells (data not shown). Thus, the loss of FAP256 reduces either the overall levels or the cortical presence of mating type proteins and this is sufficient to explain the deficiency in pair formation. To summarize, losses of three distal segment-enriched proteins in

Tetrahymena affects parameters of cilia (number, length and beat parameters) and reduce cilia-dependent functions. While ARMC9 is particularly important for ciliary motility, FAP256/CEP104 may have a role in the cilia-dependent cell-cell signaling associated with conjugation.

FAP256 is important for capping of central pair microtubules and ARMC9 affects the middle segment organization.

The ends of all complete axonemal microtubules (A-tubules and CP) carry ciliary caps, structures which plug the microtubule ends and connect them to the ciliary plasma membrane (reviewed in (Fisch and Dupuis-Williams, 2011)). The A-tubule ends have carrot-like distal filaments (DFs) and the central microtubules end with the large central microtubule cap (CMC) (Fig. 1A) (Dentler, 1980; Dentler and Rosenbaum, 1977; Sale and Satir, 1977). Based on the negatively-stained isolated axonemes, in the wild type, the CMC was present at the end of almost every CP examined (Fig. 5A). While the CMC frequency was not affected by the loss of either CHE12 or ARMC9, it was missing in most (92%, n = 76) of FAP256-KO axonemes (Fig. 5B-D). Because CMC is present in some of FAP256-KO axonemes, FAP256 is not required for the CMC presence, but it may contribute to its assembly or stability. Although the DFs are more difficult to discern, one or more were visible at the ends of A-tubules in most of wild-type and mutant axonemes (Fig. 5A-D).

A TEM analysis of thin sections of FAP256-KO and CHE12-KO cilia did not reveal abnormalities in the middle (doublet) segment (data not shown). A small fraction (7%, n=62) of ARMC9-KO cilia cross-sections lacked (partially or completely) outer dynein arms (Fig. S9A-B). Other infrequent abnormalities in ARMC9-KO included doublet microtubules that were broken or appeared to have split subfibers (Fig. S9C-H).

FAP256, CHE12 and ARMC9 control the geometry of distal segment

Based on their localizations near the ends of axonemal microtubules, the three proteins studied here may affect the positions of microtubule ends and thus influence the distal segment dimensions. TEM cross-sections through the transition area between the middle and distal segment contain both singlet and doublet microtubules. Among these cross-sections, there was a reproducible pattern in both the wild-type and mutant cilia. Namely, the B-tubules terminated at multiple positions (spread over ~126 nm), the singlet microtubules lacked radial spokes and dynein arms, and the cilium diameter was reduced when at least five doublets already transitioned into singlets (Fig. S10). Thus, in the negatively stained whole cilia, we used the level at which the cilium first decreases in diameter (when examined from the base to tip) as the proximal boundary of distal segment in all genetic backgrounds (blue arrow Fig. 5E). The loss of FAP256 did not affect cilium length (Fig. 5K) but caused a significant reduction in the length of distal segment (by ~248 nm), by shortening both the A-tubule region (by ~ 95 nm) and the CP region (by ~ 142 nm) (Fig. 5F, L). A part of the effect on the CP region is the loss of the CMC bead that is ~100 nm in size (Sale and Satir, 1977). While the entire cilium length did not change significantly, a shortening of distal segment by 248 nm would fall within the standard

deviation of the wild-type total length value. Likely, in the absence of FAP256, both the distal segment and the entire cilium shorten by ~250 nm. Remarkably, overexpression of GFP-FAP256A shortened the CP region (by ~23%) without affecting the total length of distal segment (Fig. 6A-B, D), which is consistent with elongation of A-tubules. In many cilia of cells overproducing GFP-FAP256A, the ends of A-tubules were positioned immediately below the CMC (Fig. 6A-B). Taking the loss- and gain-of-function data together, FAP256 elongates the A-tubules, and stabilizes the CMC. Surprisingly, in the cell body, overexpressed GFP-FAP256A formed long tubulin-free fibers consistent with its oligomerization at high concentration (Fig. S11, see Discussion).

In the absence of CHE12, the entire cilium was shorter by ~1.1 μm (16%) (Fig. 5K). Remarkably, the distal segment, and within it the A-tubule and CP regions, were ~530 nm, ~366 nm and ~146 nm longer, respectively (Fig. 5G, L). These changes are consistent with shortening of all microtubules, with the B-tubules being relatively more affected. Taken together with the localization near the B-tubule ends, CHE-12 most likely promotes the elongation of B-tubules. Possibly the shortening of complete microtubules (A-tubules and CP, and consequently the entire cilium) is secondary to the shortening of B-tubules (see below).

We took advantage of an available CHE-12 loss-of-function allele in *C. elegans*, *che-12(mn389),* to test whether CHE-12 promotes the B-tubule elongation in animal sensory cilia. Based on the use of KAP::GFP and OSM-3::mCherry, the markers of the middle and distal segment, respectively (Prevo et al., 2015), the loss of CHE-12 led to a 50% reduction in total length of phasmid cilia, as observed earlier (Bacaj et al., 2008). Remarkably, both the distal segment and

middle segment length were shorter by 45% and 56%, respectively (Fig. 7). The shortening of the distal segment is consistent with earlier observations done by TEM (Bacaj et al., 2008; Das et al., 2015). In addition we revealed a role of of CHE-12 in the B-tubule elongation in *C. elegans*, which based on the *Tetrahymena* studies could be the primary effect. To conclude, the B-tubule elongation activity of CHE-12 is conserved between motile protist and sensory animal cilia.

In the ARMC9-KO strain of *Tetrahymena,* cilia were longer by ~0.93 μm (14%) (Fig. 5K). However, the entire distal segment and the A-tubule region were reduced by ~200 nm and ~185 nm, respectively, whereas the CP region was not affected (Fig. 5H, L). Thus, in the ARMC9-KO cilia, the CP and A-tubules were proportionally longer, whereas the B-tubules were excessively long in relation to the A-tubules. An introduction of GFP-ARMC9B into ARMC9-KO cells rescued the abnormal geometry of distal segment (Fig. 5L). Strikingly, overexpression of GFP-ARMC9B (in the ARMC9-KO background) made the distal segment longer (by ~30%), indicating that ARMC9 shortens the B-tubules (Fig. 6C, E-G).

CHE-12 and ARMC9 affect both the geometry of distal segment and the overall cilium length (consistently in opposite ways; see the summary of *Tetrahymena* knockout phenotypes in Table S3), opening a possibility that the distal segment defects are secondary to the cilium length defects. To explore the relationship between cilium and distal segment length, we examined a *Tetrahymena* strain lacking LF4A (TTHERM_00058800), an ortholog of cilium length regulators, LF4/MOK kinases (Berman et al., 2003). While the LF4A-KO cilia are 30% longer (YJ and JG, unpublished data), the dimensions of distal segment were normal (Fig. 5J, L). This is consistent with the LF4A loss causing lengthening of all axonemal microtubules by the same

distance (and a lack of scaling). This argues that the defects observed in the ARMC9 and CHE-12 mutants are not secondary to abnormal cilium length.

Because ARMC9 and CHE12 have a negative and positive effect on the B-tubule length, respectively, we disrupted both gene families to test for interactions. The ARMC9_CHE12-KO double knockout cells grew and fed as poorly as the single knockout ARMC9-KO (data not shown and Fig. 4B). However, the length of ARMC9_CHE12-KO cilia was normal (Fig. 5K). This additive effect is consistent with ARMC9 and CHE12 influencing cilium length via two competing pathways. In other aspects the ARMC9-KO phenotype masked the CHE-12-KO phenotype, including the multiplication and phagocytosis rates. Furthermore, the distal segment and A-tubule region were 305 nm and 141 nm shorter than the wild type, respectively, and similar to the values of ARMC9-KO (Fig. 5H-I, L). Thus, ARMC9 likely does not promote the B-tubule shortening through inhibition of CHE-12. The ARMC9_CHE12-KO cilia are functionally severely deficient while have a normal overall length. This further argues that the disturbed organization of the distal segment, likely its contraction caused by the relative B-tubule lengthening, is the cause of ciliary functional defects in the absence of ARMC9 and CHE-12.

Discussion

Sizing mechanisms must operate not only at the whole cell and organelle level but also inside organelles, including those built around microtubules, such as cilia. Despite the discovery of multiple factors that promote either microtubule assembly or disassembly (Akhmanova and

Steinmetz, 2015; Bowne-Anderson et al., 2015), how the sizes of microtubules are coordinated within an organelle remains unknown. The ciliary distal segment offers a rare opportunity to address the mechanism of sizing of microtubules within a functional group. We show that three conserved proteins are enriched either at the distal (FAP256/CEP104) or proximal (CHE-12 and ARMC9) boundary of ciliary distal segment, and regulate its dimensions by controlling the lengths of specific microtubule types. While FAP256 acts on the ends of complete microtubules (A-tubules) and promotes their elongation, CHE-12 and ARMC9 act on the ends of B-tubules and mediate their elongation and shortening, respectively (Fig. 6H). Thus the distal segment geometry involves differential regulation of the ends of complete and incomplete microtubules. FAP256/CEP104 and CHE-12/crescerin likely act by promoting addition of tubulin subunits to the ends of microtubules, an activity that is already well documented for another TOG domain plus end-tracking protein, XMAP215/DIS1/STU2 that elongates cytoplasmic and mitotic microtubules (Ayaz et al., 2014; Ayaz et al., 2012; Brouhard et al., 2008; Fox et al., 2014; Widlund et al., 2011).

FAP256/CEP104 and CHE12/crescerin are likely to be directly targeted to the plus ends of either complete (A-tubules) or incomplete (B-tubules) axonemal microtubules, respectively. The lattices of A- and B-tubules have distinct protofilament curvatures (Ichikawa et al., 2017). In the case of CHE-12/crescerin (Das et al., 2015), the relative positions of its multiple tubulin-binding TOG domains may confer the preferential docking onto the microtubule lattice with the B-tubule curvature. While FAP256/CEP104 has only a single TOG domain, our observations open a possibility that FAP256 oligomerizes on the microtubule surface, in analogy to the mitotic plus end-tracking proteins, NDC80 and Dam1 (Alushin et al., 2010; Westermann et al., 2005). An

oligomerization of FAP256/CEP104 may confer its preferential recognition of the ends of complete microtubules (A-tubules and CP), and promote its persistence on the microtubule surface to allow it to remain at the tips of growing, steady-state and disassembling cilia (Satish Tammana et al., 2013).

CHE-12 and ARMC9 compete to regulate the B-tubule length. ARMC9 may be a signaling molecule (Van De Weghe et al., 2017) that either activates a microtubule end depolymerizer or inhibits a polymerization factor (that based on our data is different from CHE-12). Neither ARMC9 nor CHE-12 are absolutely required for the generation of a recessed microtubule end, but rather act as fine regulators whose activities control the exact positions of the microtubule ends.

It is intriguing that the losses of CHE-12 and ARMC9 also affect overall cilium length in a manner consistent with their effects on B-tubules (in the case of CHE-12 we documented this correlation in *Tetrahymena* and C. *elegans*). Since CHE12 and ARMC9 act on the ends of B-tubules, they are unlikely to directly regulate cilium length, as this parameter is defined by the length of the CP (or A-tubules in 9+0 cilia). It seems more likely that the effects of CHE-12 and ARMC9 on cilium length are secondary due to the changes in the B-tubules. Within the middle segment, the B-tubules are the main if not exclusive track for the anterograde intraflagellar transport (Stepanek and Pigino, 2016) an activity that delivers the building blocks needed for cilium assembly. Thus, the length of B-tubules could be rate-limiting for cilium assembly.

The distal segment lacks motility-associated protein complexes including dynein arms and radial spokes. Thus, it is unexpected that cilia in *Tetrahymena* cells lacking either FAP256/CEP104 or ARMC9 are deficient in ciliary motility. In *Tetrahymena*, in the absence of FAP256, most of the ends of central microtubules lack the CMC. Our observations are consistent with the abnormally blunt ciliary tips reported in the *Chlamydomonas* mutant lacking FAP256 (Satish Tammana et al., 2013). Possibly, in addition to its role in promoting complete microtubule elongation, FAP256 acts as a linker to reinforce the external portion of the CMC at the microtubule end. The spherical shape of the CMC bead may facilitate the twisting of the central pair (Fisch and Dupuis-Williams, 2011) and this may be important for the waveform bend propagation (Mitchell, 2003; Omoto et al., 1999; Omoto and Kung, 1979, 1980). Surprisingly the ciliary beat frequency and waveform are not affected in the CHE-12 knockout cilia despite their shorter middle segment and the corresponding reduction in the number of dynein arms. In contrast, cilia lacking ARMC9 have a longer force-producing middle segment but display severe defects in the beat frequency and waveform. The altered geometry of the distal segment could affect ciliary motility either through changes in the physical properties of the distal portions of microtubules or by disturbing the regulatory proteins (see below) that may selectively recognize the singlet microtubules. Additionally, infrequent structural defects in the middle segment of ARMC9-KO cilia (including fewer dynein arms) could reflect axoneme assembly errors that may reduce ciliary motility.

A growing body of evidence links the tips of sensory primary cilia to essential signaling during mammalian development. Defects in the Hh signaling are associated with a failure of Hh signaling molecules, Gli and Sufu, to concentrate at the ciliary tip (Haycraft et al., 2005; Liem et

al., 2009; Tukachinsky et al., 2010). Intriguingly, the length of distal segment is dynamic; in *Chlamydomonas,* the distal segment is relatively short in vegetative cells and elongates during mating, and this event correlates with ciliary accumulation of molecules involved in cell-cell adhesion (Mesland et al., 1980). We show that a loss of FAP256 in *Tetrahymena* decreases pair formation, a process that involves cell-cell communication (Love and Rotheim, 1984; Wolfe et al., 1979). In humans, mutations in FAP256 and ARMC9 cause Joubert syndrome (Srour et al., 2015; Van De Weghe et al., 2017), a ciliopathy with mostly neurological defects. None of the Joubert syndrome proteins are directly associated with ciliary motility, suggesting that defects in the sensory primary cilia cause the disease. The Joubert syndrome proteins described to date localize to either the basal body, transition zone or notably to the ciliary tip (Shaheen et al., 2016). Here we link two Joubert syndrome proteins, FAP256 and ARMC9, to the ends of specific axonemal microtubules within the distal segment. Additional ciliary tip proteins whose mutations causes Joubert syndrome are KIF7 (Dafinger et al., 2011; He et al., 2014) and KIAA0556 (Sanders et al., 2015). Interestingly, a loss of KIA0566 in *C. elegans* produces longer cilia with fewer A-tubules and occasionally doublet microtubules at the position normally occupied by the distal segment (Sanders et al., 2015), a partial phenocopy of the loss of ARMC9 described here. Thus, mutations in ciliary tip proteins may cause Joubert syndrome by changing the geometry of the distal segment.

Acknowledgements

The research reported in this publication was supported by the National Institutes of Health including grants: R01GM089912 and 1021RR194369 (to JG), R01GM110413 (to KL),

P41GM103533 (to JJM and JRY), R01GM099820 (to CGP) and R01GM098543 (to LMR). PL was supported by a predoctoral fellowship 16PRE27480028 from the American Heart Association. JG was also supported by intramural grants from the Office of Vice-President for Research and the Department of Cellular Biology at the University of Georgia. RT and CB were funded by the European Research Council (ERC) grant 278248 Multicell. DW was funded by the National Science Centre 2014/14/M/NZ3/00511 (Harmonia 6) grant. We thank Mary Ard (Georgia Electron Microscopy facility at UGA) for assistance with electron microscopy and Muthugapatti K. Kandasamy (Biomedical Microscopy Core facility at UGA) for assistance with fluorescence microscopy. We thank Joseph Frankel (University of Iowa) for critical reading of the manuscript. We thank the following researchers for providing reagents: Martin A. Gorovsky (University of Rochester) for polyE and polyG antibodies, Joseph Frankel (University of Iowa) for 12G10 antibodies (available from the Developmental Studies Hybridoma Bank, University of Iowa), and Erwin Peterman (VU University of Amsterdam) for *EJP42*. We thank Edward Kipreos for his advise on the construction of *C. elegans* strains. The *che-12(mn389) strain* was obtained from the CGC, which is funded by the NIH Office of Research Infrastructure Programs (P40 OD010440).

Author Contributions

PL, WD and JG conceived the project. PL, KKV and MG constructed and analyzed the *Tetrahymena* mutants. DFG and CGP contributed to the analyses of *Tetrahymena* mutants. PL analyzed the *C. elegans* mutant. PL, EJ, DW and WD performed electron microscopic studies. PL, RT, CNB and PDW evaluated the cilia motility. PL prepared, and JJM and JRY analyzed the BioID samples. PL and LMR performed protein structure predictions. PL, YYJ and KL

performed the TIRFM observations. JG supervised the project. PL and JG wrote the manuscript. All authors discussed and edited the manuscript.

Declaration of Interests

The authors declare no competing interests.

References

Akhmanova, A., and Steinmetz, M.O. (2015). Control of microtubule organization and dynamics: two ends in the limelight. Nature reviews Molecular cell biology *16*, 711-726.

Al-Jassar, C., Andreeva, A., Barnabas, D.D., McLaughlin, S.H., Johnson, C.M., Yu, M., and van Breugel, M. (2017). The Ciliopathy-Associated Cep104 Protein Interacts with Tubulin and Nek1 Kinase. Structure (London, England : 1993) *25*, 146-156.

Alushin, G.M., Ramey, V.H., Pasqualato, S., Ball, D.A., Grigorieff, N., Musacchio, A., and Nogales, E. (2010). The Ndc80 kinetochore complex forms oligomeric arrays along microtubules. Nature *467*, 805-810.

Ayaz, P., Munyoki, S., Geyer, E.A., Piedra, F.A., Vu, E.S., Bromberg, R., Otwinowski, Z., Grishin, N.V., Brautigam, C.A., and Rice, L.M. (2014). A tethered delivery mechanism explains the catalytic action of a microtubule polymerase. eLife *3*, e03069.

Ayaz, P., Ye, X., Huddleston, P., Brautigam, C.A., and Rice, L.M. (2012). A TOG:alphabeta-tubulin complex structure reveals conformation-based mechanisms for a microtubule polymerase. Science (New York, NY) *337*, 857-860.

Bacaj, T., Lu Y Fau - Shaham, S., and Shaham, S. (2008). The conserved proteins CHE-12 and DYF-11 are required for sensory cilium function in Caenorhabditis elegans.

Berman, S.A., Wilson, N.F., Haas, N.A., and Lefebvre, P.A. (2003). A novel MAP kinase regulates flagellar length in Chlamydomonas. Current biology : CB *13*, 1145-1149.

Bowne-Anderson, H., Hibbel, A., and Howard, J. (2015). Regulation of Microtubule Growth and Catastrophe: Unifying Theory and Experiment. Trends in cell biology *25*, 769-779.

Brenner, S. (1974). The genetics of Caenorhabditis elegans. Genetics *77*, 71-94.

Brouhard, G.J., Stear, J.H., Noetzel, T.L., Al-Bassam, J., Kinoshita, K., Harrison, S.C., Howard, J., and Hyman, A.A. (2008). XMAP215 is a processive microtubule polymerase. Cell *132*, 79-88.

Calzone, F.J., and Gorovsky, M.A. (1982). Cilia regeneration in Tetrahymena. A simple reproducible method for producing large numbers of regenerating cells. Exp Cell Res *140*, 471-476.

Cassidy-Hanley, D., Bowen, J., Lee, J.H., Cole, E., VerPlank, L.A., Gaertig, J., Gorovsky, M.A., and Bruns, P.J. (1997). Germline and somatic transformation of mating Tetrahymena thermophila by particle bombardment. Genetics *146*, 135-147.

Cervantes, M.D., Hamilton, E.P., Xiong, J., Lawson, M.J., Yuan, D., Hadjithomas, M., Miao, W., and Orias, E. (2013). Selecting one of several mating types through gene segment joining and deletion in Tetrahymena thermophila. PLoS biology *11*, e1001518.

Couvillion, M.T., and Collins, K. (2012). Biochemical approaches including the design and use of strains expressing epitope-tagged proteins. Methods in cell biology *109*, 347-355.

Dafinger, C., Liebau, M.C., Elsayed, S.M., Hellenbroich, Y., Boltshauser, E., Korenke, G.C., Fabretti, F., Janecke, A.R., Ebermann, I., Nurnberg, G.*, et al.* (2011). Mutations in KIF7 link Joubert syndrome with Sonic Hedgehog signaling and microtubule dynamics. The Journal of clinical investigation *121*, 2662-2667.

Das, A., Dickinson, D.J., Wood, C.C., Goldstein, B., and Slep, K.C. (2015). Crescerin uses a TOG domain array to regulate microtubules in the primary cilium. Molecular biology of the cell *26*, 4248-4264.

Dave, D., Wloga, D., and Gaertig, J. (2009). Manipulating ciliary protein-encoding genes in Tetrahymena thermophila. Methods in cell biology *93*, 1-20.

Dentler, W.L. (1980). Structures linking the tips of ciliary and flagellar microtubules to the membrane. Journal of cell science *42*, 207-220.

Dentler, W.L., and Rosenbaum, J.L. (1977). Flagellar elongation and shortening in Chlamydomonas. III. structures attached to the tips of flagellar microtubules and their relationship to the directionality of flagellar microtubule assembly. The Journal of cell biology *74*, 747-759.

Duan, J., and Gorovsky, M.A. (2002). Both carboxy-terminal tails of alpha- and beta-tubulin are essential, but either one will suffice. Current biology : CB *12*, 313-316.

Fawcett, D.W.a., and Porter, K.R. (1954). A study of the fine structure of ciliated epithelia. J Morphol *94*, 221-281.

Fisch, C., and Dupuis-Williams, P. (2011). Ultrastructure of cilia and flagella - back to the future! Biology of the cell / under the auspices of the European Cell Biology Organization *103*, 249-270.

Fox, J.C., Howard, A.E., Currie, J.D., Rogers, S.L., and Slep, K.C. (2014). The XMAP215 family drives microtubule polymerization using a structurally diverse TOG array. Molecular biology of the cell *25*, 2375-2392.

Funfak, A., Fisch, C., Abdel Motaal, H.T., Diener, J., Combettes, L., Baroud, C.N., and Dupuis-Williams, P. (2014). Paramecium swimming and ciliary beating patterns: a study on four RNA interference mutations. Integrative biology : quantitative biosciences from nano to macro.

Gaertig, J., Gu, L., Hai, B., and Gorovsky, M.A. (1994). High frequency vector-mediated transformation and gene replacement in Tetrahymena. Nucleic acids research *22*, 5391-5398.

Gaertig, J., Wloga, D., Vasudevan, K.K., Guha, M., and Dentler, W. (2013). Discovery and functional evaluation of ciliary proteins in Tetrahymena thermophila. Methods in enzymology *525*, 265-284.

Gorovsky, M.A. (1973). Macro- and micronuclei of Tetrahymena pyriformis: a model system for studying the structure and function of eukaryotic nuclei. J Protozool *20*, 19-25.

Goujon, M., McWilliam, H., Li, W., Valentin, F., Squizzato, S., Paern, J., and Lopez, R. (2010). A new bioinformatics analysis tools framework at EMBL–EBI. Nucleic acids research *38*, W695-W699.

Hai, B., Gaertig, J., and Gorovsky, M.A. (2000). Knockout heterokaryons enable facile mutagenic analysis of essential genes in Tetrahymena. Methods in cell biology *62*, 513-531.

Haycraft, C.J., Banizs, B., Aydin-Son, Y., Zhang, Q., Michaud, E.J., and Yoder, B.K. (2005). Gli2 and Gli3 localize to cilia and require the intraflagellar transport protein polaris for processing and function. PLoS genetics *1*, e53.

He, M., Subramanian, R., Bangs, F., Omelchenko, T., Liem, K.F., Jr., Kapoor, T.M., and Anderson, K.V. (2014). The kinesin-4 protein Kif7 regulates mammalian Hedgehog signalling by organizing the cilium tip compartment. Nature cell biology *16*, 663-672.

Ichikawa, M., Liu, D., Kastritis, P.L., Basu, K., Hsu, T.C., Yang, S., and Bui, K.H. (2017). Subnanometre-resolution structure of the doublet microtubule reveals new classes of microtubule-associated proteins. Nature communications *8*, 15035.

Jerka-Dziadosz, M., Strzyewska-Jowko, I., Wojsa-Lugowska, U., Krawczynska, W., and Krzywicka, A. (2001). The dynamics of filamentous structures in the apical band, oral crescent, fission line and the postoral meridional filament in Tetrahymena thermophila revealed by monoclonal antibody 12G9. Protist *152*, 53-67.

Jiang, K., Toedt, G., Montenegro Gouveia, S., Davey, N.E., Hua, S., van der Vaart, B., Grigoriev, I., Larsen, J., Pedersen, L.B., Bezstarosti, K.*, et al.* (2012). A Proteome-wide screen

for mammalian SxIP motif-containing microtubule plus-end tracking proteins. Current biology : CB *22*, 1800-1807.

Jiang, L., Tam, B.M., Ying, G., Wu, S., Hauswirth, W.W., Frederick, J.M., Moritz, O.L., and Baehr, W. (2015a). Kinesin family 17 (osmotic avoidance abnormal-3) is dispensable for photoreceptor morphology and function. FASEB journal : official publication of the Federation of American Societies for Experimental Biology *29*, 4866-4880.

Jiang, Y.Y., Lechtreck, K., and Gaertig, J. (2015b). Total internal reflection fluorescence microscopy of intraflagellar transport in Tetrahymena thermophila. Methods in cell biology *127*, 445-456.

Kar, A., Phadke, S.R., Das Bhowmik, A., and Dalal, A. (2018). Whole exome sequencing reveals a mutation in ARMC9 as a cause of mental retardation, ptosis, and polydactyly. American journal of medical genetics Part A *176*, 34-40.

Kubo, T., Yanagisawa, H.A., Yagi, T., Hirono, M., and Kamiya, R. (2010). Tubulin polyglutamylation regulates axonemal motility by modulating activities of inner-arm dyneins. Current biology : CB *20*, 441-445.

Larkin, M.A., Blackshields, G., Brown, N.P., Chenna, R., McGettigan, P.A., McWilliam, H., Valentin, F., Wallace, I.M., Wilm, A., Lopez, R.*, et al.* (2007). Clustal W and Clustal X version 2.0. Bioinformatics *23*, 2947-2948.

Lechtreck, K.F., and Geimer, S. (2000). Distribution of polyglutamylated tubulin in the flagellar apparatus of green flagellates. Cell motility and the cytoskeleton *47*, 219-235.

Liem, K.F., Jr., He, M., Ocbina, P.J., and Anderson, K.V. (2009). Mouse Kif7/Costal2 is a cilia-associated protein that regulates Sonic hedgehog signaling. Proceedings of the National Academy of Sciences of the United States of America *106*, 13377-13382.

Love, B., and Rotheim, M.B. (1984). Cell surface interactions in conjugation: Tetrahymena ciliary membrane vesicles. Mol Cell Biol *4*, 681-687.

McEwen, D.P., Jenkins, P.M., and Martens, J.R. (2008). Olfactory cilia: our direct neuronal connection to the external world. Current topics in developmental biology *85*, 333-370.

Mesland, D.A., Hoffman, J.L., Caligor, E., and Goodenough, U.W. (1980). Flagellar tip activation stimulated by membrane adhesions in Chlamydomonas gametes. The Journal of cell biology *84*, 599-617.

Mitchell, D.R. (2003). Orientation of the central pair complex during flagellar bend formation in Chlamydomonas. Cell motility and the cytoskeleton *56*, 120-129.

Mochizuki, K. (2008). High efficiency transformation of Tetrahymena using a codon-optimized neomycin resistance gene. Gene *425*, 79-83.

Mukhopadhyay, S., Lu, Y., Qin, H., Lanjuin, A., Shaham, S., and Sengupta, P. (2007). Distinct IFT mechanisms contribute to the generation of ciliary structural diversity in C. elegans. The EMBO journal *26*, 2966-2980.

Nelsen, E.M. (1978). Transformation in Tetrahymena thermophila. Development of an inducible phenotype. Developmental biology *66*, 17-31.

Nelsen, E.M., and Debault, L.E. (1978). Transformation in Tetrahymena pyriformis: description of an inducible phenotype. J Protozool *25*, 113-119.

Omori, Y., Chaya, T., Katoh, K., Kajimura, N., Sato, S., Muraoka, K., Ueno, S., Koyasu, T., Kondo, M., and Furukawa, T. (2010). Negative regulation of ciliary length by ciliary male germ cell-associated kinase (Mak) is required for retinal photoreceptor survival. Proceedings of the National Academy of Sciences of the United States of America *107*, 22671-22676.

Omoto, C.K., Gibbons, I.R., Kamiya, R., Shingyoji, C., Takahashi, K., and Witman, G.B. (1999). Rotation of the central pair microtubules in eukaryotic flagella. Molecular biology of the cell *10*, 1-4.

Omoto, C.K., and Kung, C. (1979). The pair of central tubules rotates during ciliary beat in Paramecium. Nature *279*, 532-534.

Omoto, C.K., and Kung, C. (1980). Rotation and twist of the central-pair microtubules in the cilia of Paramecium. The Journal of cell biology *87*, 33-46.

Orias, E., and Rasmussen, L. (1976). Dual capacity for nutrient uptake in Tetrahymena. IV. Growth without food vacuoles and its implications. Exp Cell Res *102*, 127-137.

Perkins, L.A., Hedgecock, E.M., Thomson, J.N., and Culotti, J.G. (1986). Mutant sensory cilia in the nematode Caenorhabditis elegans. Developmental biology *117*, 456-487.

Prevo, B., Mangeol, P., Oswald, F., Scholey, J.M., and Peterman, E.J. (2015). Functional differentiation of cooperating kinesin-2 motors orchestrates cargo import and transport in C. elegans cilia. Nature cell biology *17*, 1536-1545.

Rezabkova, L., Kraatz, S.H., Akhmanova, A., Steinmetz, M.O., and Kammerer, R.A. (2016). Biophysical and Structural Characterization of the Centriolar Protein Cep104 Interaction Network. The Journal of biological chemistry *291*, 18496-18504.

Roux, K.J., Kim, D.I., Raida, M., and Burke, B. (2012). A promiscuous biotin ligase fusion protein identifies proximal and interacting proteins in mammalian cells. The Journal of cell biology *196*, 801-810.

Sale, W.S., and Satir, P. (1977). The termination of the central microtubules from the cilia of Tetrahymena pyriformis. Cell biology international reports *1*, 45-49.

Salisbury, J.L., Baron, A.T., and Sanders, M.A. (1988). The centrin-based cytoskeleton of Chlamydomonas reinhardtii: distribution in interphase and mitotic cells. The Journal of cell biology *107*, 635-641.

Sanders, A.A., de Vrieze, E., Alazami, A.M., Alzahrani, F., Malarkey, E.B., Sorusch, N., Tebbe, L., Kuhns, S., van Dam, T.J., Alhashem, A.*, et al.* (2015). KIAA0556 is a novel ciliary basal body component mutated in Joubert syndrome. Genome biology *16*, 293.

Satish Tammana, T.V., Tammana, D., Diener, D.R., and Rosenbaum, J. (2013). Centrosomal protein CEP104 (Chlamydomonas FAP256) moves to the ciliary tip during ciliary assembly. Journal of cell science *126*, 5018-5029.

Schiapparelli, L.M., McClatchy, D.B., Liu, H.H., Sharma, P., Yates, J.R., 3rd, and Cline, H.T. (2014). Direct detection of biotinylated proteins by mass spectrometry. Journal of proteome research *13*, 3966-3978.

Schneider, C.A., Rasband, W.S., and Eliceiri, K.W. (2012). NIH Image to ImageJ: 25 years of image analysis. Nature methods *9*, 671-675.

Shaheen, R., Szymanska, K., Basu, B., Patel, N., Ewida, N., Faqeih, E., Al Hashem, A., Derar, N., Alsharif, H., Aldahmesh, M.A.*, et al.* (2016). Characterizing the morbid genome of ciliopathies. Genome biology *17*, 242.

Shaner, N.C., Lambert, G.G., Chammas, A., Ni, Y., Cranfill, P.J., Baird, M.A., Sell, B.R., Allen, J.R., Day, R.N., Israelsson, M.*, et al.* (2013). A bright monomeric green fluorescent protein derived from Branchiostoma lanceolatum. Nature methods *10*, 407-409.

Shang, Y., Li, B., and Gorovsky, M.A. (2002). Tetrahymena thermophila contains a conventional gamma-tubulin that is differentially required for the maintenance of different microtubule-organizing centers. The Journal of cell biology *158*, 1195-1206.

Snow, J.J., Ou, G., Gunnarson, A.L., Walker, M.R., Zhou, H.M., Brust-Mascher, I., and Scholey, J.M. (2004). Two anterograde intraflagellar transport motors cooperate to build sensory cilia on C. elegans neurons. Nature cell biology *6*, 1109-1113.

Srour, M., Hamdan, F.F., McKnight, D., Davis, E., Mandel, H., Schwartzentruber, J., Martin, B., Patry, L., Nassif, C., Dionne-Laporte, A.*, et al.* (2015). Joubert Syndrome in French Canadians and Identification of Mutations in CEP104. Am J Hum Genet *97*, 744-753.

Stepanek, L., and Pigino, G. (2016). Microtubule doublets are double-track railways for intraflagellar transport trains. Science (New York, NY) *352*, 721-724.

Suprenant, K.A., and Dentler, W.L. (1988). Release of intact microtubule-capping structures from Tetrahymena cilia. The Journal of cell biology *107*, 2259-2269.

Suryavanshi, S., Edde, B., Fox, L.A., Guerrero, S., Hard, R., Hennessey, T., Kabi, A., Malison, D., Pennock, D., Sale, W.S.*, et al.* (2010). Tubulin glutamylation regulates ciliary motility by altering inner dynein arm activity. Current biology : CB *20*, 435-440.

Tsypin, L.M., and Turkewitz, A.P. (2017). The Co-regulation Data Harvester: automating gene annotation starting from a transcriptome database. SoftwareX *6*, 165-171.

Tukachinsky, H., Lopez, L.V., and Salic, A. (2010). A mechanism for vertebrate Hedgehog signaling: recruitment to cilia and dissociation of SuFu-Gli protein complexes. The Journal of cell biology *191*, 415-428.

Urbanska, P., Song, K., Joachimiak, E., Krzemien-Ojak, L., Koprowski, P., Hennessey, T., Jerka-Dziadosz, M., Fabczak, H., Gaertig, J., Nicastro, D.*, et al.* (2015). The CSC proteins FAP61 and FAP251 build the basal substructures of radial spoke 3 in cilia. Molecular biology of the cell *26*, 1463-1475.

Van De Weghe, J.C., Rusterholz, T.D.S., Latour, B., Grout, M.E., Aldinger, K.A., Shaheen, R., Dempsey, J.C., Maddirevula, S., Cheng, Y.H., Phelps, I.G.*, et al.* (2017). Mutations in ARMC9, which Encodes a Basal Body Protein, Cause Joubert Syndrome in Humans and Ciliopathy Phenotypes in Zebrafish. Am J Hum Genet *101*, 23-36.

Westermann, S., Avila-Sakar, A., Wang, H.W., Niederstrasser, H., Wong, J., Drubin, D.G., Nogales, E., and Barnes, G. (2005). Formation of a dynamic kinetochore- microtubule interface through assembly of the Dam1 ring complex. Molecular cell *17*, 277-290.

Widlund, P.O., Stear, J.H., Pozniakovsky, A., Zanic, M., Reber, S., Brouhard, G.J., Hyman, A.A., and Howard, J. (2011). XMAP215 polymerase activity is built by combining multiple tubulin-binding TOG domains and a basic lattice-binding region. Proceedings of the National Academy of Sciences of the United States of America *108*, 2741-2746.

Williams, C.L., McIntyre, J.C., Norris, S.R., Jenkins, P.M., Zhang, L., Pei, Q., Verhey, K., and Martens, J.R. (2014). Direct evidence for BBSome-associated intraflagellar transport reveals distinct properties of native mammalian cilia. Nature communications *5*, 5813.

Wloga, D., Camba, A., Rogowski, K., Manning, G., Jerka-Dziadosz, M., and Gaertig, J. (2006). Members of the NIMA-related kinase family promote disassembly of cilia by multiple mechanisms. Molecular biology of the cell *17*, 2799-2810.

Wolfe, J., Turner, R., Jr., Barker, R., and Adair, W.S. (1979). The need for an extracellular component for cell pairing in Tetrahymena. Exp Cell Res *121*, 27-30.

Xiong, J., Lu, Y., Feng, J., Yuan, D., Tian, M., Chang, Y., Fu, C., Wang, G., Zeng, H., and Miao, W. (2013). Tetrahymena functional genomics database (TetraFGD): an integrated resource for Tetrahymena functional genomics. Database : the journal of biological databases and curation *2013*, bat008.

Ye, F., Nager, A.R., and Nachury, M.V. (2018). BBSome trains remove activated GPCRs from cilia by enabling passage through the transition zone. The Journal of cell biology.

Figure Legends

Figure 1. FAP256A localizes to the tips of cilia and unciliated basal bodies and the ends of A-tubules and CP. (A) The segmental organization of the motile cilium (the blue and green arrows mark the proximal boundary of the distal segment and the CP region, respectively). (B-E) TIRFM images of live *Tetrahymena* cells that express FAP256A-GFP under native promoter, at various times (min) before and after low pH-induced deciliation that induces cilia regeneration. (F) Differential interference contrast (DIC) and TIRFM images of the same cilium (white arrows: the two FAP256A-GFP dots at the tip) (G) An SR-SIM immunofluorescence image of a *Tetrahymena* cell expressing FAP256A-2xmNeonGreen-6xMyc-BirA* under native promoter (green: 6xMyc, red: polyE, green arrowheads: unciliated basal bodies, white arrowheads: ciliated basal bodies, white arrows: FAP256A signals at the tip, asterisk: marks the gap between the polyE tubulin and FAP256A signals). (H-I) Immunoelectron TEM localization of FAP256A-GFP. Axonemes of wild type (H) and FAP256A-GFP (I) cells were labeled with anti-GFP and gold-conjugated secondary antibodies. Red circles mark the gold particles on the axonemes. The red dots on the left side summarize the approximate positions of gold particles (1 red dot = 1 gold particle) found in a total of 14 wild-type and 14 FAP256A-GFP axonemes. The As mark the visible termination points for the A-tubules (note that less than 9 ends are visible, some of these ends could be on the non-imaged side of the axoneme or were lost during preparation) and the blue arrow marks the proximal boundary of the distal segment.

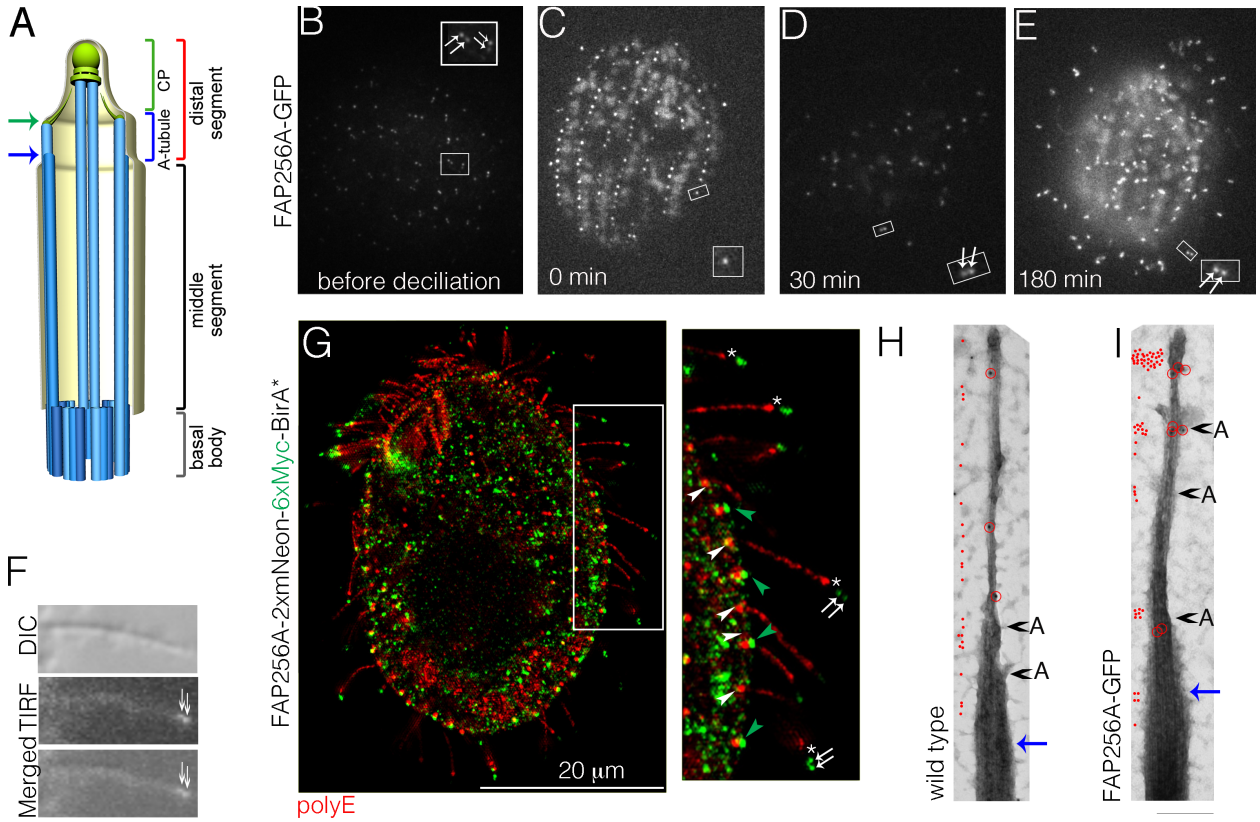
A
CP
distal segment
A-tubule
middle segment
basal body
B
FAP256A-GFP
before deciliation
C
0 min
D
30 min
E
180 min
F
DIC
Merged TIRF
G
FAP256A-2xmNeon-6xMyc-BirA*
20 µm
polyE
H
wild type
A
A
I
FAP256A-GFP
A
A
A

Figure 2. CHE12 localizes near the ends of B-tubules (A-B) SR-SIM immunofluorescence imaging of CHE12A-GFP in growing cells before and 30 min after low pH-induced deciliation (during cilia regeneration) (green: polyglycylated tubulin, red: anti-GFP). The arrow shows a short cilium with CHE12A-GFP at the tip in the cell before deciliation (A). Such cilia are numerous in the cell after deciliation (B). See Fig. S4 for negative control to evaluate the non-specific background. (C) An SR-SIM immunofluorescence imaging of CHE12B-mNeon-6xMyc. Green: poly-glycylated tubulin, red: 6xMyc, arrows point to CHE12B at the ciliary tip and the arrowheads mark the punctate signals along the cilium shaft. (D) A single TIRFM image frame taken from Movie S2. The positions of three ciliary shafts are outlined by red lines and the tips of these cilia are marked with Ts. (E) A kymograph corresponding to a single cilium (boxed in D) reveals that CHE12B undergoes diffusion (scale bar: 1 μm and 1 sec).

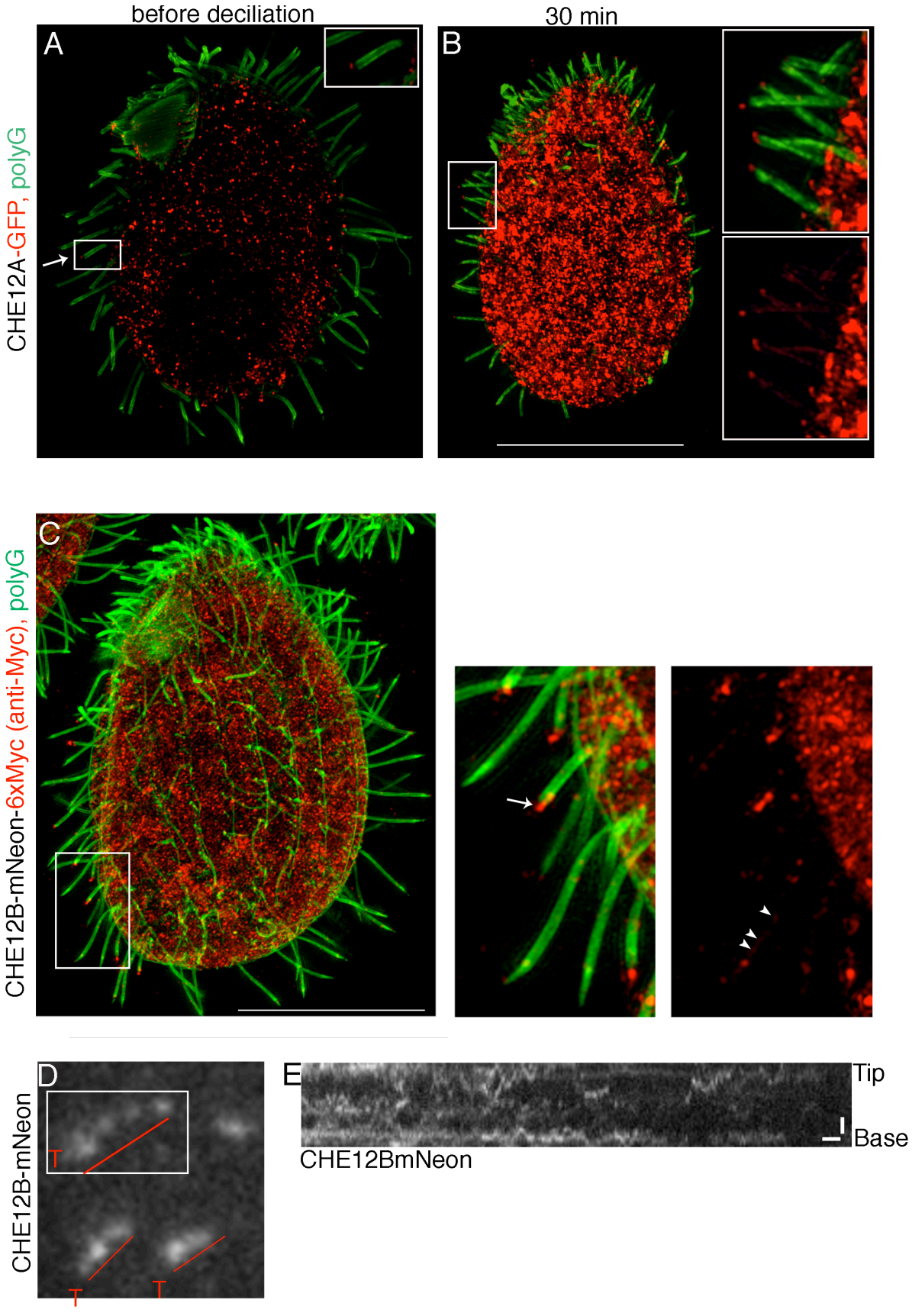
before deciliation
30 min
A
B
CHE12A-GFP, polyG
C
CHE12B-mNeon-6xMyc (anti-Myc), polyG
D
CHE12B-mNeon
T
T
T
E
Tip
Base
CHE12BmNeon

Figure 3. ARMC9 localizes near the ends of B-tubules. (A) An SR-SIM immunofluorescence image of ARMC9A-mNeon-6xMyc. The cell was labeled with polyG (green) and anti-Myc (red) antibodies (scale bar: 20 μm). ARMC9A is associated with the tips of mature full-length cilia. (B) SR-SIM images of isolated cilia (of cells expressing ARMC9A-mNeon-6xMyc) that have partially splayed microtubules (red: polyG, green: 6xMyc). (C-D) Immunogold TEM localization of ARMC9A in cilia of wild-type (C) and ARMC9A-mNeon-6xMyc expressing cells (D) using an anti-Myc primary antibody and gold-conjugated secondary antibodies. The red circles mark the gold particles on the axonemes. The red dots on the right side summarize the distribution of gold particles at these approximate positions in a total of 18 cilia per genotype. The blue arrow marks the proximal boundary of distal segment and the As point to the termination points of identifiable A-tubule ends (note that some of the ends could be on the non-imaged side of the axoneme or were lost during preparation (scale bar: 200 nm). (E) An SR-SIM image of a cell expressing ARMC9-2xmNeon-6xMyc labeled with anti-Myc antibody (red) and polyE (green) antibodies. ARMC9B is associated with the tips of assembling cilia. The box labels growing cilia of the assembling new oral apparatus (Scale bar: 20 μm). (F) An SR-SIM image of a portion of a *Tetrahymena* cell co-expressing MTT1-driven GFP-FAP256A (green: GFP) and ARMC9A-mNeon-6xMyc (red: 6xMyc) (the brackets connect the FAP256 and ARMC9 signals on the same cilium, scale bar: 5μm).

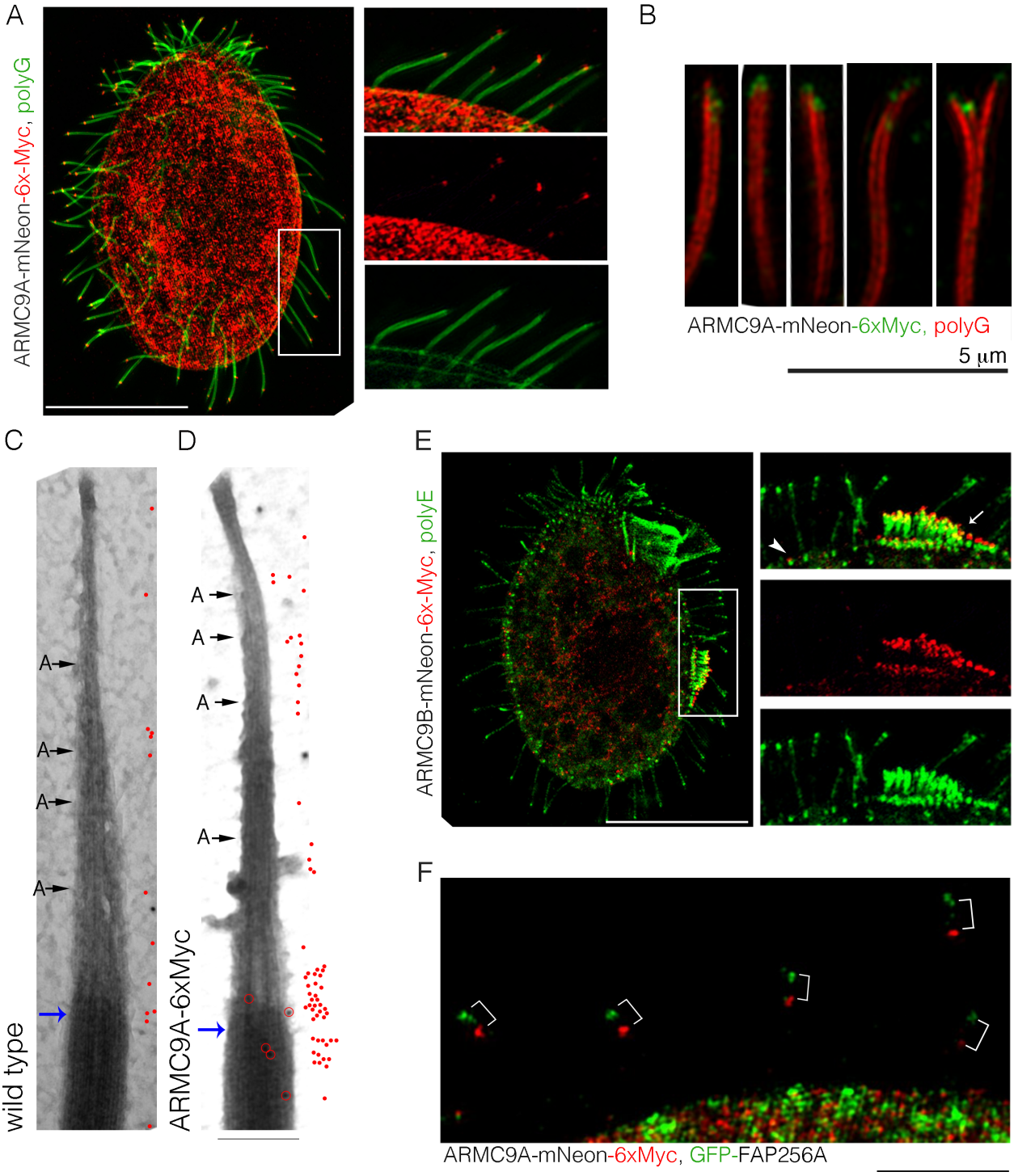
A
ARMC9A-mNeon-6x-Myc, polyG
B
ARMC9A-mNeon-6xMyc, polyG
5 μm
C
D
wild type
ARMC9A-6xMyc
A
E
ARMC9B-mNeon-6x-Myc, polyE
F
ARMC9A-mNeon-6xMyc, GFP-FAP256A

Figure 4. Losses of FAP256, CHE12 and ARMC9 affect cilia. (A) Swimming velocities of wild type (WT, 0.41 mm/sec, n=31), FAP256-KO (F-KO, 0.27 mm/sec, n=22), CHE12-KO (C-KO, 0.29 mm/sec, n=16) and ARMC9-KO (A-KO, 0.2 mm/sec, n=15) cells were measured in growing cultures by recording the paths of cells over time. The asterisks mark significant differences as compared to the wild type at $p < 0.001$. (B) The rates of phagocytosis expressed as the number of ink-filled food vacuoles per cell after 10 min of exposure to India ink (asterisks show significant differences as compared to wild type at $p < 0.05$). (C) Rates of pair formation at the onset of conjugation. Wild-type or KO cells were mixed with an equal number of wild type cells of a complementary mating type and the percentage of cells in pairs was scored 6 hr post mixing (asterisks show significant differences at $p < 0.05$). (D) The ciliary beat frequencies of wild type (39.8 +/- 4.2 hz, n= 109), FAP256-KO (34 +/- 4.4 Hz, n= 58), CHE12-KO (37 +/- 5.8 Hz, n = 95 cilia), and ARMC9-KO cells (20.5 +/- 6.2 Hz, n = 37 cilia). Error bars represent standard deviations, asterisks indicate statistical significance at $p < 0.05$ (compared to the wild type). (E-F) Space-time diagrams that document ciliary motility based on the supplemental movies S3 and S6. The x-axis represents the position of cilia along the *Tetrahymena* cell surface (A: anterior, P: posterior end of the cell). The y-axis represents time in msec. Each short diagonal line represents a single cilium moving along the cell surface over time (see Fig. S8 for further details). The red arrows mark an example of a single beat cycle, the red rectangle marks an example of a paralyzed cilium.

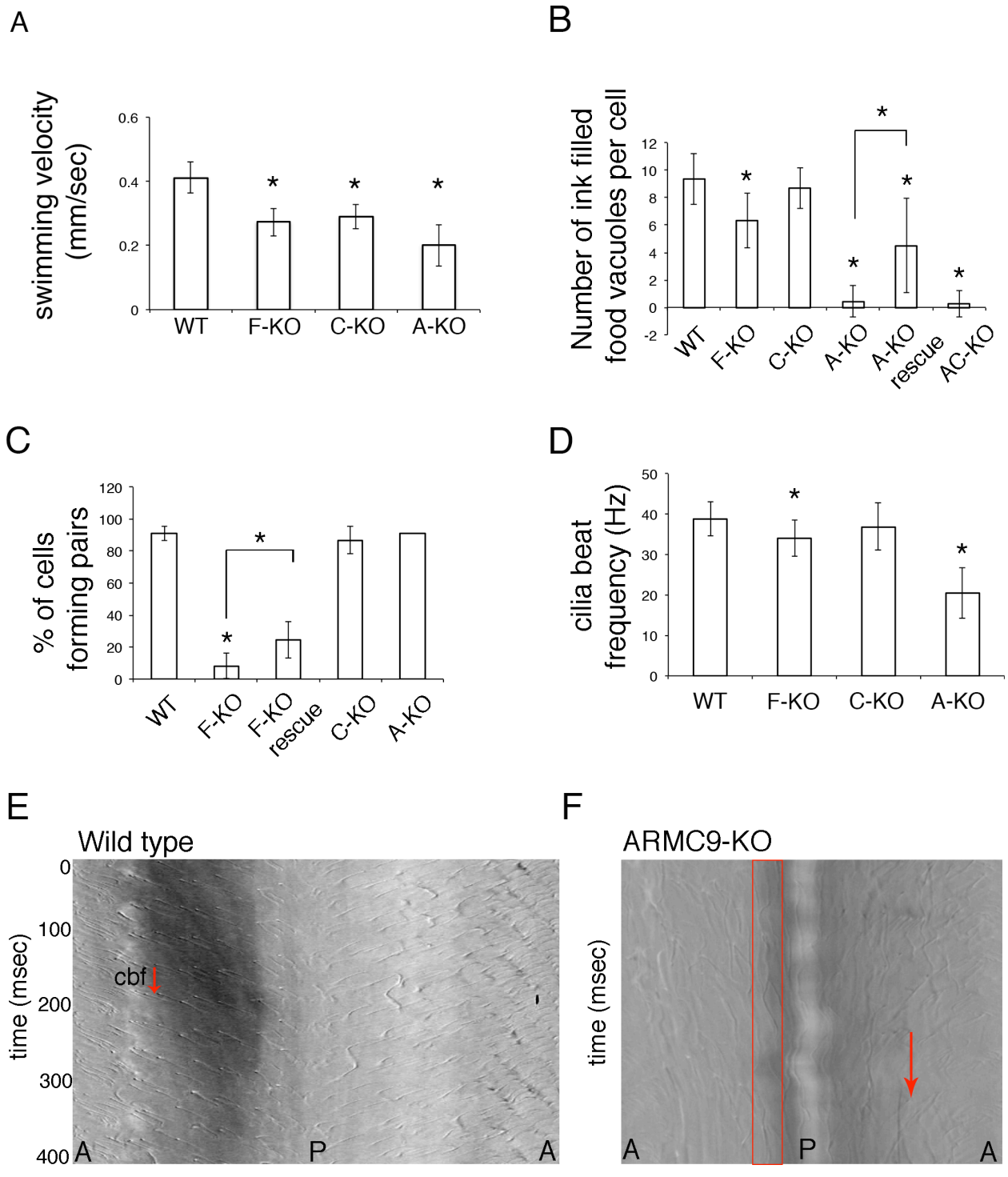
A
swimming velocity (mm/sec)
0.6
0.4
0.2
0
WT
F-KO
C-KO
A-KO
B
Number of ink filled food vacuoles per cell
12
10
8
6
4
2
0
-2
WT
F-KO
C-KO
A-KO
A-KO rescue
AC-KO
C
% of cells forming pairs
120
100
80
60
40
20
0
WT
F-KO
F-KO rescue
C-KO
A-KO
D
cilia beat frequency (Hz)
50
40
30
20
10
0
WT
F-KO
C-KO
A-KO
E
Wild type
time (msec)
0
100
200
300
400
cbf
A
P
A
F
ARMC9-KO
time (msec)
A
P
A

Figure 5. FAP256, CHE12 and ARMC9 affect the dimensions of distal segment and FAP256 is needed for assembly or stability of the CMC. (A-D) Images of negatively-stained wild type and knockout axonemes. Arrows point to the ends of the CP microtubules (the location of CMC), and arrowheads mark the proximal and distal ends of the DFs. The percentage of axonemes positive for the presence of CMC and DFs are shown below each image (wild type CMC score n = 48, DFs n = 19; FAP256-KO CMC n = 76, DFs n = 42; CHE12-KO CMC n = 11, DFs n = 7; and ARMC9-KO CMC n = 10, DFs n = 10). (E-J) Representative electron microscopy images of negatively-stained whole mount wild-type and knockout cilia (in E the blue and green brackets mark the A-tubule and CP region, respectively; the blue and green arrows mark the proximal boundary of the distal segment and CP region, respectively). (K) Cilium length was quantified using electron microscopic images of negatively-stained isolated cilia (wild type (WT): 6.9 μm, +/-0.97 n=51, CHE12-KO (C-KO): 5.8 μm, +/- 0.57, n=39, FAP256-KO (F-KO): 6.7 μm, +/- 0.79, n=49, ARMC9-KO (A-KO)-KO: 7.8 μm, +/- 0.82 n=70 and ARMC9-KO_CHE12-KO (AC-KO): 6.9 μm, +/- 0.57 n=50, asterisks show significant differences compared to wild type at $p < 0.05$). (L) Quantifications of the length of distal segment, A-tubule and CP region (averages +/- standard deviations, asterisks show significant differences as compared to the wild type at $p < 0.05$, * at the top of the column shows a significant difference in the distal segment, * on the side of each column shows a significant difference in either the CP (top) or the A-tubule region (bottom)).

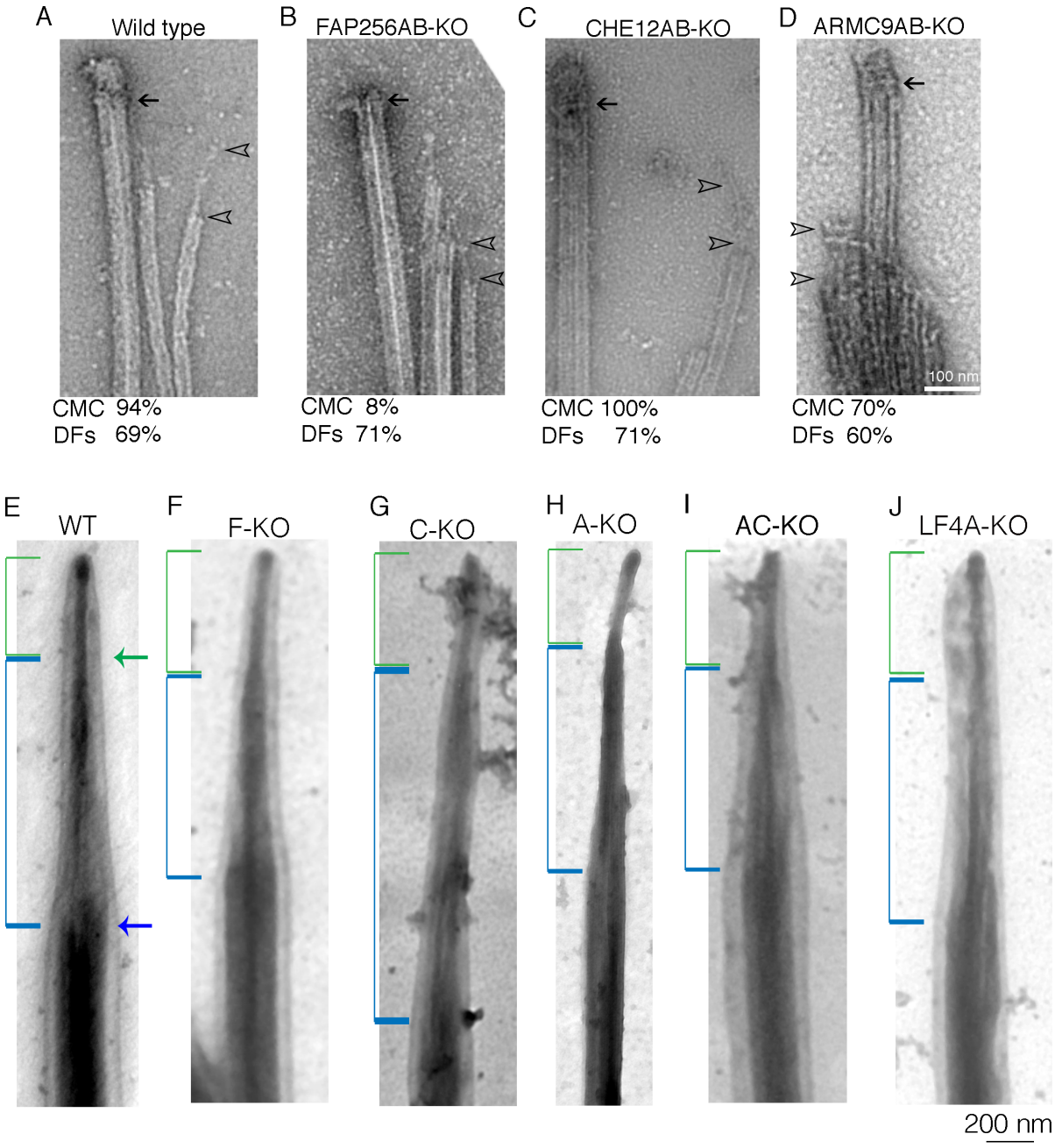
A
Wild type
CMC 94%
DFs 69%
B
FAP256AB-KO
CMC 8%
DFs 71%
C
CHE12AB-KO
CMC 100%
DFs 71%
D
ARMC9AB-KO
100 nm
CMC 70%
DFs 60%
E
WT
F
F-KO
G
C-KO
H
A-KO
I
AC-KO
J
LF4A-KO
200 nm
K
cilia length (μm)
WT
F-KO
C-KO
A-KO
A-KO rescue
AC-KO
L
length (μm)
CP region
A-tubule region
WT
F-KO
C-KO
A-KO
A-KO rescue
AC-KO
LF4A-KO

Figure 6. FAP256 activity elongates the A-tubules while ARMC9 activity shortens the B-tubules. (A-C) Negatively-stained whole cilia from a wild type (A) and cells overproducing either GFP-FAP256A (C) or GFP-ARMC9B (D) after six hr of exposure to cadmium chloride to induce the transgenes (green bracket: CP region, blue bracket: A-tubule region). (D-E) Quantifications of the length of CP-region (n = 50-60), and distal segment (n = 45-67) based on the images of negatively stained whole cilia (mean +/- standard deviation, * $p < 0.05$). (F-G) SR-SIM images of a wild type control (F) and a GFP-ARMC9B overproducing cell (in the ARMC9-KO background) (G) after 6 hr of exposure to cadmium chloride to induce the transgene overexpression (green: α-tubulin detected by 12G10 monoclonal antibody (and GFP-ARMC9B), red: polyG antibodies, scale bar: 20 μm). The anti-a-tubulin 12G10 antibody labels strongly the distal segment (as compared to the middle segment) likely due to increased accessibility of microtubules not covered by motility-related complexes. Color channels are shifted in magnified images, arrows point to the boundaries of the distal segment. (H) A summary of the functions of FAP256/CEP104, CHE-12 and ARMC9 uncovered in this study.

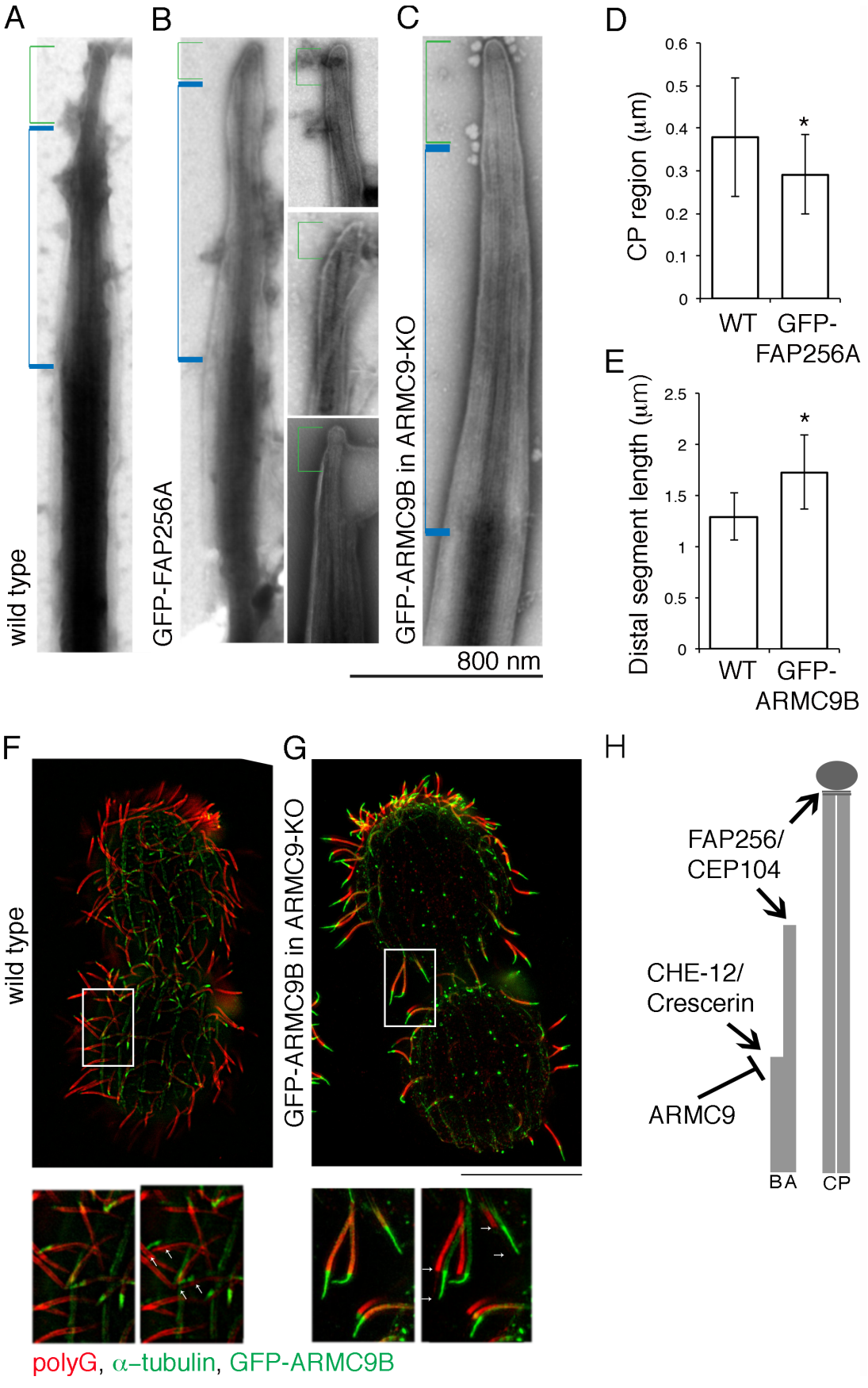
A
B
C
D
E
wild type
GFP-FAP256A
GFP-ARMC9B in ARMC9-KO
800 nm
CP region (μm)
0.6
0.5
0.4
0.3
0.2
0.1
0
*
WT
GFP-FAP256A
Distal segment length (μm)
2.5
2
1.5
1
0.5
0
*
WT
GFP-ARMC9B
F
G
H
wild type
GFP-ARMC9B in ARMC9-KO
FAP256/
CEP104
CHE-12/
Crescerin
ARMC9
BA
CP
polyG, α–tubulin, GFP-ARMC9B

Figure 7. CHE-12 loss of function shortens both the A- and B-tubules in chemosensory cilia of *C.elegans*. (A-B) Representative immunofluorescence images of two phasmid neuron cilia (PHA, PHB) of adult animals (green: KAP::GFP, red: OSM-3::mCherry, arrowheads point to the distal boundaries of the middle segment corresponding to the distal ends of KAP::GFP). (C) A quantification of the middle and distal segment lengths in phasmid cilia (error bars show standard deviations, asterisks show statistical significance at $p < 0.05$).

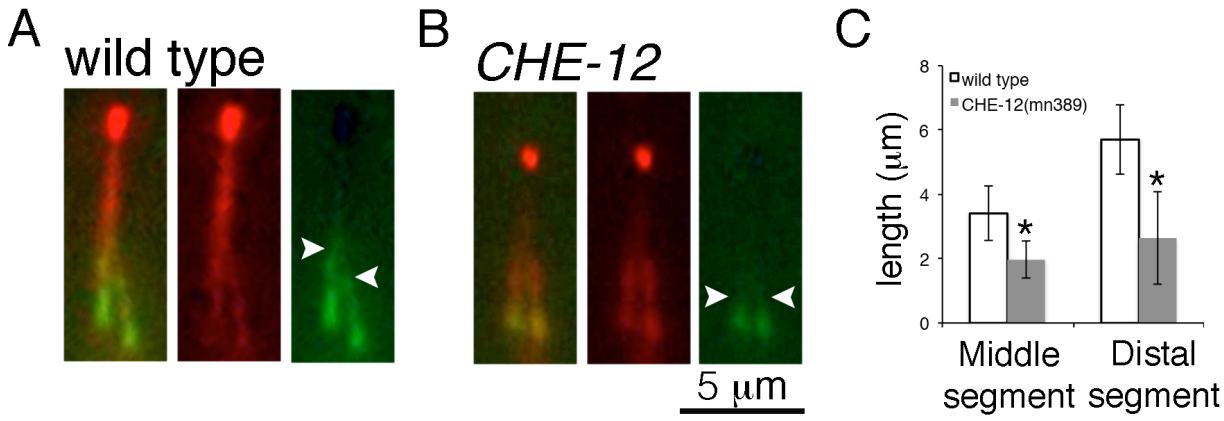
A
wild type
B
CHE-12
5 μm
C
wild type
CHE-12(mn389)
length (μm)
0
2
4
6
8
Middle segment
Distal segment
*
*

Supplementary Tables

Table S1. Primers used for amplification of coding sequences for tagging of the native loci, overexpression, gene disruptions and genotyping.

FAP256A (native locus)	
5'-Forward	AATA CCG CGG CAG AAC TAA TCA GGG AAG TAA
5'-Reverse	TATT ACG CG TGC GCC TGT AGA GCG TTC ATT AT
3'-Forward	AATA ATC GAT GCC TTA GAC AAT TGA CTT GC
3'-Reverse	TTAT GAG CTC GAG AGA CTG CTT AAC TGA TC
CHE12A (native locus)	
5'-Forward	AATA CCG CGG G AAT TAA ATG GAT AAA AGG ACT
5'-Reverse	TATT ACG CG TTC TAT CAT ATC CAT AAT TTG TT
3'-Forward	AATA ATC GAT TC TTG TAT AAT ATT CGT CAT AAA
3'-Reverse	TATT GAG CTC GTC TAT CTT AAT ATG AAT TCA C
ARMC9A (native locus)	
5'-Forward	TATT A CGC GT GC TTT TAA TAG ACC TGG AGG CGT
5'-Reverse	TATT CCG CGG ACA TCA CAA AGA GAA TTA TTT AAG
3'-Forward	TATT GAG CTC CTC ATC AAA TAT ATC ATC AAT GTC
3'-Reverse	TATT ATC GAT AAT CCT GAT GAG TGC TAA CAT A
ARMC9B (native locus)	
5'-Forward	TATT CCG CGG GAG GCA CTT AGA TAG CAT AAT A
5'-Reverse	TATT A CGC GT GC ATT ACT ATC CTC ATC TAT ATT TGA T
3'-Forward	TATT ATC GAT ATC TTC TAT TGT TTA TCT ACT TGT
3'-Reverse	TATT GAG CTC TTA TAA TGT AAA AAT GCT GAT AAC
FAP256A (overexpression)	

Forward	ATAA ACGCGT C TCT AAA TAG TAG CAA AAT ATG CA
Reverse	TTAA GGA TCC TCA GCC TGT AGA GCG TTC A
ARMC9B (overexpression)	
Forward	ATAA ACG CGT ATT TAT AAT TTG TAT TTA TAT TTT TGT G
Reverse	AATT GGA TCC TCA ATT ACT ATC CTC ATC TAT ATT T
FAP256A (gene disruption)	
5'-Forward	ATAA GGG CCC GAT ATT GCT TTT CTA AAG ATT A
5'-Reverse	AATT CCC GGG TAT TTT GGG CTT AAT TGA TAG
3'-Forward	AATT CTG CAG GGC TAG GCA CCT GAA TCT GTT C
3'-Reverse	AAT ACC GCG GAT GCT TAC GCC AGC CTT CAG
FAP256B (gene disruption)	
5'-Forward	ATAA GGG CCC TAA GAT CCA AAA CAC CTC CAC
5'-Reverse	AATT CCC GGG CAA ATA GAT ATA AAA CTT ACC AC
3'-Forward	AATA CTG CAG ACC AGA GCC AGA ACC TCC
3'-Reverse	TTAT CCG CGG GCA TAA AAG TTT CCT CCT GG
CHE12A (gene disruption)	
5'-Forward	ATA AGG GCC CAG GAC AGT TTA ACT TTA TTA GA
5'-Reverse	AAT TCC CGG GAT TGT ACG ATT TAT TTC TGT CA
3'-Forward	ATAT CTG CAG TGA TGG GTC TCT TGA AGT TA
3'-Reverse	TTAT CCG CGG TCT ATC ATA TCC ATA ATT TGT TA
CHE12B (gene disruption)	
5'-Forward	ATAA GGG CCC ATG ATG AAA GTG TAG AAA GTA A
5'-Reverse	AATT CCC GGG TGC AAA TAA GTA AGT AAT TAA GT
3'-Forward	AATT CTG CAG GTC TTG ACT GAC TAA TAA TAT T
3'-Reverse	TTAT CCG CGG TGC TTG CAA TAA TAT CTT ATA C

ARMC9A (gene disruption)	
5' Forward	ATA ACC CGG GCA AAT CAT TAA TAA ATC AAA CAA TC
5' Reverse	AAT TGG GCC CGA AAG TGA GAG ATA CAG ATT TTG
3' Forward	AATT CCG CGG ATT CCT TCT GGT AAA ACT GTC T
3' Reverse	AATA CTG CAG GAG TAC TTA GAT AAC AGA GGA G
ARMC9B (gene disruption)	
5' Forward	ATAA GAG CTC CAT ATA CTA ATT AGG AGT CTA CA
5' Reverse	AATT CCC GGG TAT AAA TCA ATC TAT TCT ATA TGC T
3' Forward	AATT GGA TCC TAA ATG GAC GTC ATT CCC TCA
3' Reverse	AATA CTC GAG GTG AAT CCA TAA TAG CTT ACT TT
FAP256A (diagnostic KO primers)	
Forward	TT AGT TCG AGT GTT TTT CCC T
Reverse	TG CAT ATT TTG CTA CTA TTT AGA
FAP256B (diagnostic KOprimers)	
Forward	AGA TGC AGA ATA CCG ACT TG
Reverse	CTT CTG CTA GAG ATT TTA GTC
CHE12A (diagnostic KO primers)	
Forward	CGA AAA ATA GTA GTG AAA ATG A
Reverse	AAG CTT GAT CTC AAA TTA TCG
CHE12B (diagnostic KO primers)	
Forward	ATA AAT CAA ACT AAT GGC TAA G
Reverse	A AGC TCT TAC CTA GTT AAA TAA
ARMC9A (diagnostic KO primers)	
Forward	TGC TGC ATT TAA CCA GTA GA

Reverse	TTA CTG AAA CTT ACA TAC ATA TTA
ARMC9B (diagnostic KO primers)	
Forward	ATG AAG AAG AAC CAA GGA AGT
Reverse	CG ATT ACA CCC ATG CTT CAC
C. elegans CHE-12 (diagnostic primers)	
Forward	CATCGACCTTATCCGCCCA
Reverse	AGATGGCATTGAGAGAAATTC

Table S2. Distal segment candidates with at least 10-fold enrichment in BirA*-NRK2-(K35R)-GFP as compared to GFP-BirA*.

Protein ID	NSAF BNG"	NSAF GB""	spectral count BNG"	spectral count GB""	seq. coverage BNG"	seq. coverage GB""	closest orthologs in other species
TTHERM_00346410	9.56E-04	0	26	0	7.90%	0	FAP103
TTHERM_00074280	5.08E-05	0	4	0	3.20%	0	FAP36
TTHERM_01123950	5.15E-04	0	14	0	13.90 %	0	ubiquitin-conjugating enzyme E2 13
TTHERM_00568000	1.70E-04	0	12	0	5.60%	0	oxysterol binding protein
TTHERM_00526990	3.54E-05	0	3	0	4.20%	0	SIRT2
TTHERM_00450990# *	8.68E-05	0	13	0	3.40%	0	dyf-5 / MAK
TTHERM_00421040	1.87E-05	0	2	0	2.40%	0	CDK5 activator-binding protein C42
TTHERM_00723450*	1.96E-05	0	4	0	1.80%	0	ARMC9
TTHERM_00030290	4.35E-04	0	16	0	15.20 %	0	UNC-44
TTHERM_00245740	0.006307045	2.42 E-05	617	2	30.90 %	8.80%	NRK2
TTHERM_00245740	0.006296822	2.42 E-05	616	2	30.90 %	8.80%	NRK2
TTHERM_00070340 9	2.01E-04	0	9	0	6.50%	0	NSFL1 cofactor p47
TTHERM_00578720	8.78E-04	0	34	0	14.00 %	0	putative methyltransferase
TTHERM_00537370	6.08E-04	0	15	0	27.70 %	0	RIIa dmain-containing protein 1
TTHERM_00105430	4.02E-04	0	11	0	7.90%	0	profilin-1
TTHERM_00794150	3.70E-04	0	9	0	11.90 %	0	cofilin-1

TTHERM_01311290	2.91E-04	0	19	0	2.20%	0	voltage-gated potassium channel subunit
TTHERM_00919560	2.13E-04	0	67	0	1.10%	0	ABC3
TTHERM_01345810	2.09E-04	0	4	0	10.40 %	0	Protein phosphatase 2A
TTHERM_01044390	1.90E-04	0	22	0	6.20%	0	HSP-70
TTHERM_00471350	1.31E-04	0	3	0	13.40 %	0	prefoldin subunit 4
TTHERM_00497990	1.15E-04	0	4	0	16.10 %	0	eukaryotic translation initiation factor
TTHERM_00433610	8.83E-05	0	6	0	4.50%	0	COP9 signalosome complex subunit 4
TTHERM_00938830	6.90E-05	0	8	0	1.90%	0	CASEIN KINASE
TTHERM_00481220	6.80E-05	0	9	0	2.90%	0	KIN1
TTHERM_00136080	5.37E-05	0	5	0	5.60%	0	UDP-galactose 4-epimerase
TTHERM_00423390	4.68E-05	0	11	0	0.60%	0	multidrug resistance protein 1
TTHERM_00526990	3.54E-05	0	3	0	4.20%	0	SIRT2
TTHERM_00283420	3.06E-05	0	3	0	2.40%	0	cytochrome P450
TTHERM_00001175 9	2.95E-05	0	4	0	1.70%	0	Mcm7
TTHERM_00050390 0	1.38E-05	0	2	0	2.00%	0	piwi-like protein
TTHERM_00772060	7.21E-06	0	2	0	0.80%	0	Translation inittiation factor
TTHERM_00149860	9.48E-04	6.01 E-05	112	6	3.40%	10.80 %	predicted phosphatase 2C

Results of proximity biotinylation (BioID)-based identification of proteins using BirA*-NRK2(K35R)-GFP overproduction. NRK2(K35R) is an inactive kinase that accumulates within the distal segment of cilia when overproduced ((Wloga et al., 2006) and Fig. S5). The Table lists 33 biotinylated proteins that were at least 10 fold enriched in cilia of BirA*-NRK2(K35R)-GFP-overproducing cells as compared to cilia of GFP-BirA*-overproducing cells. ” BirA*-NRK2(K35R)-GFP sample. ””BirA*-GFP sample. *These proteins have mRNA expression patterns that indicate co-regulation with the known distal segment protein, FAP256A. # A murine ortholog, MAK, is a ciliary-tip enriched protein (Omori et al., 2010).

Table S3. Summary of defects caused by the loss of either FAP256, or CHE12 or ARMC9 in *Tetrahymena*.

Phenotype	FAP256	CHE12	ARMC9
Growth rate	↓		↓
Phagocytosis	=	=	↓
signaling during mating	↓	=	=
Swimming velocity	30% ↓	25% ↓	47% ↓
cilia beat frequency	15% ↓	7% ↓	43% ↓
cilia density	33% ↓	38% ↓	37% ↑
cilia length	=*	16% ↓	14% ↑
CMC	↓	=	=
Distal segment	↓	↑	↓
A-tubule region	↓	↑	↓
CP region	↓	↑	=

* The cilium likely shortens by ~250 nm based on the measurements of the distal segment alone but this value is within the SD of mean length of wild-type cilia

Supplementary Figures

Figure S1. (A) Domain organization of FAP256/CEP104 *Tetrahymena* homologs based on the InterPro database (red box: TOG domain, amino acids 450-805 in FAP256A and amino acids 400-700 in FAP256B; green circle: coiled coil domain). (B) A 3D model of the TOG domain of FAP256A predicted using i-TASSER (rainbow colors), superimposed on the crystal structure of Stu2:TOG1-ab-tubulin (slate: Stu2:TOG1, pink: β-tubulin, green: α-tubulin, left: front view, right: back view). (C) A multiple sequence alignment of CEP104/FAP256 homologs. The sequences used were from *T*etrahymena *thermophila* gi|118365202 (FAP256A), *Ichthyophthirius multifiliis* gi|471221679*, Paramecium tetraurelia* gi|145521394*, Oxytricha trifallax* gi|403345233*, Stylonychia lemnae* gi|678325194 and gi|678312996*, Saimiri boliviensis boliviensis* gi|725596390, *Physcomitrella patens* gi|168045131 and *Homo sapiens* gi|33876357 (the arrowheads mark the conserved amino acids that form the interphase with curved tubulin).

A

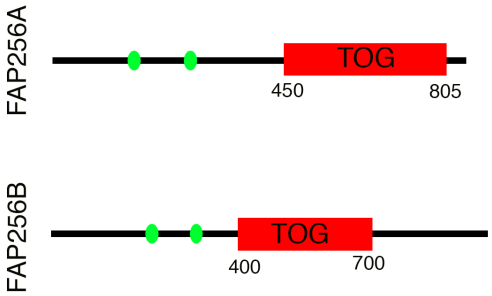
FAP256A
TOG
450
805
FAP256B
TOG
400
700

B

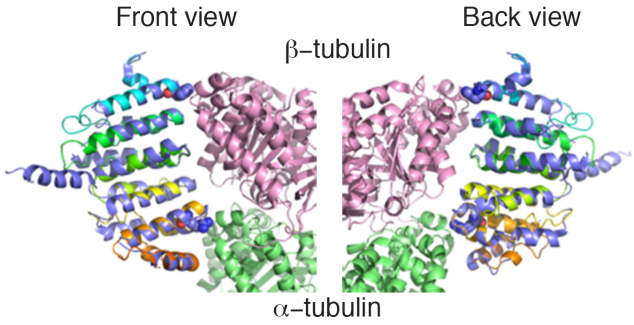
Front view
Back view
β–tubulin
α–tubulin

C

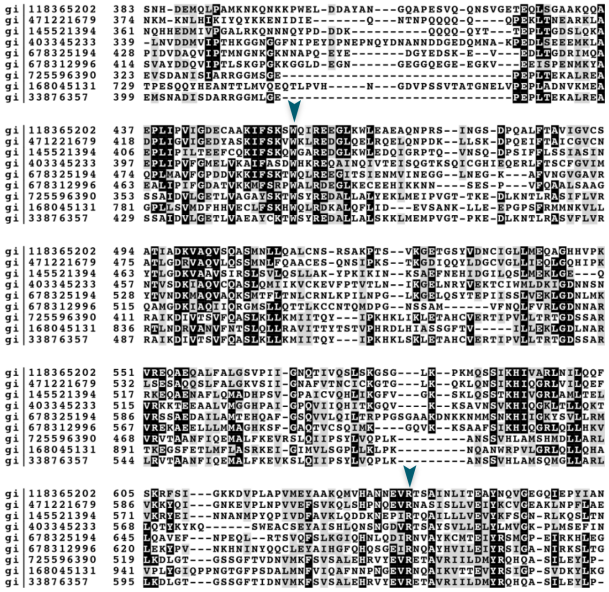

Figure S2. (A-B) Immunoelectron microscopy localization of polyglycylated tubulin (using polyG antibodies) in cilia. Representative immunoelectron micrographs of isolated axonemes labeled with either the pre-immune serum (A) or antibodies against poly-glycylated tubulin (polyG 2302) (B) and gold conjugated secondary antibodies. (C-K) Representative TEM cross-sections of wild-type cilia within the distal segment. (C) A cross section through the CP region. (D-K) Cross-sections through the A-tubule region. The percentages of cross-sections with different numbers of A-tubules (bottom right corner) were calculated in the total of 40 cross-sections. The number of cross-sections with 2 A-tubules: 6 (D), 3 A-tubules: 2 (E), 4 A-tubules: 3 (F), 5 A-tubules: 1 (G), 6 A-tubules: 1 (H), 7 A-tubules: 4 (I), 8 A-tubules: 6 (J), 9 A-tubules: 17 (K). (L) A cartoon showing the estimated positions of termination points of all A-tubules within the distal segment. The numbers on the A-tubule show the number of singlets at the position marked by red arrow. We did not find cross sections with one A-tubule. The position of each A-tubule termination is presented as the distance (in nm) from the B-tubule termination zone.

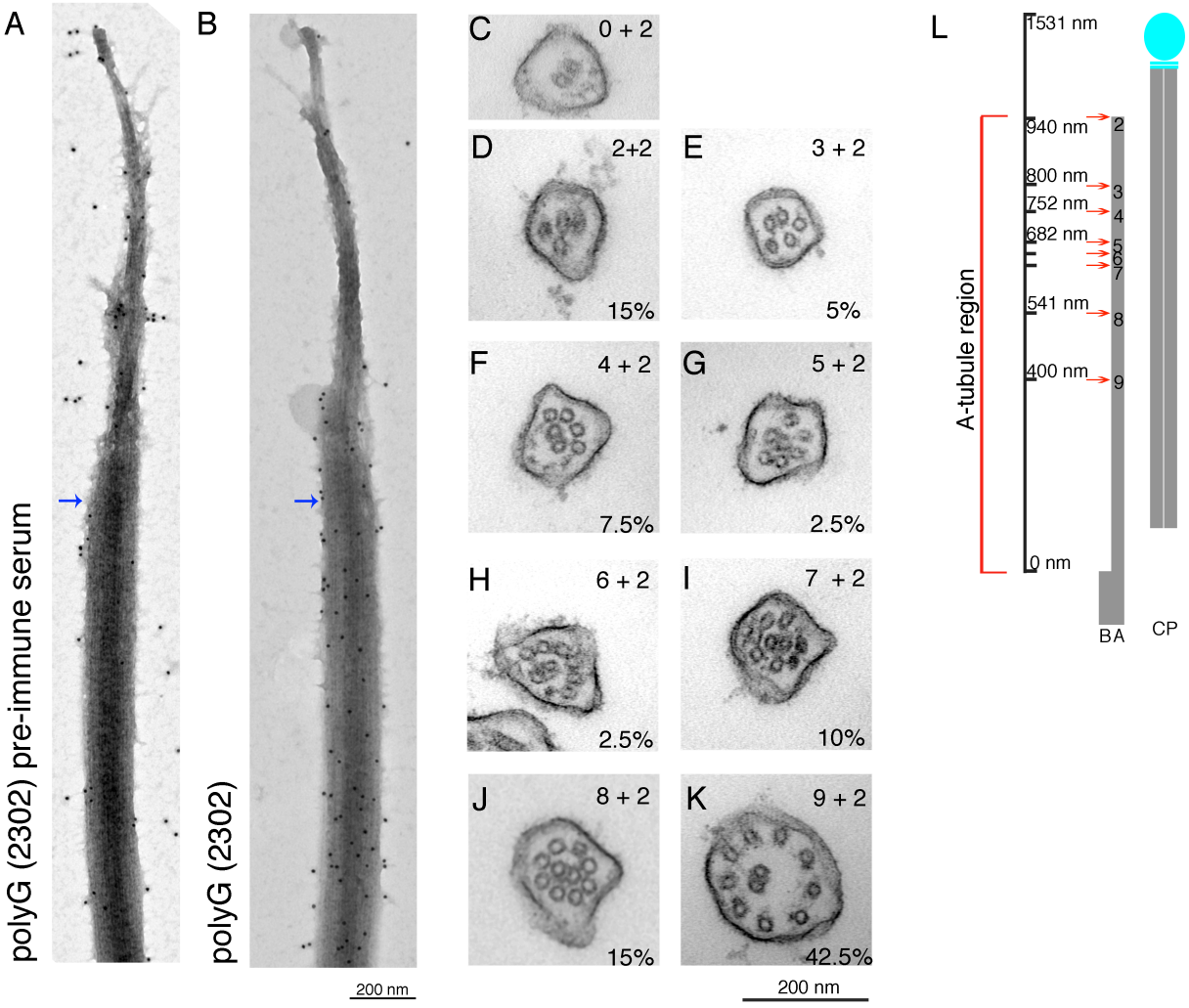
A
polyG (2302) pre-immune serum
B
polyG (2302)
200 nm
C
0 + 2
D
2+2
15%
E
3 + 2
5%
F
4 + 2
7.5%
G
5 + 2
2.5%
H
6 + 2
2.5%
I
7 + 2
10%
J
8 + 2
15%
K
9 + 2
42.5%
200 nm
L
1531 nm
940 nm
800 nm
752 nm
682 nm
541 nm
400 nm
0 nm
A-tubule region
2
3
4
5
6
7
8
9
BA
CP

Figure S3. SR-SIM immunofluorescence images of *Tetrahymena* cells expressing either FAP256A-2xmNeonGreen-6xMyc-BirA (A) or CHE12B-mNeon-6xMyc-BirA* (B) under native promoter. Cilia were labeled with polyG (panel A: green) or polyE (panel B: green), and FAP256A and CHE12B were detected using an anti-Myc antibody (red). In A, magnified cilia - the asterisk marks the gap between the FAP256A and polyG tubulin signal, B, magnified cilia - the arrow and arrowheads mark the CHE12B signal near the tip and punctate signal along the cilium respectively) (scale bar: 20 μm).

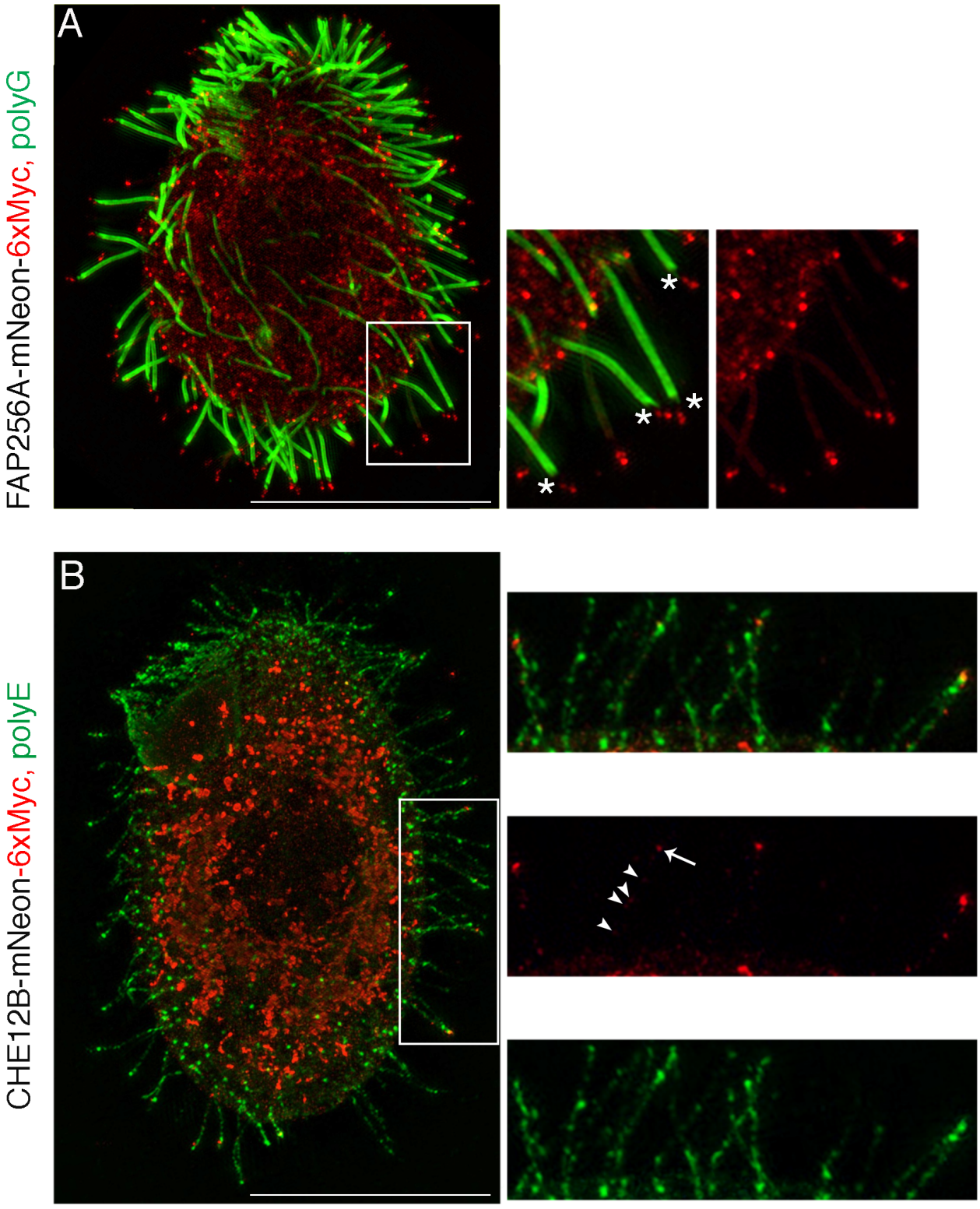
A
FAP256A-mNeon-6xMyc, polyG
B
CHE12B-mNeon-6xMyc, polyE

Figure S4. Confocal images of wild type (negative control) cells before and 30 min post deciliation labeled with antibodies against GFP (red) and polyG (green) (this is a negative control for the background signal of anti-GFP antibodies in reference to images shown in Fig. 2).

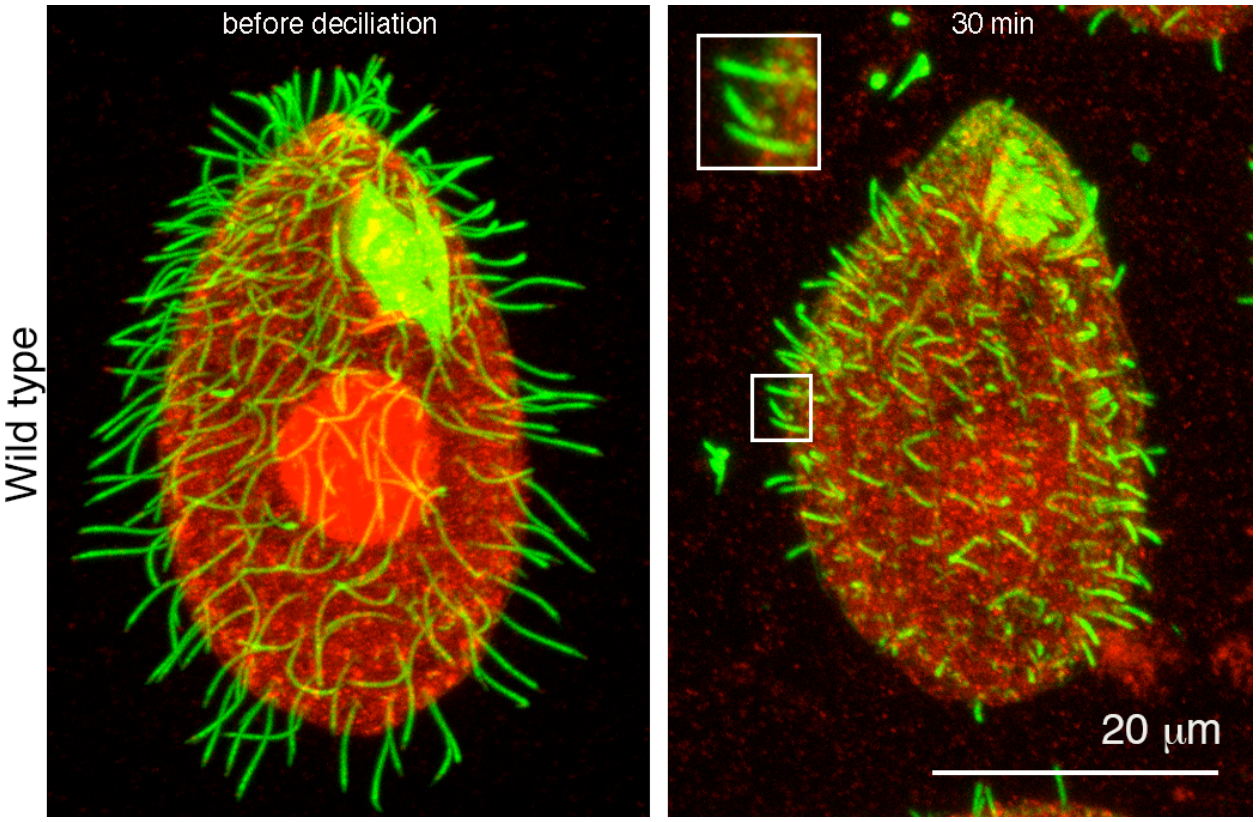

Figure S5. NRK2(K35R)-GFP and BirA*-NRK2(K35R)-GFP localize to the tips of cilia.

(A) Negatively stained whole cilia 2 hr post induction of NRK2-(K35R)-GFP overexpression (arrows point to the sites of accumulation of NRK2-(K35R)-GFP). (B-C) Confocal immunofluorescence images of BirA*-NRK2-(K35R)-GFP in the presence and absence of biotin (blue: polyG, red: biotinylated proteins labeled with streptavidin-cy3, green: GFP).

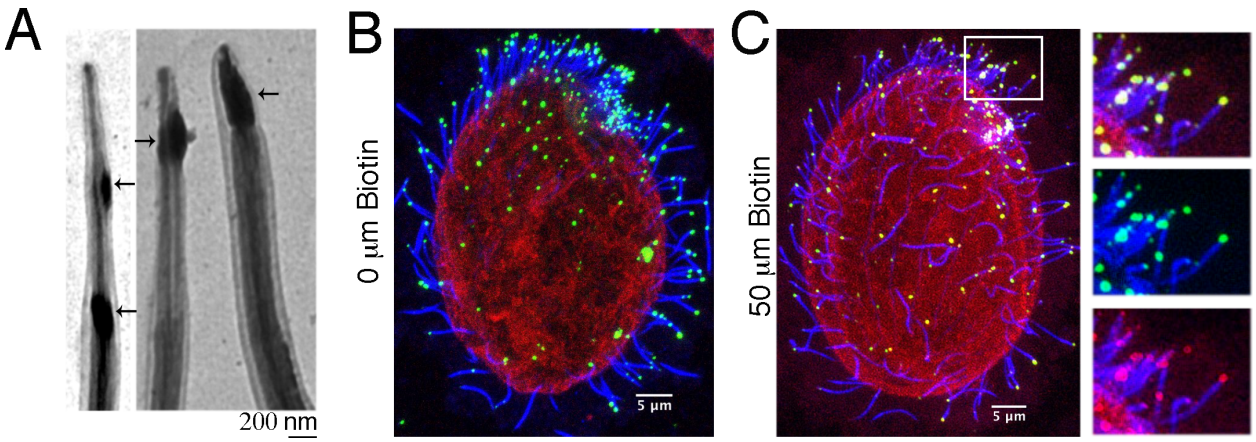

Figure S6. The morphology, growth rates and ciliation of the wild-type and knockout strains. (A-D) Confocal immunofluorescence images of wild-type, FAP256-KO, CHE12-KO and ARMC9-KO cells stained with polyG antibodies (green) and anti-centrin (red). Growth curves of wild-type and ARMC9 knockout cultures in SPP (E) and MEPP media (F). (G) Cilia densities (number of cilia per μm of cell circumference) were calculated by dividing the number of visible cilia at the widest cell circumference by the length of the circumference (WT: 0.27 cilia/μm, +/- 0.05 n = 10, F-KO: 0.18 cilia/μm, +/- 0.02 n= 8, C-KO: 0.18 cilia/μm, +/- 0.05 n=12 and A-KO: 0.34 cilia/μm, +/- 0.06 n=10, asterisks show significant differences compared to wild type at $p < 0.05$).).

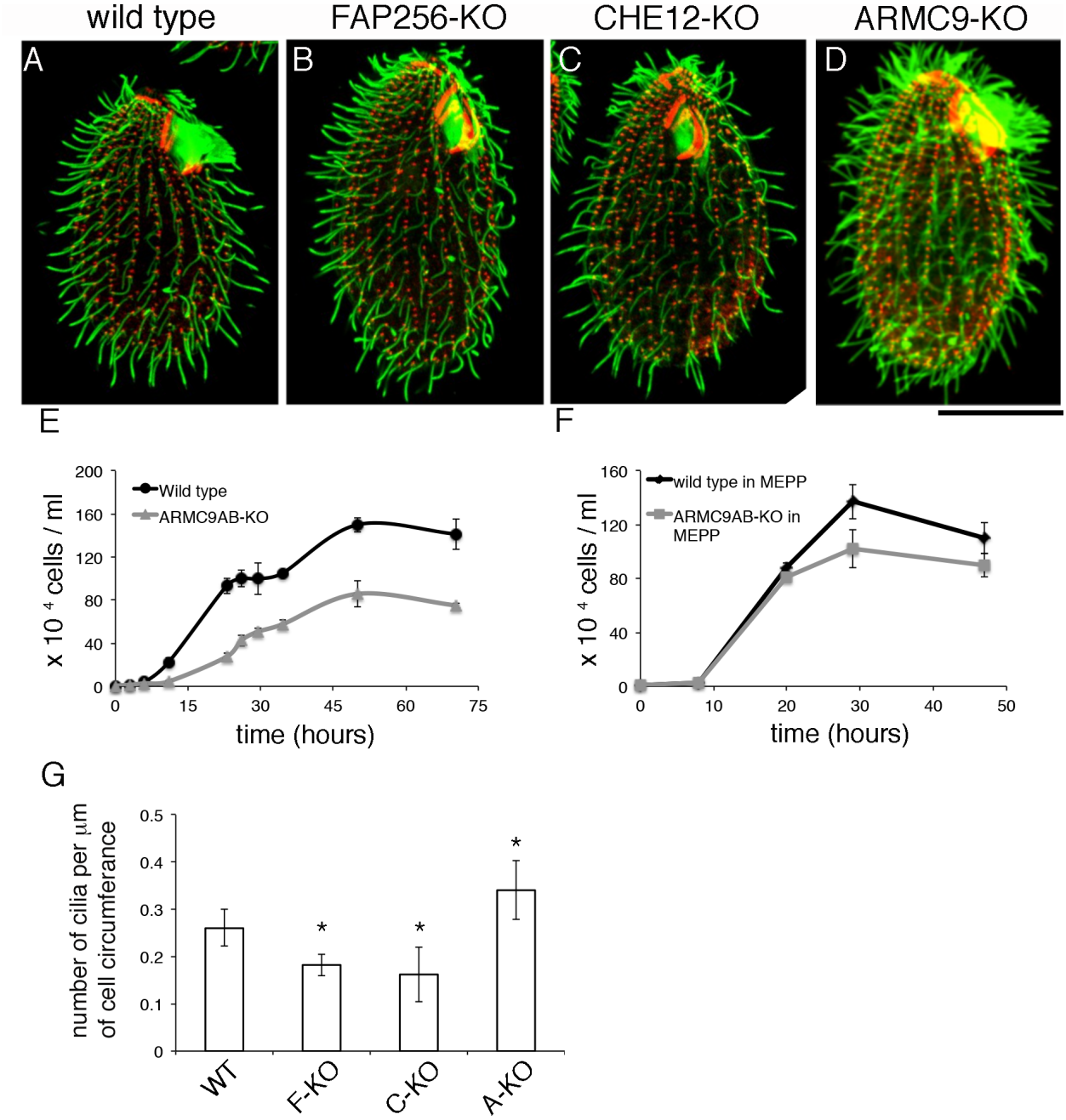
wild type
FAP256-KO
CHE12-KO
ARMC9-KO
A
B
C
D
E
F
x 10 4 cells / ml
Wild type
ARMC9AB-KO
time (hours)
wild type in MEPP
ARMC9AB-KO in MEPP
G
number of cilia per μm of cell circumferance
WT
F-KO
C-KO
A-KO

Figure S7. The cortical presence of mating type proteins is affected by the loss of FAP256. SR-SIM images of wild type (A, C) and FAP256AB-KO cells (B, D) expressing either MTA4-GFP (A,B) or MTB4-GFP (C,D) based on engineering the native loci (scale bar: 20 μm).

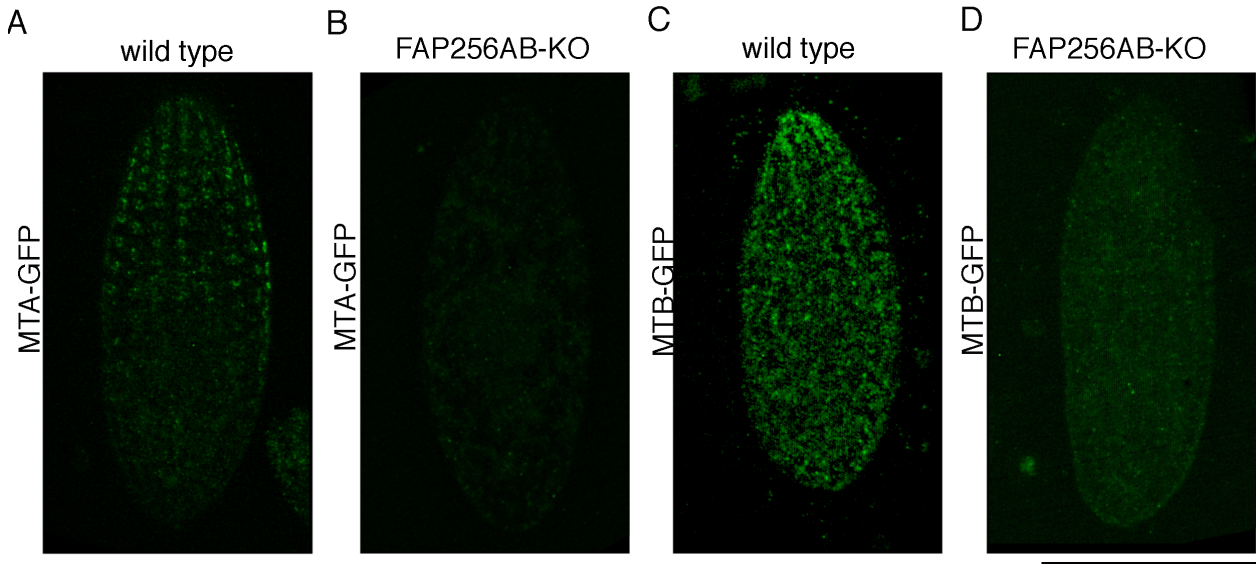
A
wild type
MTA-GFP
B
FAP256AB-KO
MTA-GFP
C
wild type
MTB-GFP
D
FAP256AB-KO
MTB-GFP

Figure S8. Imaging of beating cilia. (A) The areas containing the cell body (blue) and cilia (green) were marked at the first frame of a high speed movie and used to manually track the same cell over the course of the movie. Using a Matlab application the cilia area was extracted and unfolded. All cilia movies have the same orientation (left: anterior, middle: posterior, right: anterior area of the cell). (B) A representative still image of a movie representing the green area shown in A. The red line marks the position selected to create a kymograph. (C-E) Kymograph prepared from extracted cilia movies of wild type (C), FAP256-KO (D) and CHE12-KO (E) cells. The short diagonal lines represent single cilia as they move along the cell surface. The red arrow shows an example of a single beat cycle (A: anterior, P: posterior of the cell).

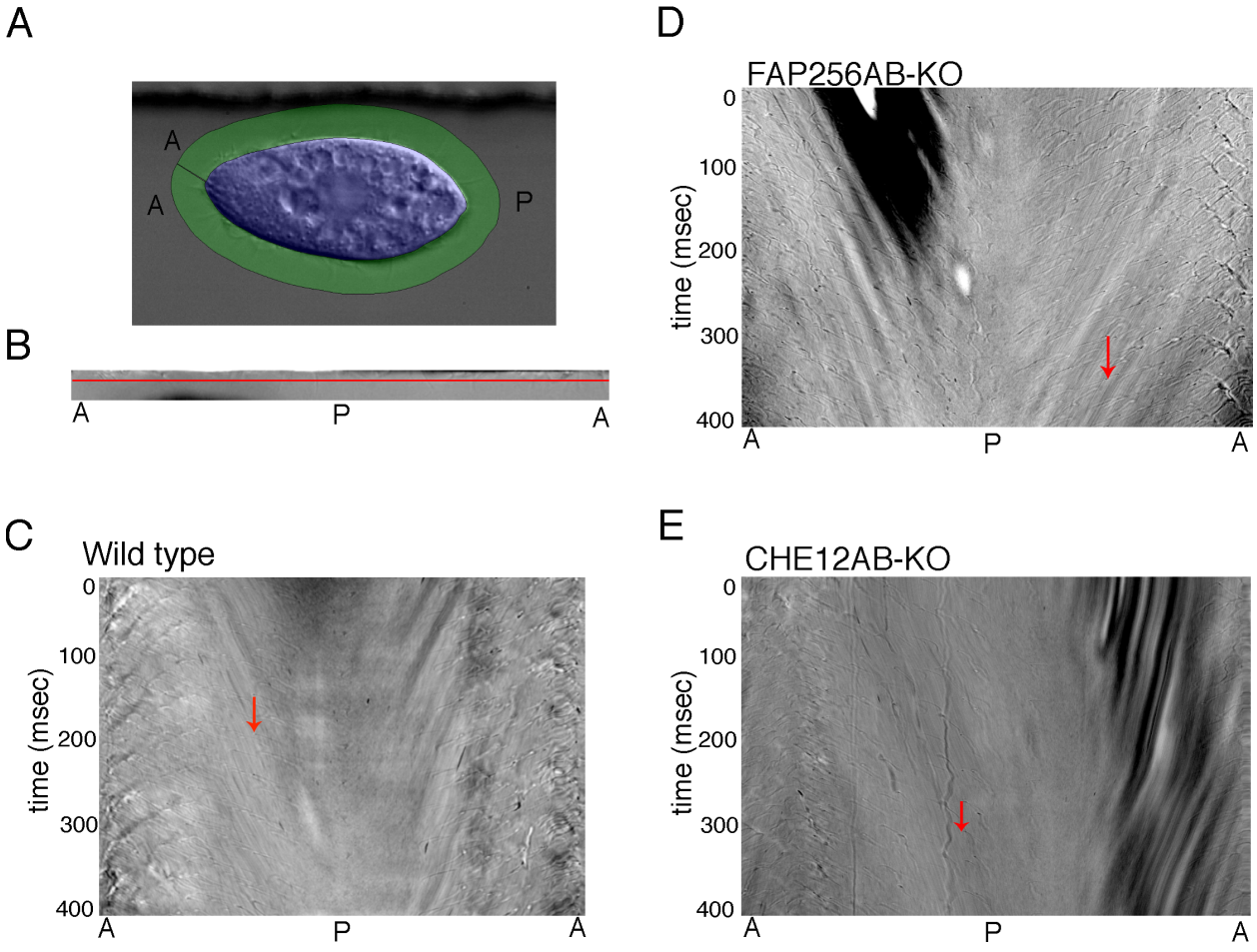
A
A
A
P
B
A
P
A
D
FAP256AB-KO
0
100
200
300
400
time (msec)
A
P
A
C
Wild type
0
100
200
300
400
time (msec)
A
P
A
E
CHE12AB-KO
0
100
200
300
400
time (msec)
A
P
A

Figure S9. A loss of ARMC9 causes infrequent structural defects in the middle segment. Representative cross section of a wild type cilium (A), and ARMC9-KO cilia showing missing outer dynein arms (B), a doublet that is 90^{o} rotated in relation to the CP (C) and a split doublet (D). Longitudinal sections showing areas of extensive bend (E-G) and collapsed outer doublets (H) (scale bar 200 nm).

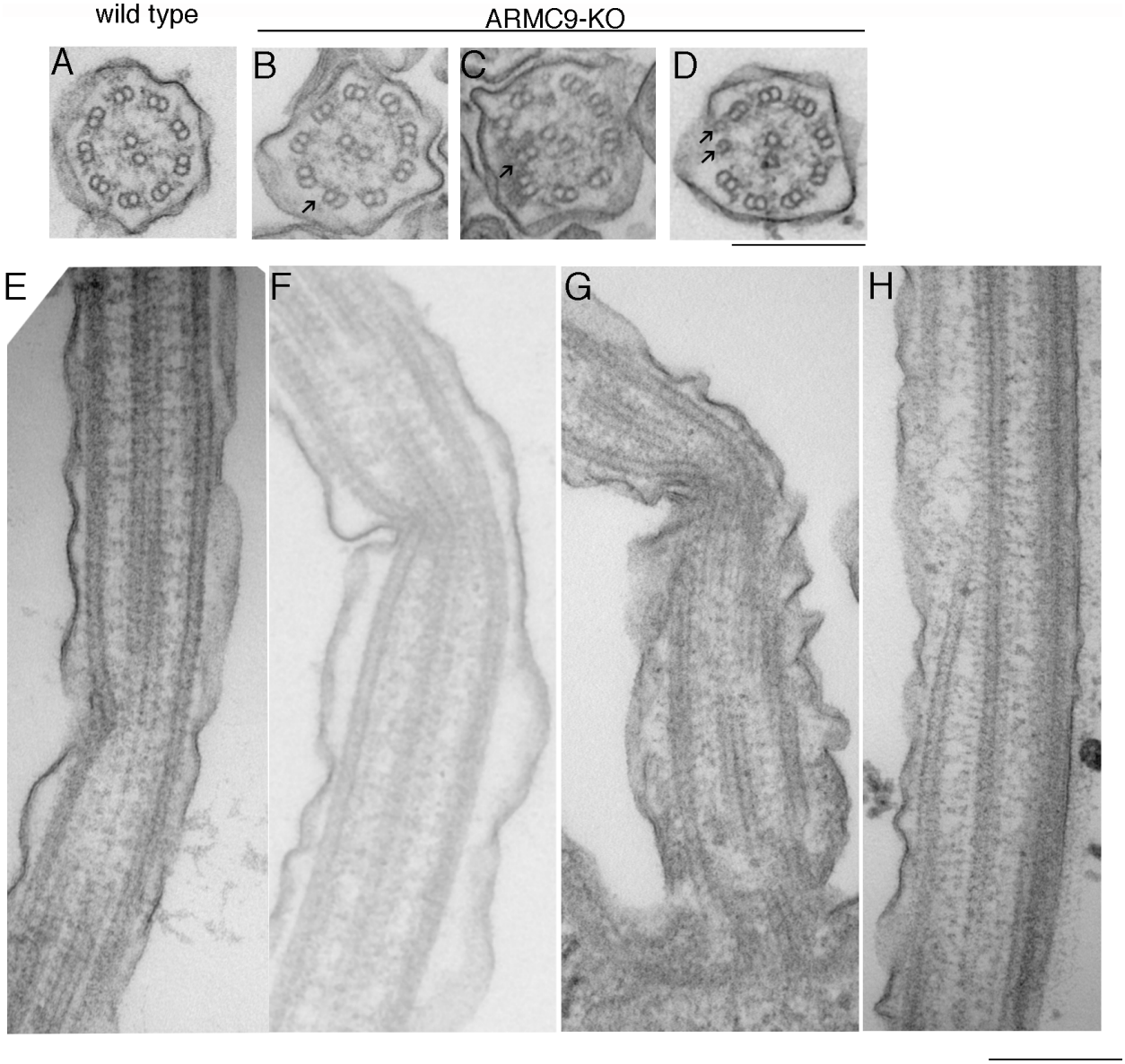
wild type
ARMC9-KO
A
B
C
D
E
F
G
H

Figure S10. The transition from middle to distal segment correlates with a decrease in the cilium diameter. Representative cross sections through the transition zone from doublets to singlets in wild type (A-C), and ARMC9-KO (D-F). Termination of the 96 nm repeat proteins correlates with the termination of B-tubules in wild type and knockout strains (Scale bar: 200 nm).

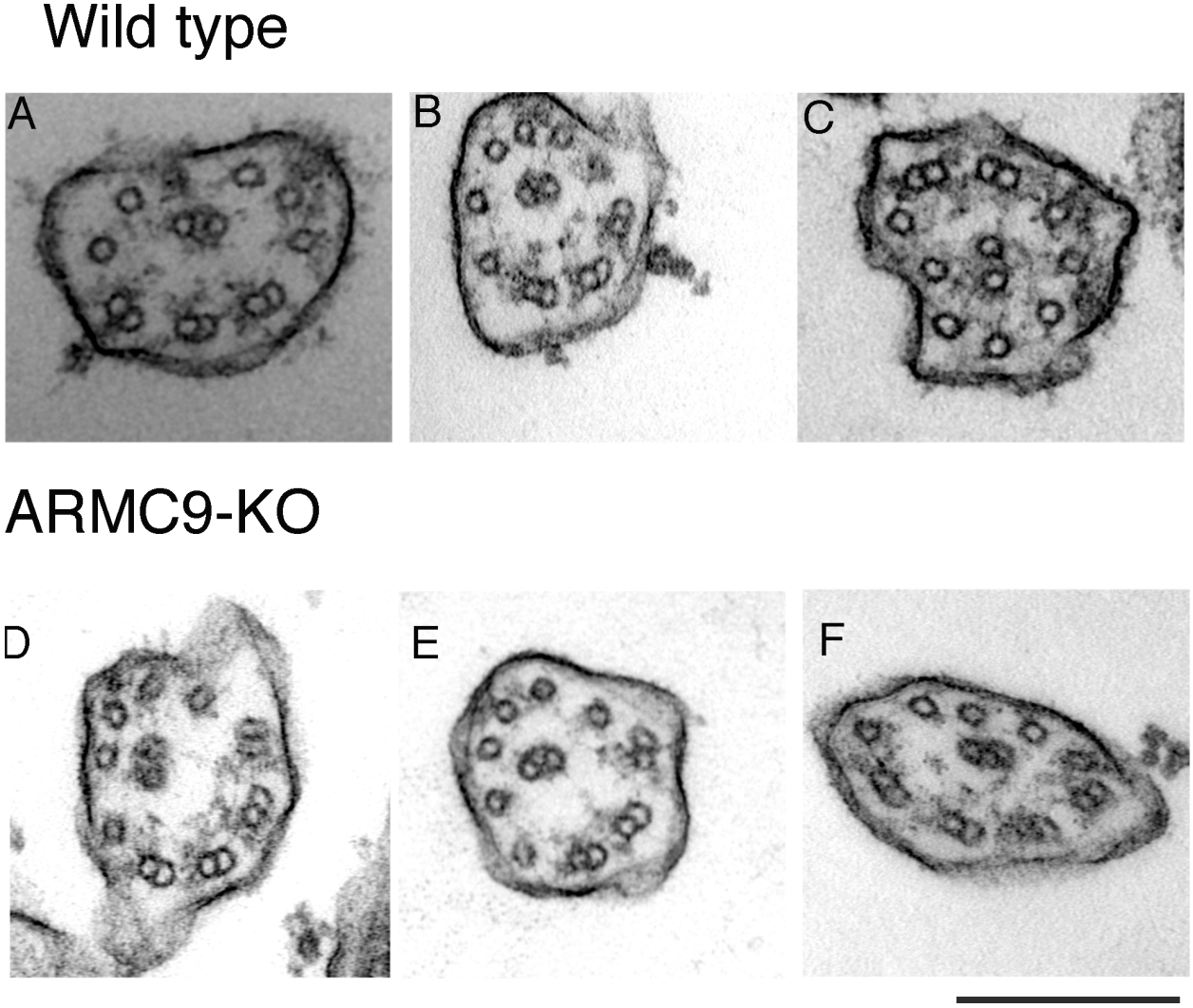
Wild type
A
B
C
ARMC9-KO
D
E
F

Figure S11. Overexpressed GFP-FAP256A forms long fibers in the cell body. Confocal immunofluorescence images of *Tetrahymena* cells expressing GFP-FAP256A under the control of the cadmium inducible promoter *MTT1*. Cells were fixed before transgene induction, three and six hrs after induction with 2.5 μg/ml $CdCl_2$ (green: GFP-FAP256A, blue: DAPI, red: α-tubulin, polyG and centrin).

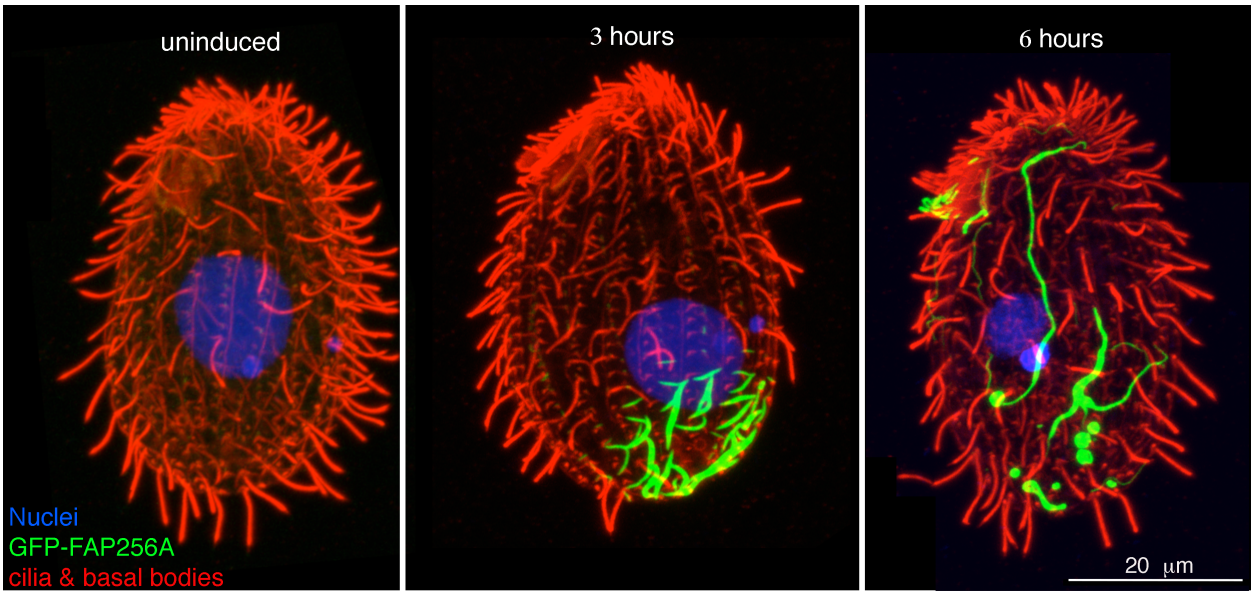
uninduced
3 hours
6 hours
Nuclei
GFP-FAP256A
cilia & basal bodies
20 μm

Supplementary Movies

Movie S1: A TIRFM movie of a cell expressing FAP256-GFP, notice the two adjacent FAP256 foci move together. Videos are played at 7 frames per second.

Movie S2: A TIRFM movie of a cell expressing CHE12B-mNeonGreen. Videos are played at 7 frames per second.

Movies S3-S6: High speed movies of wild-type (movie S3), FAP256-KO (movie S4), CHE12-KO (movie S5), and ARMC9-KO (movie S6) cells freely swimming in microfluidic channels. The movies were recorded at 2000 frames per second, the videos are played at 10 frames per second.

Multiple Sequence alignment

Multiple sequence alignment of CEP104/FAP256 was performed using ClustalW (Goujon et al., 2010; Larkin et al., 2007). The sequences used were *T*etrahymena *thermophila* gi|118365202, *Ichthyophthirius multifiliis* gi|471221679*, Paramecium tetraurelia* gi|145521394*, Oxytricha trifallax* gi|403345233*, Stylonychia lemnae* gi|678325194 and gi|678312996*, Saimiri boliviensis boliviensis* gi|725596390*, Physcomitrella patens* gi|168045131 and *Homo sapiens* AAH01640.1.

Multiplication rates of Tetrahymena strains

Growing cultures of wild-type and knockout strains were adjusted to 1x 10^4 cells/ml and cell concentration was measured after 3, 6, 9, 18, 24, 36 hrs (n = 3 independent experiments).

CHAPTER 3

CONCLUSIONS

My dissertation begun as a quest for the identification of proteins that make up the ciliary cap structures with an overarching goal of understanding the function of caps. This project was driven by our curiosity to find out why the ends of axonemal microtubules, which are the sites of microtubule and cilium length regulation, are capped. Our lab in collaboration with William Dentler (Kansas State University) who identified the caps in the early 80's, were pursuing this question for many years. We reasoned that *Tetrahymena* model may be ideal due to its large density of cilia and consequently of caps. From the beginning we knew that the project may be challenging as the cap components are predictive to represent only a small fraction of the total ciliary protein. To identify the cap proteins, William Dentler fractionated cilia under conditions that release the caps (in high magnesium chloride concentration) (Suprenant and Dentler, 1988) and the proteins in this fraction were identified by mass spectrometry. This approach generated a rather long list of cap candidates and previous lab members characterized some of these candidates, but have not identified any genuine cap components. On this list there were the two proteins, FAP256/CEP104 and CHE-12/Crescerin, predicted to have TOG domains. These two proteins attracted our attention because at that time other well studied TOG domain proteins (namely members of the Stu2/XMAP215 family) were known to recognize a curved tubulin conformation that is present at the plus end of microtubules. My contribution to this project was to determine if FAP256/CEP104 and CHE-12/Crescerin are components of the caps. As

described in Chapter 2, we found that both proteins localize to the tip of cilia, but they are not cap components, themselves. Out of the ~14 cap candidates examined in detail by our lab none of them turned out to be a cap protein, suggesting the biochemical fractionation based on the high salt extraction did not lead to a sufficient enrichment of cap proteins to enable their detection by mass spectrometry. We subsequently used a proximity biotinylation method (BioID) to label proteins at the tip of cilia in live cells. BioID utilizes a promiscuous biotin ligase as a protein tag (BirA*) that induces biotinylation of proteins within a 10 nm radius (Roux et al., 2012). We first delivered BirA* to the tip of cilia using FAP256/CEP104 that we earlier found to be located near the ends of complete axonemal microtubules, but this approach failed to identify any additional tip proteins, likely due to the low concentration of FAP256 at the tips of cilia. Next we delivered BirA* to the tip of cilia using an overproduced NRK2 kinase that extensively labels the tip area. NRK2 is a NIMA-related kinase that was shown by our lab to accumulate at the tip of cilia upon overexpression. A kinase dead version of the protein was used as bait in BioID to prevent cilia shortening that is associated with the activity of NRK2 (Wloga et al., 2006). This approach led to the identification of ARMC9, a ciliary-tip enriched protein, which turned out not to be a cap component either. However, by studying the localizations and functions of FAP256/CEP104, CHE-12 and ARMC9 we linked all of them to the ends of axonemal microtubules. Furthermore, we showed that the three proteins either elongate or trim the ends of axonemal microtubules and regulate the dimensions of the distal segment. Our studies led to significant discoveries related to the biogenesis and function of the distal segment in cilia.

All cilia studied to date have a distal segment, a compartment composed of only singlet microtubules, which has remained largely unstudied. The length of distal segment varies in

different species and types of cilia and several observations suggest a correlation between its length and sensory functions of cilia. FAP256/CEP104, CHE12/Crescerin and ARMC9 localize to the ends of different subsets of axonemal microtubules where they regulate microtubule length, and consequently, determine the distal segment geometry. By generating loss-of-function alleles, we discovered an unexpected role of the distal segment-associated proteins (and presumably the distal segment itself) in ciliary motility and cilia-based signaling. Mutations in two of the proteins we studied here, FAP256/CEP104 and ARMC9, cause a severe ciliopathy, Joubert syndrome. Thus, our work provides a link between the distal segment geometry and human disease.

FAP256/CEP104 was first identified as a binding partner and likely cargo of EB1 and was shown to localize to the distal end of centrioles (Jiang et al., 2012). In ciliated cells FAP256/CEP104 localizes to the daughter centriole and the tip of the cilium, near the ends of CP and outer doublets but its ciliary function was unclear (Satish Tammana et al., 2013). Specifically loss of FAP256 in *Chlamydomonas* and mammalian cultured cells reduced the ability of cells to make cilia or made them shorter. In *Chlamydomonas*, the tips of cilia of cells with an insertional mutation in the FAP256 gene are abnormally blunt, which suggest that the cap structures are missing. In addition in the absence of FAP256 (in *Chlamydomomas*), all axonemal microtubules are of about equal length and the motility associated 96 nm repeat proteins extend all the way to the end of the cilium (Satish Tammana et al., 2013). In humans mutations in CEP104 cause Joubert syndrome, a ciliopathy (Srour et al., 2015), suggesting that FAP256 has an important function in cilia. FAP256/CEP104 could be delivered to the tip of cilia by EB1 and maintained at the tip either through interaction with EB1 or in direct association with the microtubule plus-end. We asked if FAP256 contains any of the known microtubule binding

domains that cytoplasmic +TIP proteins utilize to interact with the microtubule plus-end. Using structural prediction software, we found that FAP256/CEP104 has a single TOG domain. During the course of our study, the crystal structure of FAP256/CEP104 TOG-domain was published, confirming our *in silico* structural predictions (Al-Jassar et al., 2017; Lenka Rezabkova, 2016). Therefore, similarly to the cytoplasmic microtubules (Ayaz et al., 2014; Ayaz et al., 2012; Fox et al., 2014; Leano et al., 2013; Widlund et al., 2011), TOG-domains may mediate protein binding to the plus-end of axonemal microtubules. CHE-12 is also a TOG domain protein and together with the mammalian orthologs comprise the Crescerins protein family (Das et al., 2015). Loss of CHE-12 shortens sensory cilia of *C. elegans* (Bacaj et al., 2008; Das et al., 2015; Perkins et al., 1986). Based on crystallography the TOG domains of CHE-12 bind to curved tubulin and *in vitro* single TOG domains promote microtubule polymerization, suggesting CHE-12 is a ciliary microtubule polymerase (Das et al., 2015). We showed that CHE-12 diffuses inside cilia and accumulates near the ends of B-tubules. The third protein we studied was ARMC9. Mutations in ARMC9 cause Joubert syndrome (Kar et al., 2018; Van De Weghe et al., 2017). In mammalian cells, ARMC9 localizes to basal body of the primary cilium and its loss reduces cilia density in zebra fish (Van De Weghe et al., 2017). We show that ARMC9 is a novel ciliary distal segment protein and it localizes to the ends of B-tubules. Thus, we identified one protein that localizes to the ends of complete tubules (FAP256/CEP104) and two proteins that localize to the ends of incomplete tubules (CHE-12 and ARMC9), showing that the ends of microtubule subtypes in cilia are biochemically distinct.

Recent cryo-EM analysis of the doublet structure showed that there is a difference in the local curvature between the A and B-tubule of the doublet (Ichikawa et al., 2017). This difference likely creates different tubulin interface on the outside and luminal surface of A and

B-tubules, which may contribute to the compartmentalization of ciliary MAPs, like FAP256/CEP104, CHE12 and ARMC9, to a subset of microtubules. One possibility is that TOG domains recognize conformational differences on different microtubule subtypes. TOG domains from different families share a common structure and tubulin interacting motifs, but their curvature varies. For example, TOG domains of the CLASP family proteins are more curved across the tubulin binding surface compared to the TOG domains of the XMAP215 family proteins, allowing them to bind to the relatively more curved plus-end of depolymerizing microtubules (Leano et al., 2013). Similarly, differences in the curvature of the tubulin binding surfaces of the TOG domains may provide the specificity to an axonemal microtubule subtype. Alternatively, the arrangement of the multiple TOG domains in CHE-12 may support selectivity for incomplete microtubules. Interestingly, overexpression of CHE-12 in cultured mammalian cells promotes microtubule bundling (Das et al., 2015). Thus, it is possible that CHE-12 mediates lateral microtubule interactions, for example, at the junction between the A and B-tubules. It is unclear how ARMC9 localizes to the ends of B-tubules. ARMC9 contains an N-terminal LisH domain and armadillo (ARM) repeats that are not known to be microtubule end binding domains. Therefore further work is needed to determine if ARMC9 localizes to the end of B-tubules directly or indirectly through interaction with other B-tubule end proteins. Typically, proteins that localize to the microtubule plus-end are involved in the regulation of microtubule dynamics or mediate linking of microtubule ends to other structures. One possibility is that FAP256/CEP104 links the A-tubules and CP to their caps.

To study the function of FAP256, CHE-12 and ARMC9, we created knockout strains in *Tetrahymena* lacking these proteins. Initial phenotypic analysis showed that all knockout strains swam slowly and had cilia-related deficiencies: (1) the loss of FAP256 inhibited pair formation

during mating (a process that involves cilia-based cell-cell signaling), and reduced ciliary beat frequency; (2) the loss of CHE-12 did not cause any detectable defects in cilia function; (3) the loss of ARMC9 severely affected ciliary motility and the oral cilia became non-functional and the posterior locomotory were almost completely paralyzed. The diversity of ciliary phenotypes shows that FAP256, CHE12 and ARMC9 have different molecular roles in cilia. To understand their function we explored each ciliary phenotype in greater detail.

We were surprised to find that cells lacking FAP256 failed to form pairs at the onset of conjugation. While the molecular mechanism of pair formation is not known, the experiments by Wolfe and Love demonstrated that pair formation depends on cell-to-cell communication through exchange of secreted signals of unknown nature (Love and Rotheim, 1984; Wolfe et al., 1979). Unpublished work from our lab also showed that cilia are essential for pair formation, as bald mutants never form pairs. We ruled out a possibility that pair formation is affected by the slow motility of FAP256-KO cells, by showing that mutants that swim slower and have fewer cilia form pairs with higher efficiency. To test if FAP256-KO cells are defective in cell-to-cell communication, we crossed wild type cells to FAP256-KO in the presence of wild type cells of the same mating type (mt IV) as FAP256-KO (50% wild type : 25% FAP256-KO : 25% wild type mt IV). In this "triple strain" mating experiment, the wild type cells provide the secreted signals required to stimulate pair formation, thus allowing us to test if FAP256 can respond to mating signals. We observed a ~50% mating efficiency in this experiment (compared to ~100% in the control), demonstrating that even in the presence of mating signals (contributed by wild type mt IV) FAP256-KO cells failed to form pairs. Therefore, we concluded that loss of FAP256 affects cell-to-cell communication. Successful mating involves a period of initiation that occurs under starvation (Bruns and Brussard, 1974). During this time cells undergo developmental

changes including changes in gene expression, shortening of some cilia and increase in cilia density. Two proteins, MTA and MTB, are expressed under starvation and are essential for mating. Different mating type cells express different variants of MTA and MTB that are generated by differential DNA level rearrangements (Cervantes et al., 2013). We failed to detect GFP tagged MTA and MTB in the FAP256-KO cells. However, the FAP256-KO cells develop a differentiated mating type because a small fraction of the population formed pairs with wild type cells of all mating types except mating type IV (indicating that this particular strain successfully rearranged the mating type loci and expressed a single mating type, specifically mating type IV). Preliminary results showed no change in the mRNA levels of MTA and MTB in FAP256-KO. To test further whether the FAP256-KO cells undergo a normal initiation for mating during starvation, we quantified the mRNA levels of another gene expressed only in starvation (NgoA) (Xiong et al., 2013), as well as measured the length and density of cilia under starvation. Preliminary results showed that the transcript levels of NgoA in starved FAP256-KO cells were higher than in the wild type cells (data not shown). Starved FAP256-KO cells were able to increase cilia density but shorten cilia by twice as much as the wild type did. Therefore, we show that the loss of FAP256 affects the developmental changes that occur under starvation including changes in gene expression and cilia length. Loss of FAP256 also led to loss of the CP cap (CMC), which may contribute to the mating defect. Even though the composition of the CP cap is not known, its elaborate structure including a spherical bead, two plates and helical filaments suggests that this is a multi-protein complex, and thus in the absence of FAP256 many more proteins are likely missing from cilia.

The loss of CMC in absence of FAP256 raised the possibility that FAP256 might be a part of the cap. However, FAP256 remains associated with axonemes under conditions that

solubilize the cap (Suprenant and Dentler, 1988) (our unpublished data). Furthermore, a small fraction of axonemes do assemble caps without FAP256. Therefore, FAP256 is unlikely to be part of the CMC, but it might be important for stabilizing the cap at the end of CP microtubules. FAP256 is also present at the ends of A-tubules. However, its loss did not affect the A-tubule caps, the DFs. This suggests that the CP and A-tubule caps are not only structurally different, but also differ on how they associate with the microtubule end. Stabilization of the CMC at the end of CP cannot be mediated exclusively through FAP256 since FAP256 is also present at the ends of A-tubules. This raises the possibility that the plus-ends of A-tubules and CP are also biochemically distinct.

To understand the cause of beat frequency defects in the knockout strains, we examined the cilium ultrastructure. Our collaborator Dorota Wloga (Nencki Institute of Experimental Biology of Polish Academy of Sciences) who performed TEM sectioning of cilia, noticed that in longitudinal sections, CHE12-KO cilia seemed to have an excessively long distal segment. This observation meant that we obtained mutants with defective distal segment dimensions that would allow us to explore the function of the distal segment. To investigate this observation further, we quantified the distal segment length in negatively stained whole cilia. The use of whole cilia (either isolated or on cells) for the length measurements allowed us to obtain rapidly a very large number of specimens that could be measured, in contrast to thin sections that rarely cover the entire distal segment. The proximal boundary of the distal segment is defined by the termination of B-tubules, which correlates with a decrease in the cilium diameter in wild type and knockout cilia. We also quantified the dimension of the A-tubule and CP region that are defined by the termination of A-tubules as well as the overall cilium length defined by the length of the CP. We found that in the absence of FAP256, cilia length is wild type but the distal segment is short. In

the absence of CHE12 cilia are shorter and have a longer distal segment. Whereas, in the absence of ARMC9 cilia are longer and have shorter distal segment compared to wild type. The decrease in the distal segment length in FAP256-KO cilia can be partially attributed to loss of the CP cap. Examinations of the A-tubule and CP region revealed that A-tubules are shorter in the absence of FAP256. Because FAP256 has a TOG domain similar to Stu2 TOG1 domain that is involved in microtubule polymerization (Ayaz et al., 2014; Ayaz et al., 2012; Brouhard et al., 2008) we asked if FAP256 acts as an A-tubule polymerase. Overexpression of FAP256 resulted in significant lengthening of the A-tubules, which in many cases terminated almost at the same level as the CP. No statistically significant increase in the distal segment length was observed. These observations indicate that FAP256/CEP104 acts as a polymerase for the A-tubules and the cap linker for the CP. Because CHE-12 and ARMC9 localize to the ends of B-tubules we hypothesized they are involved in the positive and negative regulation of B-tubule length, respectively. A role for CHE-12 as a B-tubule polymerase is supported by *in vitro* experiments demonstrating increased microtubule polymerization rate in the presence of CHE-12 TOG domains (Das et al., 2015). Overexpression of ARMC9 caused a dramatic elongation of the distal segment, which supports a role of ARMC9 in the shortening of B-tubules. Because ARMC9 lacks any known domains that affect microtubule dynamics, we hypothesize it is a regulatory molecule that induces the B-tubule depolymerization through either inhibition of assembly factors or activation of depolymerization factors. To test if ARMC9 induces B-tubule elongation through inhibition of CHE12 we deleted both proteins in the same cell. Combined loss of CHE-12 and ARMC9 resulted in an intermediate phenotype. Specifically, B-tubules in double knockout cilia were longer than wild type, but shorter than B-tubules in ARMC9-KO cilia. Thus, ARMC9 function does not depend entirely on CHE-12. Therefore the biochemical differences at

the plus-ends of complete and incomplete microtubules reflect the independent regulation of their dynamics and consequently of their length. This is a significant discovery showing that the independent regulation of microtubule dynamics may underline the mechanism that regulates the relative length of axonemal microtubules to establish the distal segment.

We also discovered a correlation between the B-tubule and the overall cilium length. CHE12-KO cells have shorter cilia and B-tubules, whereas ARMC9-KO cilia have longer cilia and B-tubules. This raises a possibility that the B-tubule length defect is secondary to the overall cilium length defect. However we showed that under conditions that lengthen and shorten cilia, the dimensions of the distal segment did not change. Thus, the cilium length defect observed in the absence of CHE-12 and ARMC9 is secondary to the B-tubule defects. This argues in favor of a role of B-tubules in the regulation of the overall cilium length. However, in the absence of both CHE-12 and ARMC9, cilia are wild type in length and have shorter distal segment (aka longer B-tubules). This result complicates our interpretation of the correlation between the B-tubule and cilium length. To test our hypothesis that the B-tubule length determines the overall cilium length we will overexpress CHE12 to induce elongation of B-tubules and test its effect on the overall cilium length. Our hypothesis is also supported by Kubo's finding that a decrease in poly-glutamylation due to loss of TTLL9 in *Chlamydomonas* reduced the rate of cilia disassembly and tubulin turnover without any effect on IFT (Kubo et al., 2015). Poly-glutamylation is mainly present on B-tubules ((Kubo et al., 2010; Lechtreck and Geimer, 2000; Suryavanshi et al., 2010) and our work, see chapter 2) and similar to our observations, showed that B-tubule defects affect the overall cilium length. To further explore the correlation between the B-tubule length and cilium length we will examine the distal segment geometry in mutants with abnormal B-tubule

PTMs and cilia length. For example, *Tetrahymena* cells overexpressing TTLL6 have hyperglutamylated and shorter cilia (Wloga et al., 2010).

Overall, our results support the presence of another layer in the cilium length regulation involving the regulation of axonemal microtubule dynamics. This idea has been proposed before based on evidence that depolymerizing kinesins such as Kif7 (He et al., 2014) and Kif19A (Niwa et al., 2012; Wang et al., 2016) affect the length of cilia likely through depolymerization of microtubules. However, it is not known if these kinesins depolymerize all axonemal microtubules or a specific subtype. Our work specifically links B-tubule length defects to the overall cilium length, which is not intuitive given that B-tubules are the shortest microtubules in cilia.

The most important question now is if there is a functional defect associated with changes in the distal segment length. Lengthening of the distal segment in CHE12-KO did not correlate with defects in cilia function. Surprisingly, shortening of the distal segment in FAP256-KO and ARMC9-KO correlated with reduced cilia beat frequency and altered waveform (in the case of ARMC9). However, FAP256-KO and ARMC9-KO cilia have similar distal segment dimensions, but ciliary motility is more severely affected in ARMC9-KO. Thus, the distal segment dimensions cannot solely explain the ciliary motility defects. Cilia beat frequency is dependent on the activity of outer dynein arms (Kamiya, 2002). We noticed that changes in the distal segment length correlated with changes in the length of 96 nm repeat proteins on A-tubules. Thus, it is intriguing that a shorter force producing middle segment does not compromise cilia function, whereas a longer force producing middle segment does. Electron microscopy did not reveal any detects in the presence of 96 nm repeat proteins in CHE12-KO and FAP256-KO cilia. However, the reduced motility in FAP256-KO could be due to loss of the CP cap, which was

speculated to be involved in cilia bend propagation (Mitchell, 2003; Omoto et al., 1999; Omoto and Kung, 1979, 1980). In addition to the short distal segment in ARMC9-KO cilia, we observed some infrequent structural abnormalities like loss of outer dynein arms, broken and translocate doublets. These defects could be caused by erroneous tubulin addition during the B-tubule assembly. Loss of outer dynein arms is intriguing because these proteins are attached to the A-tubule lattice, raising a possibility that structural defects on B-tubules may lead to loss of dynein arms from the A-tubule. However, these defects are rare and the main defect contributing to the reduced cilia beat frequency in ARMC9-KO remains unknown. Our results propose that shortening of the distal segment compromises ciliary motility. We will overexpress FAP256 in the ARMC9-KO background to induce lengthening of the A-tubules and test if restoring the length of the singlet A-tubule extensions in the absence of ARMC9 will partially rescue the motility defects. This will prove that the distal segment organization affects ciliary motility. In addition we will overexpress CHE12 to promote elongation of B-tubules and mimic the ARMC9-KO structural defect. If elongation of B-tubules in wild type background compromises ciliary motility, it will further support our finding that the distal segment geometry is involved in the regulation of cilia beat frequency.

The molecular mechanisms that regulate cilia beat frequency are not completely understood but it is known to involve sensory functions of motile cilia (Bloodgood, 2010). For example, bitter taste receptors localize to the tip of airway cilia and activate a signaling pathway leading to Ca^{2+} influx and increased ciliary beating for removing noxious substances from the airway (Shah et al., 2009). Signaling molecules that reduce cilia beat frequency have not yet been identified. We hypothesize that shortening of the distal segment may affect the localization of signaling proteins that regulate cilia beat frequency. Alternatively, proteins at the ends of

axonemal microtubules may serve as binding sites for signaling molecules. Cytoplasmic microtubules serve as docking sides for signaling molecules, which is essential for the organization of microtubule networks in response to stimuli (Janmey, 1998). In *C. elegans* mutations that affect the depolymerization of 15 protofilament microtubules in touch receptor neurons interfere with posttranscriptional regulation of proteins (Bounoutas et al., 2011). This is reminiscent of the effect of loss of FAP256 on MTA and MTB. As discussed earlier loss of FAP256 did not affect the mRNA levels of MTA and MTB. However, the proteins where undetected. Perhaps FAP256 or the structural defects caused by loss of FAP256 affect the localization or activity of proteins involved in postrascriptional regulation. Recently, it was shown that the microtubule plus end binding protein Kif7 retains G-protein coupled receptors at the tip of cilia upon pathway activation (Ye et al., 2018). In analogy to this, it is possible that loss of FAP256 and ARMC9 may affect the localization of signaling molecules involved in cilia beat frequency.

Our observation of an inverse correlation between the distal segment length and length of 96 nm repeat proteins on the A-tubule is intriguing. It shows that the doublet portion of A-tubules is different from the singlet portion. Recently, the first cryo-EM study of the singlet A-tubule region reported the presence of different luminal structures in the A-tubule singlet and doublet region in human sperm flagellum (Zabeo et al., 2018) providing further evidence for the longitudinal compartmentalization of A-tubules. Since 96 nm repeat proteins interact with CP projections to power cilia beating, we asked if CP projections are also restricted to the middle segment. Hydin, a CP projection protein was shown by immunogold to be present along the CP but did not label its distal end (Lechtreck and Witman, 2007). Fluorescently tagged hydin and PF16 (a CP projection protein), co-localize with polyG (Mayukh Guha and JG unpublished

data), which labels only the middle segment and thus marks the length of B-tubules (our study and (Kubo et al., 2010; Lechtreck and Geimer, 2000; Suryavanshi et al., 2010)). Thus, we conclude that CP projections are also limited to the middle segment and we propose that B-tubules organize the motility machinery of cilia.

To test if the function of FAP256, CHE12 and ARMC9 in motile cilia of a protist is conserved in animal cilia, we took advantage of an existing *C. elegans* mutant strain expressing truncated CHE12 (Bacaj et al., 2008). GFP tagged CHE-12 showed punctate localization in *C. elegans* cilia and mammalian cells *in vitro* (Bacaj et al., 2008; Das et al., 2015). We showed in *Tetrahymena* that the punctate localization of CHE12 along the cilium is due to its diffusion inside cilia (chapter 2). It was previously shown that GFP tagged CHE-12 did not localize to *C. elegans* cilia in some IFT mutants, and although IFT like movement of CHE-12 was not observed inside cilia of wild type animals, the authors proposed that CHE-12 may partially require IFT for its localization (Bacaj et al., 2008). However, the lack of CHE-12 detection in IFT mutant cilia could be due to the structural defects caused by loss of IFT. For example, amphid cilia are extremely short in *osm-5* mutants (Bacaj et al., 2008; Haycraft et al., 2001). An accumulation of CHE-12 near the ends of B-tubules was not detected in mammalian cells and *C. elegans* cilia (Bacaj et al., 2008; Das et al., 2015). However, this could be due to the low-resolution imaging used in these studies. We showed that mutations in CHE-12 cause shortening of both the middle and distal segment in phasmid sensory cilia of *C. elegans*. Loss of CHE-12 in both *C. elegans* and *Tetrahymena* shortened both the A and B-tubules. Therefore, our results confirmed a conserved function of CHE12 in the regulation of B-tubule length. Further examination of the function of FAP256 and ARMC9 in the sensory cilia of *C. elegans* will be

done using an existing FAP256 mutant strain and creating an ARMC9 knockout strain using CRISPR.

FAP256 and ARMC9 are mutated in the human ciliopathy Joubert syndrome (Srour et al., 2015; Van De Weghe et al., 2017). Joubert syndrome is an autosomal recessive disease with mainly neurological defects. Almost all known Joubert syndrome proteins are ciliary proteins that localize either to the basal body, transition zone or the tip of cilia. None of the known Joubert syndrome proteins are motility-associated proteins suggesting that defects in primary cilia function cause Joubert syndrome. Primary cilia in the brain are involved in the regulation of cell cycle progression, Hedgehog and WNT signaling, which are essential for brain development (Youn and Han, 2018). Since many functionally diverse proteins cause the same disease phenotype, it is likely that loss of each protein may converge to the same functional deficit. Only Hedgehog signaling has been linked to the tip of cilia (Haycraft et al., 2005; Liem et al., 2009; Tukachinsky et al., 2010). Our work links two Joubert syndrome proteins to the ends of specific microtubules in cilia and suggests that structural defects at the distal segment may cause Joubert syndrome. Our hypothesis is supported by the phenotype of loss of Kif7 (He et al., 2014) and KIAA0556 (Sanders et al., 2015), two additional Joubert syndrome proteins that localize to the distal segment of cilia. Kif7 is likely a +TIP microtubule depolymerase, the loss of which results in formation of longer cilia with structural defects at the tip and defects in Hedgehog signaling (He et al., 2014). KIAA0556 is a protein that likely binds to and stabilizes microtubules and in its absence cilia become longer and have structural abnormalities that resemble ARMC9-KO defects in *Tetrahymena,* such as presence of doublets within the distal segment indicative of longer B-tubules (Sanders et al., 2015). Taken together, we propose that defects in the distal segment geometry may underline at least a subset of the Joubert syndrome pathology. It is not

unreasonable to consider that even in the cases of mutations of proteins of the basal body or transition zone the direct cause of the JS pathology is a dysfunction of the distal segment. For example, a defect in the transition zone could lead to an abnormal content of the distal segment proteins, which in turn could affect its properties. In the future it will be of interest to examine the distal segment in cilia of JS patients carrying mutations in proteins that normally are not enriched at the ciliary tip.

Although in this study we did not identify any cap proteins, we created a mutant that lacks the CP cap and showed that it is not essential for CP assembly and ciliary motility. Thus the quest for the identification of cap components continues and perhaps should be focused on the DFs. However, my dissertation work led to a number of different findings including the discovery of the independent regulation of the dynamics of complete and incomplete microtubules and consequently their length, a novel role of the distal segment in ciliary motility and implication of the distal segment geometry in Joubert syndrome. We also brought B-tubules to the spotlight by showing that they orchestrate the motility machinery of cilia and that their length correlates with the overall cilium length. In addition to new findings, our work raised many questions for the future. One of the most important questions is how the length of B-tubules affects the overall cilium length. How cells regulate the size of their organelles is a fundamental question in cellular biology. The cilia field is heavily invested in addressing these questions by utilizing the easily quantifiable length of cilia. Most of the research on cilia length regulation is focused on understanding the function of IFT that regulates the quantity of tubulin in cilia (Craft et al., 2015) and very little is known about the ability of microtubules to respond to changes in tubulin levels. Our finding that the dynamics of complete and incomplete microtubules are independently regulated to determine their length and subsequently the length

of cilia paves the road for future research in exploring the role of microtubule dynamics in cilia length regulation. We provide candidates for forward genetic screens to identify additional components of the regulation of microtubule dynamics in cilia. For example, CHE-12 mutants in *C. elegans* are dye-filling defective and a suppressor can potentially be selected based on the reversal of dye-filling defect. This can lead to the identification of proteins that promote B-tubule depolymerization. We can also perform a suppressor screen for ARMC9-KO in *Tetrahymena* by selecting mutants with a normal growth rate. A suppressor screen for ARMC9-KO can lead to the identification of proteins that affect microtubule dynamics and are regulated by ARMC9. Such candidates can be used to manipulate the length of B-tubules and test its effect on the overall cilium length. Our lab has recently worked out the methodology needed for identification of genetic interactors in Tetrahymena and the paper describing the first genetic suppressor in this model is under review (Yuyang Jiang and JG).

Another question of clinical importance is how changes in the length of distal segment cause Joubert syndrome. Loss of two out of the four distal segment proteins that cause Joubert syndrome also cause defects in Hedgehog signaling (Breslow et al., 2017; He et al., 2014). It remains to be tested if loss of FAP256 and KIAA0556 also affect Hedgehog signaling. We hypothesize that proteins at the ends of microtubules or proteins that localize within the distal segment are important for the localization and activation of signaling proteins in primary cilia. Our work provides tools to further explore biochemically the composition of the distal segment in order to address its function and the importance of compartmentalization in cilia.

References

Afzelius, B.A. (1976). A human syndrome caused by immotile cilia. Science (New York, NY) *193*, 317-319.

Akhmanova, A., and Steinmetz, M.O. (2008). Tracking the ends: a dynamic protein network controls the fate of microtubule tips. Nature reviews Molecular cell biology *9*, 309-322.

Akhmanova, A., and Steinmetz, M.O. (2010). Microtubule +TIPs at a glance. Journal of cell science *123*, 3415-3419.

Akhmanova, A., and Steinmetz, M.O. (2015). Control of microtubule organization and dynamics: two ends in the limelight. Nature reviews Molecular cell biology *16*, 711-726.

Al-Bassam, J., and Chang, F. (2011). Regulation of microtubule dynamics by TOG-domain proteins XMAP215/Dis1 and CLASP. Trends in cell biology *21*, 604-614.

Al-Bassam, J., Larsen, N.A., Hyman, A.A., and Harrison, S.C. (2007). Crystal structure of a TOG domain: conserved features of XMAP215/Dis1-family TOG domains and implications for tubulin binding. Structure (London, England : 1993) *15*, 355-362.

Al-Jassar, C., Andreeva, A., Barnabas, D.D., McLaughlin, S.H., Johnson, C.M., Yu, M., and van Breugel, M. (2017). The Ciliopathy-Associated Cep104 Protein Interacts with Tubulin and Nek1 Kinase. Structure (London, England : 1993) *25*, 146-156.

Aldaz, H., Rice, L.M., Stearns, T., and Agard, D.A. (2005). Insights into microtubule nucleation from the crystal structure of human gamma-tubulin. Nature *435*, 523-527.

Alushin, G.M., Lander, G.C., Kellogg, E.H., Zhang, R., Baker, D., and Nogales, E. (2014). High-resolution microtubule structures reveal the structural transitions in alphabeta-tubulin upon GTP hydrolysis. Cell *157*, 1117-1129.

Alushin, G.M., Ramey, V.H., Pasqualato, S., Ball, D.A., Grigorieff, N., Musacchio, A., and Nogales, E. (2010). The Ndc80 kinetochore complex forms oligomeric arrays along microtubules. Nature *467*, 805-810.

Ayaz, P., Munyoki, S., Geyer, E.A., Piedra, F.A., Vu, E.S., Bromberg, R., Otwinowski, Z., Grishin, N.V., Brautigam, C.A., and Rice, L.M. (2014). A tethered delivery mechanism explains the catalytic action of a microtubule polymerase. eLife *3*, e03069.

Ayaz, P., Ye, X., Huddleston, P., Brautigam, C.A., and Rice, L.M. (2012). A TOG:alphabeta-tubulin complex structure reveals conformation-based mechanisms for a microtubule polymerase. Science (New York, NY) *337*, 857-860.

Bacaj, T., Lu Y Fau - Shaham, S., and Shaham, S. (2008). The conserved proteins CHE-12 and DYF-11 are required for sensory cilium function in Caenorhabditis elegans.

Berman, S.A., Wilson, N.F., Haas, N.A., and Lefebvre, P.A. (2003). A novel MAP kinase regulates flagellar length in Chlamydomonas. Current biology : CB *13*, 1145-1149.

Bloodgood, R.A. (2010). Sensory reception is an attribute of both primary cilia and motile cilia. Journal of cell science *123*, 505-509.

Bounoutas, A., Kratz, J., Emtage, L., Ma, C., Nguyen, K.C., and Chalfie, M. (2011). Microtubule depolymerization in Caenorhabditis elegans touch receptor neurons reduces gene expression through a p38 MAPK pathway. Proceedings of the National Academy of Sciences of the United States of America *108*, 3982-3987.

Bower, R., Tritschler, D., Vanderwaal, K., Perrone, C.A., Mueller, J., Fox, L., Sale, W.S., and Porter, M.E. (2013). The N-DRC forms a conserved biochemical complex that maintains outer doublet alignment and limits microtubule sliding in motile axonemes. Molecular biology of the cell *24*, 1134-1152.

Bowne-Anderson, H., Hibbel, A., and Howard, J. (2015). Regulation of Microtubule Growth and Catastrophe: Unifying Theory and Experiment. Trends in cell biology *25*, 769-779.

Brenner, S. (1974). The genetics of Caenorhabditis elegans. Genetics *77*, 71-94.

Breslow, D.K., Hoogendoorn, S., Kopp, A.R., Morgens, D.W., Vu, B.K., Han, K., Li, A., Hess, G.T., Bassik, M.C., Chen, J.K.*, et al.* (2017). A comprehensive portrait of cilia and ciliopathies from a CRISPR-based screen for Hedgehog signaling. bioRxiv.

Briggs, L.J., Davidge, J.A., Wickstead, B., Ginger, M.L., and Gull, K. (2004). More than one way to build a flagellum: comparative genomics of parasitic protozoa. Current biology : CB *14*, R611-612.

Brokaw, C.J., and Kamiya, R. (1987). Bending patterns of Chlamydomonas flagella: IV. Mutants with defects in inner and outer dynein arms indicate differences in dynein arm function. Cell motility and the cytoskeleton *8*, 68-75.

Brouhard, G.J., Stear, J.H., Noetzel, T.L., Al-Bassam, J., Kinoshita, K., Harrison, S.C., Howard, J., and Hyman, A.A. (2008). XMAP215 is a processive microtubule polymerase. Cell *132*, 79-88.

Brownell, J.E., Zhou, J., Ranalli, T., Kobayashi, R., Edmondson, D.G., Roth, S.Y., and Allis, C.D. (1996). Tetrahymena histone acetyltransferase A: a homolog to yeast Gcn5p linking histone acetylation to gene activation. Cell *84*, 843-851.

Bruns, P.J., and Brussard, T.B. (1974). Pair formation in tetrahymena pyriformis, an inducible developmental system. The Journal of experimental zoology *188*, 337-344.

Calzone, F.J., and Gorovsky, M.A. (1982). Cilia regeneration in Tetrahymena. A simple reproducible method for producing large numbers of regenerating cells. Exp Cell Res *140*, 471-476.

Carlier, M.F., and Pantaloni, D. (1981). Kinetic analysis of guanosine 5'-triphosphate hydrolysis associated with tubulin polymerization. Biochemistry *20*, 1918-1924.

Cassidy-Hanley, D., Bowen, J., Lee, J.H., Cole, E., VerPlank, L.A., Gaertig, J., Gorovsky, M.A., and Bruns, P.J. (1997). Germline and somatic transformation of mating Tetrahymena thermophila by particle bombardment. Genetics *146*, 135-147.

Cassimeris, L., Pryer, N.K., and Salmon, E.D. (1988). Real-time observations of microtubule dynamic instability in living cells. The Journal of cell biology *107*, 2223-2231.

Cervantes, M.D., Hamilton, E.P., Xiong, J., Lawson, M.J., Yuan, D., Hadjithomas, M., Miao, W., and Orias, E. (2013). Selecting one of several mating types through gene segment joining and deletion in Tetrahymena thermophila. PLoS biology *11*, e1001518.

Chalfie, M., and Thomson, J.N. (1982). Structural and functional diversity in the neuronal microtubules of Caenorhabditis elegans. The Journal of cell biology *93*, 15-23.

Chang, P., Giddings, T.H., Jr., Winey, M., and Stearns, T. (2003). Epsilon-tubulin is required for centriole duplication and microtubule organization. Nature cell biology *5*, 71-76.

Chang, P., and Stearns, T. (2000). Delta-tubulin and epsilon-tubulin: two new human centrosomal tubulins reveal new aspects of centrosome structure and function. Nature cell biology *2*, 30-35.

Chretien, D., Metoz, F., Verde, F., Karsenti, E., and Wade, R.H. (1992). Lattice defects in microtubules: protofilament numbers vary within individual microtubules. The Journal of cell biology *117*, 1031-1040.

Cole, D.G., Diener Dr Fau - Himelblau, A.L., Himelblau Al Fau - Beech, P.L., Beech Pl Fau - Fuster, J.C., Fuster Jc Fau - Rosenbaum, J.L., and Rosenbaum, J.L. (1998). Chlamydomonas kinesin-II-dependent intraflagellar transport (IFT): IFT particles contain proteins required for ciliary assembly in Caenorhabditis elegans sensory neurons.

Comartin, D., Gupta, G.D., Fussner, E., Coyaud, E., Hasegan, M., Archinti, M., Cheung, S.W., Pinchev, D., Lawo, S., Raught, B.*, et al.* (2013). CEP120 and SPICE1 cooperate with CPAP in centriole elongation. Current biology : CB *23*, 1360-1366.

Couvillion, M.T., and Collins, K. (2012). Biochemical approaches including the design and use of strains expressing epitope-tagged proteins. Methods in cell biology *109*, 347-355.

Craft, J.M., Harris, J.A., Hyman, S., Kner, P., and Lechtreck, K.F. (2015). Tubulin transport by IFT is upregulated during ciliary growth by a cilium-autonomous mechanism. The Journal of cell biology *208*, 223-237.

Cullen, C.F., Deak, P., Glover, D.M., and Ohkura, H. (1999). mini spindles: A gene encoding a conserved microtubule-associated protein required for the integrity of the mitotic spindle in Drosophila. The Journal of cell biology *146*, 1005-1018.

Dafinger, C., Liebau, M.C., Elsayed, S.M., Hellenbroich, Y., Boltshauser, E., Korenke, G.C., Fabretti, F., Janecke, A.R., Ebermann, I., Nurnberg, G.*, et al.* (2011). Mutations in KIF7 link Joubert syndrome with Sonic Hedgehog signaling and microtubule dynamics. The Journal of clinical investigation *121*, 2662-2667.

Das, A., Dickinson, D.J., Wood, C.C., Goldstein, B., and Slep, K.C. (2015). Crescerin uses a TOG domain array to regulate microtubules in the primary cilium. Molecular biology of the cell *26*, 4248-4264.

Dave, D., Wloga, D., and Gaertig, J. (2009). Manipulating ciliary protein-encoding genes in Tetrahymena thermophila. Methods in cell biology *93*, 1-20.

Dawson, S.C., Sagolla, M.S., Mancuso, J.J., Woessner, D.J., House, S.A., Fritz-Laylin, L., and Cande, W.Z. (2007). Kinesin-13 regulates flagellar, interphase, and mitotic microtubule dynamics in Giardia intestinalis. Eukaryotic cell *6*, 2354-2364.

de Forges, H., Pilon, A., Cantaloube, I., Pallandre, A., Haghiri-Gosnet, A.M., Perez, F., and Pous, C. (2016). Localized Mechanical Stress Promotes Microtubule Rescue. Current biology : CB *26*, 3399-3406.

Dentler, W.L. (1980). Structures linking the tips of ciliary and flagellar microtubules to the membrane. Journal of cell science *42*, 207-220.

Dentler, W.L. (1984). Attachment of the cap to the central microtubules of Tetrahymena cilia. Journal of cell science *66*, 167-173.

Dentler, W.L., and Rosenbaum, J.L. (1977). Flagellar elongation and shortening in Chlamydomonas. III. structures attached to the tips of flagellar microtubules and their relationship to the directionality of flagellar microtubule assembly. The Journal of cell biology *74*, 747-759.

Desai, A., and Mitchison, T.J. (1997). Microtubule polymerization dynamics. Annual review of cell and developmental biology *13*, 83-117.

Dimitrov, A., Quesnoit, M., Moutel, S., Cantaloube, I., Pous, C., and Perez, F. (2008). Detection of GTP-tubulin conformation in vivo reveals a role for GTP remnants in microtubule rescues. Science (New York, NY) *322*, 1353-1356.

Duan, J., and Gorovsky, M.A. (2002). Both carboxy-terminal tails of alpha- and beta-tubulin are essential, but either one will suffice. Current biology : CB *12*, 313-316.

Dupuis-Williams, P., Fleury-Aubusson, A., de Loubresse, N.G., Geoffroy, H., Vayssie, L., Galvani, A., Espigat, A., and Rossier, J. (2002). Functional role of epsilon-tubulin in the assembly of the centriolar microtubule scaffold. The Journal of cell biology *158*, 1183-1193.

Dutcher, S.K., Morrissette, N.S., Preble, A.M., Rackley, C., and Stanga, J. (2002). Epsilon-tubulin is an essential component of the centriole. Molecular biology of the cell *13*, 3859-3869.

Dutcher, S.K., and Trabuco, E.C. (1998). The UNI3 gene is required for assembly of basal bodies of Chlamydomonas and encodes delta-tubulin, a new member of the tubulin superfamily. Molecular biology of the cell *9*, 1293-1308.

Endoh-Yamagami, S., Evangelista, M., Wilson, D., Wen, X., Theunissen, J.W., Phamluong, K., Davis, M., Scales, S.J., Solloway, M.J., de Sauvage, F.J.*, et al.* (2009). The mammalian Cos2 homolog Kif7 plays an essential role in modulating Hh signal transduction during development. Current biology : CB *19*, 1320-1326.

Euteneuer, U., and McIntosh, J.R. (1980). Polarity of midbody and phragmoplast microtubules. The Journal of cell biology *87*, 509-515.

Fawcett, D.W.a., and Porter, K.R. (1954). A study of the fine structure of ciliated epithelia. J Morphol *94*, 221-281.

Fisch, C., and Dupuis-Williams, P. (2011). Ultrastructure of cilia and flagella - back to the future! Biology of the cell / under the auspices of the European Cell Biology Organization *103*, 249-270.

Fox, J.C., Howard, A.E., Currie, J.D., Rogers, S.L., and Slep, K.C. (2014). The XMAP215 family drives microtubule polymerization using a structurally diverse TOG array. Molecular biology of the cell *25*, 2375-2392.

Funfak, A., Fisch, C., Abdel Motaal, H.T., Diener, J., Combettes, L., Baroud, C.N., and Dupuis-Williams, P. (2014). Paramecium swimming and ciliary beating patterns: a study on four RNA interference mutations. Integrative biology : quantitative biosciences from nano to macro.

Gadadhar, S., Bodakuntla, S., Natarajan, K., and Janke, C. (2017). The tubulin code at a glance. Journal of cell science *130*, 1347-1353.

Gaertig, J., Gu, L., Hai, B., and Gorovsky, M.A. (1994). High frequency vector-mediated transformation and gene replacement in Tetrahymena. Nucleic acids research *22*, 5391-5398.

Gaertig, J., Wloga, D., Vasudevan, K.K., Guha, M., and Dentler, W. (2013). Discovery and functional evaluation of ciliary proteins in Tetrahymena thermophila. Methods in enzymology *525*, 265-284.

Garcia-Gonzalo, F.R., and Reiter, J.F. (2017). Open Sesame: How Transition Fibers and the Transition Zone Control Ciliary Composition. Cold Spring Harbor perspectives in biology *9*.

Gardner, M.K., Zanic, M., Gell, C., Bormuth, V., and Howard, J. (2011). Depolymerizing kinesins Kip3 and MCAK shape cellular microtubule architecture by differential control of catastrophe. Cell *147*, 1092-1103.

Garreau de Loubresse, N., Ruiz, F., Beisson, J., and Klotz, C. (2001). Role of delta-tubulin and the C-tubule in assembly of Paramecium basal bodies. BMC cell biology *2*, 4.

Gibbons, I.R., and Rowe, A.J. (1965). Dynein: A Protein with Adenosine Triphosphatase Activity from Cilia. Science (New York, NY) *149*, 424-426.

Goodwin, S.S., and Vale, R.D. (2010). Patronin regulates the microtubule network by protecting microtubule minus ends. Cell *143*, 263-274.

Gorovsky, M.A. (1973). Macro- and micronuclei of Tetrahymena pyriformis: a model system for studying the structure and function of eukaryotic nuclei. J Protozool *20*, 19-25.

Goshima, G., Wollman, R., Stuurman, N., Scholey, J.M., and Vale, R.D. (2005). Length control of the metaphase spindle. Current biology : CB *15*, 1979-1988.

Goujon, M., McWilliam, H., Li, W., Valentin, F., Squizzato, S., Paern, J., and Lopez, R. (2010). A new bioinformatics analysis tools framework at EMBL–EBI. Nucleic acids research *38*, W695-W699.

Greider, C.W., and Blackburn, E.H. (1985). Identification of a specific telomere terminal transferase activity in Tetrahymena extracts. Cell *43*, 405-413.

Guichard, P., Hamel, V., and Gonczy, P. (2018). The Rise of the Cartwheel: Seeding the Centriole Organelle. BioEssays : news and reviews in molecular, cellular and developmental biology.

Hai, B., Gaertig, J., and Gorovsky, M.A. (2000). Knockout heterokaryons enable facile mutagenic analysis of essential genes in Tetrahymena. Methods in cell biology *62*, 513-531.

Han, Y.G., Kwok, B.H., and Kernan, M.J. (2003). Intraflagellar transport is required in Drosophila to differentiate sensory cilia but not sperm. Current biology : CB *13*, 1679-1686.

Harris, J.A., Liu, Y., Yang, P., Kner, P., and Lechtreck, K.F. (2016). Single-particle imaging reveals intraflagellar transport-independent transport and accumulation of EB1 in Chlamydomonas flagella. Molecular biology of the cell *27*, 295-307.

Haycraft, C.J., Banizs, B., Aydin-Son, Y., Zhang, Q., Michaud, E.J., and Yoder, B.K. (2005). Gli2 and Gli3 localize to cilia and require the intraflagellar transport protein polaris for processing and function. PLoS genetics *1*, e53.

Haycraft, C.J., Swoboda, P., Taulman, P.D., Thomas, J.H., and Yoder, B.K. (2001). The C. elegans homolog of the murine cystic kidney disease gene Tg737 functions in a ciliogenic pathway and is disrupted in osm-5 mutant worms. Development *128*, 1493-1505.

He, M., Subramanian, R., Bangs, F., Omelchenko, T., Liem, K.F., Jr., Kapoor, T.M., and Anderson, K.V. (2014). The kinesin-4 protein Kif7 regulates mammalian Hedgehog signalling by organizing the cilium tip compartment. Nature cell biology *16*, 663-672.

Hilton, L.K., Gunawardane, K., Kim, J.W., Schwarz, M.C., and Quarmby, L.M. (2013). The kinases LF4 and CNK2 control ciliary length by feedback regulation of assembly and disassembly rates. Current biology : CB *23*, 2208-2214.

Hoyle, H.D., Turner, F.R., and Raff, E.C. (2008). Axoneme-dependent tubulin modifications in singlet microtubules of the Drosophila sperm tail. Cell motility and the cytoskeleton *65*, 295-313.

Huang, B., Piperno, G., and Luck, D.J. (1979). Paralyzed flagella mutants of Chlamydomonas reinhardtii. Defective for axonemal doublet microtubule arms. The Journal of biological chemistry *254*, 3091-3099.

Huangfu, D., Liu, A., Rakeman, A.S., Murcia, N.S., Niswander, L., and Anderson, K.V. (2003). Hedgehog signalling in the mouse requires intraflagellar transport proteins. Nature *426*, 83-87.

Hyman, A.A., Salser, S., Drechsel, D.N., Unwin, N., and Mitchison, T.J. (1992). Role of GTP hydrolysis in microtubule dynamics: information from a slowly hydrolyzable analogue, GMPCPP. Molecular biology of the cell *3*, 1155-1167.

Ichikawa, M., Liu, D., Kastritis, P.L., Basu, K., Hsu, T.C., Yang, S., and Bui, K.H. (2017). Subnanometre-resolution structure of the doublet microtubule reveals new classes of microtubule-associated proteins. Nature communications *8*, 15035.

Inglis, P.N., Ou, G., Leroux, M.R., and Scholey, J.M. (2007). The sensory cilia of Caenorhabditis elegans. WormBook : the online review of C elegans biology, 1-22.

Ishikawa, T. (2013). 3D structure of eukaryotic flagella/cilia by cryo-electron tomography. Biophysics *9*, 141-148.

Jana, S.C., Bettencourt-Dias, M., Durand, B., and Megraw, T.L. (2016). Drosophila melanogaster as a model for basal body research. Cilia *5*, 22.

Janmey, P.A. (1998). The cytoskeleton and cell signaling: component localization and mechanical coupling. Physiological reviews *78*, 763-781.

Jerka-Dziadosz, M., Strzyewska-Jowko, I., Wojsa-Lugowska, U., Krawczynska, W., and Krzywicka, A. (2001). The dynamics of filamentous structures in the apical band, oral crescent, fission line and the postoral meridional filament in Tetrahymena thermophila revealed by monoclonal antibody 12G9. Protist *152*, 53-67.

Jiang, K., Toedt, G., Montenegro Gouveia, S., Davey, N.E., Hua, S., van der Vaart, B., Grigoriev, I., Larsen, J., Pedersen, L.B., Bezstarosti, K.*, et al.* (2012). A Proteome-wide screen for mammalian SxIP motif-containing microtubule plus-end tracking proteins. Current biology : CB *22*, 1800-1807.

Jiang, L., Tam, B.M., Ying, G., Wu, S., Hauswirth, W.W., Frederick, J.M., Moritz, O.L., and Baehr, W. (2015a). Kinesin family 17 (osmotic avoidance abnormal-3) is dispensable for photoreceptor morphology and function. FASEB journal : official publication of the Federation of American Societies for Experimental Biology *29*, 4866-4880.

Jiang, Y.Y., Lechtreck, K., and Gaertig, J. (2015b). Total internal reflection fluorescence microscopy of intraflagellar transport in Tetrahymena thermophila. Methods in cell biology *127*, 445-456.

Jiang, Y.Y., Maier, W., Baumeister, R., Minevich, G., Joachimiak, E., Ruan, Z., Kannan, N., Clarke, D., Frankel, J., and Gaertig, J. (2017). The Hippo Pathway Maintains the Equatorial Division Plane in the Ciliate Tetrahymena. Genetics *206*, 873-888.

Johnson, K.A. (1998). The axonemal microtubules of the Chlamydomonas flagellum differ in tubulin isoform content. Journal of cell science *111 (Pt 3)*, 313-320.

Johnson, K.A., and Rosenbaum, J.L. (1992). Polarity of flagellar assembly in Chlamydomonas. The Journal of cell biology *119*, 1605-1611.

Kamiya, R. (2002). Functional diversity of axonemal dyneins as studied in Chlamydomonas mutants. Int Rev Cytol *219*, 115-155.

Kar, A., Phadke, S.R., Das Bhowmik, A., and Dalal, A. (2018). Whole exome sequencing reveals a mutation in ARMC9 as a cause of mental retardation, ptosis, and polydactyly. American journal of medical genetics Part A *176*, 34-40.

Kochanski, R.S., and Borisy, G.G. (1990). Mode of centriole duplication and distribution. The Journal of cell biology *110*, 1599-1605.

Kollman, J.M., Merdes, A., Mourey, L., and Agard, D.A. (2011). Microtubule nucleation by gamma-tubulin complexes. Nature reviews Molecular cell biology *12*, 709-721.

Kozminski, K.G., Beech, P.L., and Rosenbaum, J.L. (1995). The Chlamydomonas kinesin-like protein FLA10 is involved in motility associated with the flagellar membrane. The Journal of cell biology *131*, 1517-1527.

Kozminski, K.G., Johnson, K.A., Forscher, P., and Rosenbaum, J.L. (1993). A motility in the eukaryotic flagellum unrelated to flagellar beating. Proceedings of the National Academy of Sciences of the United States of America *90*, 5519-5523.

Kruger, K., Grabowski, P.J., Zaug, A.J., Sands, J., Gottschling, D.E., and Cech, T.R. (1982). Self-splicing RNA: autoexcision and autocyclization of the ribosomal RNA intervening sequence of Tetrahymena. Cell *31*, 147-157.

Kubo, A., Yuba-Kubo, A., Tsukita, S., Tsukita, S., and Amagai, M. (2008). Sentan: a novel specific component of the apical structure of vertebrate motile cilia. Molecular biology of the cell *19*, 5338-5346.

Kubo, T., Hirono, M., Aikawa, T., Kamiya, R., and Witman, G.B. (2015). Reduced tubulin polyglutamylation suppresses flagellar shortness in Chlamydomonas. Molecular biology of the cell *26*, 2810-2822.

Kubo, T., Yanagisawa, H.A., Yagi, T., Hirono, M., and Kamiya, R. (2010). Tubulin polyglutamylation regulates axonemal motility by modulating activities of inner-arm dyneins. Current biology : CB *20*, 441-445.

Larkin, M.A., Blackshields, G., Brown, N.P., Chenna, R., McGettigan, P.A., McWilliam, H., Valentin, F., Wallace, I.M., Wilm, A., Lopez, R.*, et al.* (2007). Clustal W and Clustal X version 2.0. Bioinformatics *23*, 2947-2948.

Leano, J.B., Rogers, S.L., and Slep, K.C. (2013). A cryptic TOG domain with a distinct architecture underlies CLASP-dependent bipolar spindle formation. Structure (London, England : 1993) *21*, 939-950.

Lechtreck, K.F. (2015). IFT-Cargo Interactions and Protein Transport in Cilia. Trends in biochemical sciences *40*, 765-778.

Lechtreck, K.F., and Geimer, S. (2000). Distribution of polyglutamylated tubulin in the flagellar apparatus of green flagellates. Cell motility and the cytoskeleton *47*, 219-235.

Lechtreck, K.F., Gould, T.J., and Witman, G.B. (2013). Flagellar central pair assembly in Chlamydomonas reinhardtii. Cilia *2*, 15.

Lechtreck, K.F., Van De Weghe, J.C., Harris, J.A., and Liu, P. (2017). Protein transport in growing and steady-state cilia. Traffic (Copenhagen, Denmark) *18*, 277-286.

Lechtreck, K.F., and Witman, G.B. (2007). Chlamydomonas reinhardtii hydin is a central pair protein required for flagellar motility. The Journal of cell biology *176*, 473-482.

Lenka Rezabkova, S.H.W.K., Anna Akhmanova, Michel O. Steinmetz, and Richard A. Kammerer (2016). Biophysical and Structural Characterization of the Centriolar Protein Cep104 Interaction Network. J Biol Chem *v1*.

Lewin, R.A. (1954). Mutants of Chlamydomonas moewusii with impaired motility. Journal of general microbiology *11*, 358-363.

Liem, K.F., Jr., He, M., Ocbina, P.J., and Anderson, K.V. (2009). Mouse Kif7/Costal2 is a cilia-associated protein that regulates Sonic hedgehog signaling. Proceedings of the National Academy of Sciences of the United States of America *106*, 13377-13382.

Lin, Y.N., Wu, C.T., Lin, Y.C., Hsu, W.B., Tang, C.J., Chang, C.W., and Tang, T.K. (2013). CEP120 interacts with CPAP and positively regulates centriole elongation. The Journal of cell biology *202*, 211-219.

Loreng, T.D., and Smith, E.F. (2017). The Central Apparatus of Cilia and Eukaryotic Flagella. Cold Spring Harbor perspectives in biology *9*.

Love, B., and Rotheim, M.B. (1984). Cell surface interactions in conjugation: Tetrahymena ciliary membrane vesicles. Mol Cell Biol *4*, 681-687.

Ludington, W.B., Ishikawa, H., Serebrenik, Y.V., Ritter, A., Hernandez-Lopez, R.A., Gunzenhauser, J., Kannegaard, E., and Marshall, W.F. (2015). A systematic comparison of mathematical models for inherent measurement of ciliary length: how a cell can measure length and volume. Biophys J *108*, 1361-1379.

Lwoff, A. (1923). Sur la nutrition des infusoires. C R Acad Sci *176*, 928-930.

Mahjoub, M.R., Xie, Z., and Stearns, T. (2010). Cep120 is asymmetrically localized to the daughter centriole and is essential for centriole assembly. The Journal of cell biology *191*, 331-346.

Marshall, W.F., and Rosenbaum, J.L. (2001). Intraflagellar transport balances continuous turnover of outer doublet microtubules: implications for flagellar length control. The Journal of cell biology *155*, 405-414.

Maurer, S.P., Fourniol, F.J., Bohner, G., Moores, C.A., and Surrey, T. (2012). EBs recognize a nucleotide-dependent structural cap at growing microtubule ends. Cell *149*, 371-382.

McEwen, D.P., Jenkins, P.M., and Martens, J.R. (2008). Olfactory cilia: our direct neuronal connection to the external world. Current topics in developmental biology *85*, 333-370.

Mesland, D.A., Hoffman, J.L., Caligor, E., and Goodenough, U.W. (1980). Flagellar tip activation stimulated by membrane adhesions in Chlamydomonas gametes. The Journal of cell biology *84*, 599-617.

Miller, J.M., Wang, W., Balczon, R., and Dentler, W.L. (1990). Ciliary microtubule capping structures contain a mammalian kinetochore antigen. The Journal of cell biology *110*, 703-714.

Mitchell, D.R. (2003). Orientation of the central pair complex during flagellar bend formation in Chlamydomonas. Cell motility and the cytoskeleton *56*, 120-129.

Mitchell, D.R., and Smith, B. (2009). Analysis of the central pair microtubule complex in Chlamydomonas reinhardtii. Methods in cell biology *92*, 197-213.

Mitchison, H.M., and Valente, E.M. (2017). Motile and non-motile cilia in human pathology: from function to phenotypes. The Journal of pathology *241*, 294-309.

Mitchison, T., and Kirschner, M. (1984). Dynamic instability of microtubule growth. Nature *312*, 237-242.

Mochizuki, K. (2008). High efficiency transformation of Tetrahymena using a codon-optimized neomycin resistance gene. Gene *425*, 79-83.

Mukhopadhyay, S., Lu, Y., Qin, H., Lanjuin, A., Shaham, S., and Sengupta, P. (2007). Distinct IFT mechanisms contribute to the generation of ciliary structural diversity in C. elegans. The EMBO journal *26*, 2966-2980.

Multigner, L., Pignot-Paintrand, I., Saoudi, Y., Job, D., Plessmann, U., Rudiger, M., and Weber, K. (1996). The A and B tubules of the outer doublets of sea urchin sperm axonemes are composed of different tubulin variants. Biochemistry *35*, 10862-10871.

Nakata, T., Niwa, S., Okada, Y., Perez, F., and Hirokawa, N. (2011). Preferential binding of a kinesin-1 motor to GTP-tubulin-rich microtubules underlies polarized vesicle transport. The Journal of cell biology *194*, 245-255.

Nakazawa, Y., Ariyoshi, T., Noga, A., Kamiya, R., and Hirono, M. (2014). Space-dependent formation of central pair microtubules and their interactions with radial spokes. PLoS One *9*, e110513.

Nechipurenko, I.V., Berciu, C., Sengupta, P., and Nicastro, D. (2017). Centriolar remodeling underlies basal body maturation during ciliogenesis in Caenorhabditis elegans. eLife *6*.

Nelsen, E.M. (1978). Transformation in Tetrahymena thermophila. Development of an inducible phenotype. Developmental biology *66*, 17-31.

Nelsen, E.M., and Debault, L.E. (1978). Transformation in Tetrahymena pyriformis: description of an inducible phenotype. J Protozool *25*, 113-119.

Nicastro, D., Schwartz, C., Pierson, J., Gaudette, R., Porter, M.E., and McIntosh, J.R. (2006). The molecular architecture of axonemes revealed by cryoelectron tomography. Science (New York, NY) *313*, 944-948.

Nicholson, W.V., Lee, M., Downing, K.H., and Nogales, E. (1999). Cryo-electron microscopy of GDP-tubulin rings. Cell biochemistry and biophysics *31*, 175-183.

Niwa, S., Nakajima, K., Miki, H., Minato, Y., Wang, D., and Hirokawa, N. (2012). KIF19A is a microtubule-depolymerizing kinesin for ciliary length control. Developmental cell *23*, 1167-1175.

Nonaka, S., Tanaka, Y., Okada, Y., Takeda, S., Harada, A., Kanai, Y., Kido, M., and Hirokawa, N. (1998). Randomization of left-right asymmetry due to loss of nodal cilia generating leftward flow of extraembryonic fluid in mice lacking KIF3B motor protein. Cell *95*, 829-837.

O'Hagan, R., Piasecki, B.P., Silva, M., Phirke, P., Nguyen, K.C., Hall, D.H., Swoboda, P., and Barr, M.M. (2011). The tubulin deglutamylase CCPP-1 regulates the function and stability of sensory cilia in C. elegans. Current biology : CB *21*, 1685-1694.

O'Toole, E.T., Giddings, T.H., McIntosh, J.R., and Dutcher, S.K. (2003). Three-dimensional organization of basal bodies from wild-type and delta-tubulin deletion strains of Chlamydomonas reinhardtii. Molecular biology of the cell *14*, 2999-3012.

Oda, T., Yanagisawa, H., Yagi, T., and Kikkawa, M. (2014). Mechanosignaling between central apparatus and radial spokes controls axonemal dynein activity. The Journal of cell biology *204*, 807-819.

Ogawa, T., Nitta, R., Okada, Y., and Hirokawa, N. (2004). A common mechanism for microtubule destabilizers-M type kinesins stabilize curling of the protofilament using the class-specific neck and loops. Cell *116*, 591-602.

Omori, Y., Chaya, T., Katoh, K., Kajimura, N., Sato, S., Muraoka, K., Ueno, S., Koyasu, T., Kondo, M., and Furukawa, T. (2010). Negative regulation of ciliary length by ciliary male germ cell-associated kinase (Mak) is required for retinal photoreceptor survival. Proceedings of the National Academy of Sciences of the United States of America *107*, 22671-22676.

Omoto, C.K., Gibbons, I.R., Kamiya, R., Shingyoji, C., Takahashi, K., and Witman, G.B. (1999). Rotation of the central pair microtubules in eukaryotic flagella. Molecular biology of the cell *10*, 1-4.

Omoto, C.K., and Kung, C. (1979). The pair of central tubules rotates during ciliary beat in Paramecium. Nature *279*, 532-534.

Omoto, C.K., and Kung, C. (1980). Rotation and twist of the central-pair microtubules in the cilia of Paramecium. The Journal of cell biology *87*, 33-46.

Omoto, C.K., and Witman, G.B. (1981). Functionally significant central-pair rotation in a primitive eukaryotic flagellum. Nature *290*, 708-710.

Orias, E., and Rasmussen, L. (1976). Dual capacity for nutrient uptake in Tetrahymena. IV. Growth without food vacuoles and its implications. Exp Cell Res *102*, 127-137.

Paintrand, M., Moudjou, M., Delacroix, H., and Bornens, M. (1992). Centrosome organization and centriole architecture: their sensitivity to divalent cations. Journal of structural biology *108*, 107-128.

Pathak, N., Austin, C.A., and Drummond, I.A. (2011). Tubulin tyrosine ligase-like genes ttll3 and ttll6 maintain zebrafish cilia structure and motility. The Journal of biological chemistry *286*, 11685-11695.

Pazour, G.J., Dickert, B.L., Vucica, Y., Seeley, E.S., Rosenbaum, J.L., Witman, G.B., and Cole, D.G. (2000). Chlamydomonas IFT88 and its mouse homologue, polycystic kidney disease gene tg737, are required for assembly of cilia and flagella. The Journal of cell biology *151*, 709-718.

Pazour, G.J., Dickert, B.L., and Witman, G.B. (1999). The DHC1b (DHC2) isoform of cytoplasmic dynein is required for flagellar assembly. The Journal of cell biology *144*, 473-481.

Pazour, G.J., Wilkerson, C.G., and Witman, G.B. (1998). A dynein light chain is essential for the retrograde particle movement of intraflagellar transport (IFT). The Journal of cell biology *141*, 979-992.

Pedersen, L.B., Geimer, S., Sloboda, R.D., and Rosenbaum, J.L. (2003). The Microtubule plus end-tracking protein EB1 is localized to the flagellar tip and basal bodies in Chlamydomonas reinhardtii. Current biology : CB *13*, 1969-1974.

Pedersen, L.B., Miller, M.S., Geimer, S., Leitch, J.M., Rosenbaum, J.L., and Cole, D.G. (2005). Chlamydomonas IFT172 is encoded by FLA11, interacts with CrEB1, and regulates IFT at the flagellar tip. Current biology : CB *15*, 262-266.

Perkins, L.A., Hedgecock, E.M., Thomson, J.N., and Culotti, J.G. (1986). Mutant sensory cilia in the nematode Caenorhabditis elegans. Developmental biology *117*, 456-487.

Piao, T., Luo, M., Wang, L., Guo, Y., Li, D., Li, P., Snell, W.J., and Pan, J. (2009). A microtubule depolymerizing kinesin functions during both flagellar disassembly and flagellar assembly in Chlamydomonas. Proceedings of the National Academy of Sciences of the United States of America *106*, 4713-4718.

Portman, R.W., LeCluyse, E.L., and Dentler, W.L. (1987). Development of microtubule capping structures in ciliated epithelial cells. Journal of cell science *87 (Pt 1)*, 85-94.

Prevo, B., Mangeol, P., Oswald, F., Scholey, J.M., and Peterman, E.J. (2015). Functional differentiation of cooperating kinesin-2 motors orchestrates cargo import and transport in C. elegans cilia. Nature cell biology *17*, 1536-1545.

Prigent, Y., Kann, M.L., Lach-Gar, H., Pechart, I., and Fouquet, J.P. (1996). Glutamylated tubulin as a marker of microtubule heterogeneity in the human sperm flagellum. Mol Hum Reprod *2*, 573-581.

Randall, J., Warr, J.R., Hopkins, J.M., and McVittie, A. (1964). A Single-Gene Mutation of Chlamydomonas Reinhardii Affecting Motility: A Genetic and Electron Microscope Study. Nature *203*, 912-914.

Reese, T.S. (1965). Olfactory Cilia in the Frog. The Journal of cell biology *25*, 209-230.

Reiter, J.F., and Leroux, M.R. (2017). Genes and molecular pathways underpinning ciliopathies. Nature reviews Molecular cell biology *18*, 533-547.

Rezabkova, L., Kraatz, S.H., Akhmanova, A., Steinmetz, M.O., and Kammerer, R.A. (2016). Biophysical and Structural Characterization of the Centriolar Protein Cep104 Interaction Network. The Journal of biological chemistry *291*, 18496-18504.

Rice, L.M., Montabana, E.A., and Agard, D.A. (2008). The lattice as allosteric effector: structural studies of alphabeta- and gamma-tubulin clarify the role of GTP in microtubule assembly. Proceedings of the National Academy of Sciences of the United States of America *105*, 5378-5383.

Rodionov, V.I., and Borisy, G.G. (1997). Microtubule treadmilling in vivo. Science (New York, NY) *275*, 215-218.

Roostalu, J., and Surrey, T. (2017). Microtubule nucleation: beyond the template. Nature reviews Molecular cell biology *18*, 702-710.

Rothwell, S.W., Grasser, W.A., and Murphy, D.B. (1985). Direct observation of microtubule treadmilling by electron microscopy. The Journal of cell biology *101*, 1637-1642.

Roux, K.J., Kim, D.I., Raida, M., and Burke, B. (2012). A promiscuous biotin ligase fusion protein identifies proximal and interacting proteins in mammalian cells. The Journal of cell biology *196*, 801-810.

Ruehle, M.D., Orias, E., and Pearson, C.G. (2016). Tetrahymena as a Unicellular Model Eukaryote: Genetic and Genomic Tools. Genetics *203*, 649-665.

Sale, W.S., and Satir, P. (1977). The termination of the central microtubules from the cilia of Tetrahymena pyriformis. Cell biology international reports *1*, 45-49.

Salisbury, J.L., Baron, A.T., and Sanders, M.A. (1988). The centrin-based cytoskeleton of Chlamydomonas reinhardtii: distribution in interphase and mitotic cells. The Journal of cell biology *107*, 635-641.

Sanders, A.A., de Vrieze, E., Alazami, A.M., Alzahrani, F., Malarkey, E.B., Sorusch, N., Tebbe, L., Kuhns, S., van Dam, T.J., Alhashem, A.*, et al.* (2015). KIAA0556 is a novel ciliary basal body component mutated in Joubert syndrome. Genome biology *16*, 293.

Sarpal, R., Todi, S.V., Sivan-Loukianova, E., Shirolikar, S., Subramanian, N., Raff, E.C., Erickson, J.W., Ray, K., and Eberl, D.F. (2003). Drosophila KAP interacts with the kinesin II motor subunit KLP64D to assemble chordotonal sensory cilia, but not sperm tails. Current biology : CB *13*, 1687-1696.

Satir, P. (1968). Studies on cilia. 3. Further studies on the cilium tip and a "sliding filament" model of ciliary motility. The Journal of cell biology *39*, 77-94.

Satish Tammana, T.V., Tammana, D., Diener, D.R., and Rosenbaum, J. (2013). Centrosomal protein CEP104 (Chlamydomonas FAP256) moves to the ciliary tip during ciliary assembly. Journal of cell science *126*, 5018-5029.

Saxton, W.M., and McIntosh, J.R. (1987). Interzone microtubule behavior in late anaphase and telophase spindles. The Journal of cell biology *105*, 875-886.

Schiapparelli, L.M., McClatchy, D.B., Liu, H.H., Sharma, P., Yates, J.R., 3rd, and Cline, H.T. (2014). Direct detection of biotinylated proteins by mass spectrometry. Journal of proteome research *13*, 3966-3978.

Schneider, C.A., Rasband, W.S., and Eliceiri, K.W. (2012). NIH Image to ImageJ: 25 years of image analysis. Nature methods *9*, 671-675.

Seetapun, D., Castle, B.T., McIntyre, A.J., Tran, P.T., and Odde, D.J. (2012). Estimating the microtubule GTP cap size in vivo. Current biology : CB *22*, 1681-1687.

Shah, A.S., Ben-Shahar, Y., Moninger, T.O., Kline, J.N., and Welsh, M.J. (2009). Motile cilia of human airway epithelia are chemosensory. Science (New York, NY) *325*, 1131-1134.

Shaheen, R., Szymanska, K., Basu, B., Patel, N., Ewida, N., Faqeih, E., Al Hashem, A., Derar, N., Alsharif, H., Aldahmesh, M.A.*, et al.* (2016). Characterizing the morbid genome of ciliopathies. Genome biology *17*, 242.

Shaner, N.C., Lambert, G.G., Chammas, A., Ni, Y., Cranfill, P.J., Baird, M.A., Sell, B.R., Allen, J.R., Day, R.N., Israelsson, M.*, et al.* (2013). A bright monomeric green fluorescent protein derived from Branchiostoma lanceolatum. Nature methods *10*, 407-409.

Shang, Y., Li, B., and Gorovsky, M.A. (2002). Tetrahymena thermophila contains a conventional gamma-tubulin that is differentially required for the maintenance of different microtubule-organizing centers. The Journal of cell biology *158*, 1195-1206.

Sharma, A., Gerard, S.F., Olieric, N., and Steinmetz, M.O. (2018). Cep120 promotes microtubule formation through a unique tubulin binding C2 domain. Journal of structural biology.

Shipley, K., Hekmat-Nejad, M., Turner, J., Moores, C., Anderson, R., Milligan, R., Sakowicz, R., and Fletterick, R. (2004). Structure of a kinesin microtubule depolymerization machine. The EMBO journal *23*, 1422-1432.

Signor, D., Wedaman, K.P., Orozco, J.T., Dwyer, N.D., Bargmann, C.I., Rose, L.S., and Scholey, J.M. (1999). Role of a class DHC1b dynein in retrograde transport of IFT motors and IFT raft particles along cilia, but not dendrites, in chemosensory neurons of living Caenorhabditis elegans. The Journal of cell biology *147*, 519-530.

Sirajuddin, M., Rice, L.M., and Vale, R.D. (2014). Regulation of microtubule motors by tubulin isotypes and post-translational modifications. Nature cell biology *16*, 335-344.

Snow, J.J., Ou, G., Gunnarson, A.L., Walker, M.R., Zhou, H.M., Brust-Mascher, I., and Scholey, J.M. (2004). Two anterograde intraflagellar transport motors cooperate to build sensory cilia on C. elegans neurons. Nature cell biology *6*, 1109-1113.

Srour, M., Hamdan, F.F., McKnight, D., Davis, E., Mandel, H., Schwartzentruber, J., Martin, B., Patry, L., Nassif, C., Dionne-Laporte, A.*, et al.* (2015). Joubert Syndrome in French Canadians and Identification of Mutations in CEP104. Am J Hum Genet *97*, 744-753.

Stepanek, L., and Pigino, G. (2016). Microtubule doublets are double-track railways for intraflagellar transport trains. Science (New York, NY) *352*, 721-724.

Summers, K.E., and Gibbons, I.R. (1971). Adenosine triphosphate-induced sliding of tubules in trypsin-treated flagella of sea-urchin sperm. Proceedings of the National Academy of Sciences of the United States of America *68*, 3092-3096.

Suprenant, K.A., and Dentler, W.L. (1988). Release of intact microtubule-capping structures from Tetrahymena cilia. The Journal of cell biology *107*, 2259-2269.

Suryavanshi, S., Edde, B., Fox, L.A., Guerrero, S., Hard, R., Hennessey, T., Kabi, A., Malison, D., Pennock, D., Sale, W.S.*, et al.* (2010). Tubulin glutamylation regulates ciliary motility by altering inner dynein arm activity. Current biology : CB *20*, 435-440.

Thazhath, R., Liu, C., and Gaertig, J. (2002). Polyglycylation domain of beta-tubulin maintains axonemal architecture and affects cytokinesis in Tetrahymena. Nature cell biology *4*, 256-259.

Thoma, C.R., Matov, A., Gutbrodt, K.L., Hoerner, C.R., Smole, Z., Krek, W., and Danuser, G. (2010). Quantitative image analysis identifies pVHL as a key regulator of microtubule dynamic instability. The Journal of cell biology *190*, 991-1003.

Tilney, L.G., Bryan, J., Bush, D.J., Fujiwara, K., Mooseker, M.S., Murphy, D.B., and Snyder, D.H. (1973). Microtubules: evidence for 13 protofilaments. The Journal of cell biology *59*, 267-275.

Tran, P.T., Walker, R.A., and Salmon, E.D. (1997). A metastable intermediate state of microtubule dynamic instability that differs significantly between plus and minus ends. The Journal of cell biology *138*, 105-117.

Tropini, C., Roth, E.A., Zanic, M., Gardner, M.K., and Howard, J. (2012). Islands containing slowly hydrolyzable GTP analogs promote microtubule rescues. PLoS One *7*, e30103.

Tsypin, L.M., and Turkewitz, A.P. (2017). The Co-regulation Data Harvester: automating gene annotation starting from a transcriptome database. SoftwareX *6*, 165-171.

Tukachinsky, H., Lopez, L.V., and Salic, A. (2010). A mechanism for vertebrate Hedgehog signaling: recruitment to cilia and dissociation of SuFu-Gli protein complexes. The Journal of cell biology *191*, 415-428.

Turk, E., Wills, A.A., Kwon, T., Sedzinski, J., Wallingford, J.B., and Stearns, T. (2015). Zeta-Tubulin Is a Member of a Conserved Tubulin Module and Is a Component of the Centriolar Basal Foot in Multiciliated Cells. Current biology : CB *25*, 2177-2183.

Urbanska, P., Song, K., Joachimiak, E., Krzemien-Ojak, L., Koprowski, P., Hennessey, T., Jerka-Dziadosz, M., Fabczak, H., Gaertig, J., Nicastro, D.*, et al.* (2015). The CSC proteins FAP61 and FAP251 build the basal substructures of radial spoke 3 in cilia. Molecular biology of the cell *26*, 1463-1475.

Van De Weghe, J.C., Rusterholz, T.D.S., Latour, B., Grout, M.E., Aldinger, K.A., Shaheen, R., Dempsey, J.C., Maddirevula, S., Cheng, Y.H., Phelps, I.G.*, et al.* (2017). Mutations in ARMC9, which Encodes a Basal Body Protein, Cause Joubert Syndrome in Humans and Ciliopathy Phenotypes in Zebrafish. Am J Hum Genet *101*, 23-36.

van Haren, J., Charafeddine, R.A., Ettinger, A., Wang, H., Hahn, K.M., and Wittmann, T. (2018). Local control of intracellular microtubule dynamics by EB1 photodissociation. Nature cell biology *20*, 252-261.

Vasudevan, K.K., Jiang, Y.Y., Lechtreck, K.F., Kushida, Y., Alford, L.M., Sale, W.S., Hennessey, T., and Gaertig, J. (2015). Kinesin-13 regulates the quantity and quality of tubulin inside cilia. Molecular biology of the cell *26*, 478-494.

Verhey, K.J., and Gaertig, J. (2007). The tubulin code. Cell cycle (Georgetown, Tex) *6*, 2152-2160.

Viswanadha, R., Hunter, E.L., Yamamoto, R., Wirschell, M., Alford, L.M., Dutcher, S.K., and Sale, W.S. (2014). The ciliary inner dynein arm, I1 dynein, is assembled in the cytoplasm and transported by IFT before axonemal docking. Cytoskeleton *71*, 573-586.

Voter, W.A., O'Brien, E.T., and Erickson, H.P. (1991). Dilution-induced disassembly of microtubules: relation to dynamic instability and the GTP cap. Cell motility and the cytoskeleton *18*, 55-62.

Wade, R.H., Chretien, D., and Job, D. (1990). Characterization of microtubule protofilament numbers. How does the surface lattice accommodate? Journal of molecular biology *212*, 775-786.

Walker, R.A., Inoue, S., and Salmon, E.D. (1989). Asymmetric behavior of severed microtubule ends after ultraviolet-microbeam irradiation of individual microtubules in vitro. The Journal of cell biology *108*, 931-937.

Walker, R.A., O'Brien, E.T., Pryer, N.K., Soboeiro, M.F., Voter, W.A., Erickson, H.P., and Salmon, E.D. (1988). Dynamic instability of individual microtubules analyzed by video light microscopy: rate constants and transition frequencies. The Journal of cell biology *107*, 1437-1448.

Walker, R.A., Pryer, N.K., and Salmon, E.D. (1991). Dilution of individual microtubules observed in real time in vitro: evidence that cap size is small and independent of elongation rate. The Journal of cell biology *114*, 73-81.

Wang, D., Nitta, R., Morikawa, M., Yajima, H., Inoue, S., Shigematsu, H., Kikkawa, M., and Hirokawa, N. (2016). Motility and microtubule depolymerization mechanisms of the Kinesin-8 motor, KIF19A. eLife *5*.

Wang, J.T., Kong, D., Hoerner, C.R., Loncarek, J., and Stearns, T. (2017). Centriole triplet microtubules are required for stable centriole formation and inheritance in human cells. eLife *6*.

Weisenberg, R.C., Deery, W.J., and Dickinson, P.J. (1976). Tubulin-nucleotide interactions during the polymerization and depolymerization of microtubules. Biochemistry *15*, 4248-4254.

Westermann, S., Avila-Sakar, A., Wang, H.W., Niederstrasser, H., Wong, J., Drubin, D.G., Nogales, E., and Barnes, G. (2005). Formation of a dynamic kinetochore- microtubule interface through assembly of the Dam1 ring complex. Molecular cell *17*, 277-290.

Widlund, P.O., Stear, J.H., Pozniakovsky, A., Zanic, M., Reber, S., Brouhard, G.J., Hyman, A.A., and Howard, J. (2011). XMAP215 polymerase activity is built by combining multiple

tubulin-binding TOG domains and a basic lattice-binding region. Proceedings of the National Academy of Sciences of the United States of America *108*, 2741-2746.

Williams, C.L., McIntyre, J.C., Norris, S.R., Jenkins, P.M., Zhang, L., Pei, Q., Verhey, K., and Martens, J.R. (2014). Direct evidence for BBSome-associated intraflagellar transport reveals distinct properties of native mammalian cilia. Nature communications *5*, 5813.

Wloga, D., Camba, A., Rogowski, K., Manning, G., Jerka-Dziadosz, M., and Gaertig, J. (2006). Members of the NIMA-related kinase family promote disassembly of cilia by multiple mechanisms. Molecular biology of the cell *17*, 2799-2810.

Wloga, D., Dave, D., Meagley, J., Rogowski, K., Jerka-Dziadosz, M., and Gaertig, J. (2010). Hyperglutamylation of tubulin can either stabilize or destabilize microtubules in the same cell. Eukaryotic cell *9*, 184-193.

Wloga, D., Joachimiak, E., Louka, P., and Gaertig, J. (2017). Posttranslational Modifications of Tubulin and Cilia. Cold Spring Harbor perspectives in biology *9*.

Wolfe, J., Turner, R., Jr., Barker, R., and Adair, W.S. (1979). The need for an extracellular component for cell pairing in Tetrahymena. Exp Cell Res *121*, 27-30.

Xia, L., Hai, B., Gao, Y., Burnette, D., Thazhath, R., Duan, J., Bre, M.H., Levilliers, N., Gorovsky, M.A., and Gaertig, J. (2000). Polyglycylation of tubulin is essential and affects cell motility and division in Tetrahymena thermophila. The Journal of cell biology *149*, 1097-1106.

Xiong, J., Lu, Y., Feng, J., Yuan, D., Tian, M., Chang, Y., Fu, C., Wang, G., Zeng, H., and Miao, W. (2013). Tetrahymena functional genomics database (TetraFGD): an integrated resource for Tetrahymena functional genomics. Database : the journal of biological databases and curation *2013*, bat008.

Ye, F., Nager, A.R., and Nachury, M.V. (2018). BBSome trains remove activated GPCRs from cilia by enabling passage through the transition zone. The Journal of cell biology.

Youn, Y.H., and Han, Y.G. (2018). Primary Cilia in Brain Development and Diseases. The American journal of pathology *188*, 11-22.

Zabeo, D., Heumann, J.M., Schwartz, C.L., Suzuki-Shinjo, A., Morgan, G., Widlund, P.O., and Hoog, J.L. (2018). A lumenal interrupted helix in human sperm tail microtubules. Scientific reports *8*, 2727.

Zanic, M., Stear, J.H., Hyman, A.A., and Howard, J. (2009). EB1 recognizes the nucleotide state of tubulin in the microtubule lattice. PLoS One *4*, e7585.

Zhang, R., Alushin, G.M., Brown, A., and Nogales, E. (2015). Mechanistic Origin of Microtubule Dynamic Instability and Its Modulation by EB Proteins. Cell *162*, 849-859.